CHALMERS
UNIVERSITY OF TECHNOLOGY

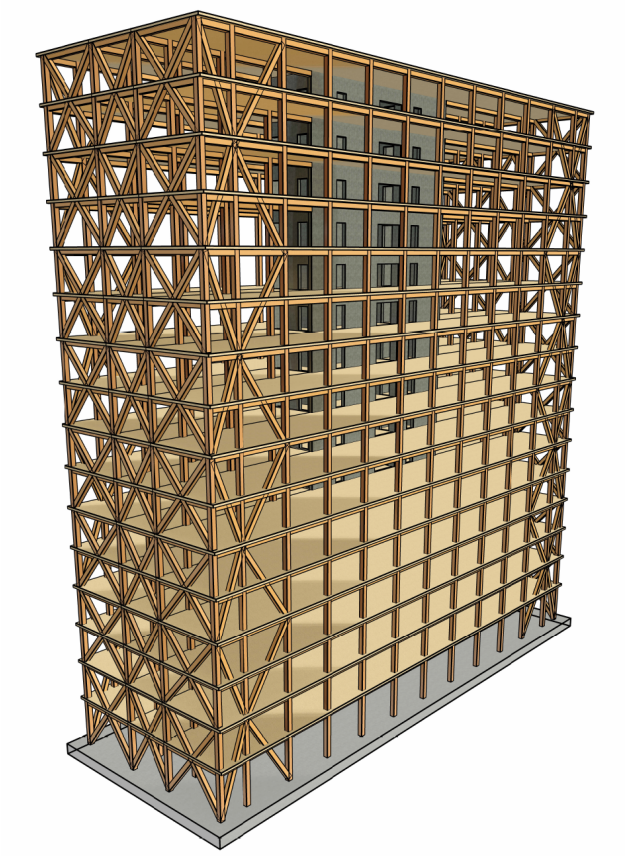

Hybrid Office Towers under Wind Loads

A Parametric Study of Dynamic Performance and Structural Stability

Master's thesis in Structural Engineering and Building Technology

NOUR EMAD AWADALLA ATTIA
MARCUS INGEMARSSON

DEPARTMENT OF ARCHITECTURE AND CIVIL ENGINEERING
CHALMERS UNIVERSITY OF TECHNOLOGY
Gothenburg, Sweden 2025
www.chalmers.se

Master's thesis ACEX30, 2025

Hybrid Office Towers under Wind Loads

A Parametric Study of Dynamic Performance and Structural Stability

NOUR EMAD AWADALLA ATTIA
MARCUS INGEMARSSON

CHALMERS
UNIVERSITY OF TECHNOLOGY

Department of Architecture and Civil Engineering
Division of Structural Engineering
Chalmers University of Technology
Gothenburg, Sweden 2025

Hybrid Office Towers under Wind Loads
A Parametric Study of Dynamic Performance and Structural Stability
NOUR EMAD AWADALLA ATTIA
MARCUS INGEMARSSON

Supervisor: Thomas Hallgren, Structural Engineer, COWI
Examiner: Mohammad al-Emrani, Full professor, Department of Architecture and Civil Engineering

Master's thesis ACEX30, 2025
Department of Architecture and Civil Engineering
Division of Structural Engineering
Chalmers University of Technology
SE-412 96 Gothenburg
Telephone +46 31 772 1000

Cover: Structural System of the Office Tower.
Typeset in LaTeX
Printed by Chalmers Reproservice
Gothenburg, Sweden 2025

Hybrid Office Towers under Wind Loads
A Parametric Study of Dynamic Performance and Structural Stability
NOUR EMAD AWADALLA ATTIA
MARCUS INGEMARSSON
Department of Architecture and Civil Engineering
Chalmers University of Technology

Abstract

As the demand for sustainable and space-efficient urban development increases, hybrid timber-concrete buildings offer an environmentally friendly alternative to conventional construction. However, due to timber's high strength-to-weight ratio, these structures tend to be relatively light, making them more sensitive to wind-induced motion. This highlights the need for deeper investigation into their dynamic and structural behaviour to ensure both occupant comfort and safety in taller buildings.

This thesis investigates the structural and dynamic performance of hybrid high-rise office buildings composed of timber and concrete, with a focus on wind-induced acceleration under the Serviceability Limit State and structural capacity under the Ultimate Limit State. Using a finite element model developed in FEM-Design, alongside hand calculations, the study analyses how different configurations, such as core thickness, core placement, concrete slab layout, and boundary conditions, affect the results.

A parametric study was conducted on a 15-, 20-, and 25-storey timber-concrete hybrid building with a concrete core and cross-laminated timber slabs, where concrete was added either by thickening the core or additional concrete slabs at the top of the building. Core placement was also varied to assess its impact on stiffness and torsional response. For each configuration, eigenfrequencies, equivalent mass, and peak accelerations were calculated and compared against comfort criteria defined in SS-ISO 10137:2008. Structural capacity was verified through analysis based on Eurocode and the Swedish annex EKS 12.

Wind-induced acceleration was the governing criterion in all cases. Adding concrete slabs at the top improved dynamic performance more effectively than increasing core thickness. While thicker cores helped with strength and stability, they were less efficient for improving comfort. Different core placements performed similarly overall. The most concrete-efficient strategy is to first use thick concrete slabs at the top of the building to improve comfort, followed by adding additional slabs if further improvement is needed. However, there is a point where adding more slabs becomes less effective than increasing core thickness, which then becomes the better option.

Keywords: hybrid building, concrete, timber, cross-laminated timber, glulam, high-rise buildings, wind-induced acceleration, comfort criteria, finite element analysis

Hybrida Kontorsbyggnader Under Vindlast
En Parametrisk Studie av Dynamisk Prestanda och Strukturell Stabilitet
NOUR EMAD AWADALLA ATTIA
MARCUS INGEMARSSON
Avdelningen för Arkitektur och Samhällsbyggnadsteknik
Chalmers Tekniska Högskola

Sammanfattning

I takt med att intresset för hållbarhet och förtätning av städer ökar, blir hybrida trä-betongbyggnader ett allt mer relevant alternativ till traditionella stomlösningar. Träets låga vikt i förhållande till hållfasthet medför dock att dessa byggnader blir mer känsliga för rörelser på grund av vindlaster, vilket kan påverka komforten negativt. Detta kräver noggrann analys av byggnadens dynamiska och strukturella beteende för att säkerställa både komfort och säkerhet.

I detta examensarbete studeras höga kontorsbyggnader med stomme av trä och betong, med särskilt fokus på byggnadens acceleration på grund av vind i bruksgränstillståndet och bärförmåga i brottgränstillståndet. Analyserna genomfördes med hjälp av FEM-Design i kombination med handberäkningar, och omfattade olika parametrar såsom kärntjocklek, kärnplacering, antal och tjocklek på betongbjälklag samt randvillkor.

En parameterstudie utfördes för byggnader med 15, 20 och 25 våningar, där betongkärna kombinerades med korslimmat träbjälklag. Betong tillfördes antingen genom tjockare kärna eller genom extra bjälklag i byggnadens topp. Även kärnans placering varierades för att studera effekten på byggnadens styvhet och vridstyvhet. För varje konfiguration beräknades egenfrekvens, ekvivalent massa och toppaccelerationer, vilka jämfördes med komfortkraven enligt SS-ISO 10137:2008. Bärförmågan utvärderades enligt Eurocode och EKS 12.

Acceleration på grund av vind var det begränsande kriteriet för att komma upp i höjd. Att lägga till tjocka bjälklag i byggnadens övre delar gav störst förbättring av komforten, medan tjockare kärna hade större påverkan på bärförmågan men var mindre effektiv för att minska accelerationerna. Olika kärnplaceringar gav i stort sett likvärdiga resultat. Den mest betongeffektiva lösningen är att först använda tjocka betongbjälklag i byggnadens översta delar för att förbättra komforten. Om ytterligare förbättring krävs kan fler bjälklag läggas till, men det finns en gräns där det blir mindre effektivt än att istället öka kärnans tjocklek, vilket då blir det bättre alternativet.

Nyckelord: Hybrida byggnader, trä, betong, korslimmat trä, limträ, höga byggnader, acceleration, komfortkrav, finita elementmetoden

Acknowledgements

This master thesis marks the completion of our Master of Science degree in Structural Engineering and Building Technology at Chalmers University of Technology. The project was carried out in collaboration between the Department of Architecture and Civil Engineering at Chalmers and the engineering consultancy COWI. The work was conducted between January and June 2025.

We would like to express our sincere gratitude to our supervisor, Thomas Hallgren at COWI, for his valuable guidance, support, and practical insights throughout the project. We would like to thank COWI for supporting this project and providing access to the necessary resources and tools to carry out the research.

We also wish to extend our thanks to our examiner, Professor Mohammad Al-Emrani, for his expert advice and constructive feedback.

Nour Emad Awadalla Attia & Marcus Ingemarsson, Gothenburg, June 2025

List of Acronyms

Below is the list of acronyms that have been used throughout this thesis listed in alphabetical order:

CLT	Cross Laminated Timber
TMD	Tuned Mass Damper
ULS	Ultimate Limit State
SLS	Serviceability Limit State
FE	Finite Element
FEM	Finite Element Method
EC	Eurocode
EKS 12	Swedish national annex specifying how Eurocodes should be applied in accordance with Boverket's building regulations
SS-EN 1990	Eurocode: Basis of structural design
SS-EN 1991-1-3	Eurocode 1: Actions on structures – General actions – Snow loads
SS-EN 1991-1-4	Eurocode 1: Actions on structures – General actions – Wind actions
SS-EN 1992-1-1	Eurocode 2: Design of concrete structures – General rules and rules for buildings
SS-EN 1995-1-1	Eurocode 5: Design of timber structures – General – Common rules and rules for buildings

Notations

Roman upper-case letters

B^2	Background response factor representing low-frequency turbulence
F_w	External wind pressure on buildings
H	Horizontal force
H_{xi}	Horizontal force acting on bracing member i in x-direction
H_{yi}	Horizontal force acting on bracing member i in y-direction
$I_v(z)$	Turbulence intensity
R^2	Amplification factor due to resonance with natural frequency
S_{bi}	Bending stiffness of wall i
S_{si}	Shear stiffness of wall i
S_T	Global torsional stiffness
S_{xi}	Stiffness of bracing member i in x-direction
S_{yi}	Stiffness of bracing member i in y-direction
T	Reference time
T_a	Return period
W_e	Wind pressure acting on external surfaces
$\ddot{X}_{\max}$	Peak acceleration due to wind

Roman lower-case letters

a_i	Distance from arbitrary position to center of bracing unit i in x-direction
b	Cross-dimension perpendicular to wind direction
b_i	Distance from arbitrary position to center of bracing unit i in y-direction
$c_o(z)$	Topography factor
c_f	Force coefficient
$c_{f,0}$	Force coefficient without free-end flow
$c_s c_d$	Structural factor accounting for dynamic effects
$c_r(z)$	Roughness factor
e	Eccentricity
f	Frequency
f_0	First natural frequency of a building
h	Height of the structure

h_{ref}	Reference height of 10 m
k_b	Bending factor dependent on load case
k_p	Peak factor
k_r	Terrain factor
k_s	Shear factor dependent on load case
l_i	Length of a shear wall for bracing member i
m	Mass
m_e	Equivalent mass
$n_{1,x}$	Fundamental frequency
q_b	Reference velocity pressure
$q_m(h)$	Mean velocity pressure at height h
$q_p(z)$	Peak wind pressure at height z
v	Up-crossing frequency
v_b	Reference wind velocity
$v_m(z)$	Mean wind speed at height z
$v_m(h)$	Mean wind speed at height h
v_{T_a}	Wind speed for given return period
x_t	Rotational center of building in x-direction
y_t	Rotational center of building in y-direction
y_C	Frequency factor
z	Height over ground surface
z_0	Roughness length
$z_{0,II}$	Reference height (0.05 m)
$z_{\max}$	Maximum height
$z_{\min}$	Minimum height
z_a	Reference height

Greek letters

δ_a	Aerodynamic damping
δ_s	Structural damping
ρ	Air density
$\sigma_{\ddot{x}}(z)$	Std. deviation of acceleration
$\phi_{1,x}(z)$	Mode shape function
ψ_λ	Reduction factor for end effects
ψ_r	Reduction factor for rounded edges
Φ_h	Reduction factor for height effects
Φ_b	Reduction factor for width effects
ν	Cross-up frequency

Contents

List of Figures

List of Tables

1

Introduction

This thesis focuses on timber buildings and investigates how a hybrid timber-concrete system can enable the construction of taller office buildings. The study focuses on wind loads and analyses dynamic oscillations to ensure structural safety and occupant comfort. This chapter provides an overview of the thesis by introducing the background and context of the study, followed by a description of the research problem. It describes the aims and objectives of the project, presents the scope and limitations, and briefly describes the methodology.

1.1 Background

Densification uses land more efficiently by increasing population density in urban areas (Smith & Coull, 1991). This approach helps preserve natural and agricultural spaces while reducing the need for urban sprawl. Concentrating resources improves infrastructure, such as public transport and utilities, leading to vibrant city centers with lower car reliance and reduced carbon emissions. High-rise buildings offer an effective solution to support urban densification.

Timber has gained popularity in high-rise construction due to its renewable properties and potential to reduce environmental impact. Compared to steel and concrete, timber has a significantly lower carbon footprint (Blaß & Sandhaas, 2017). As a renewable material capable of storing carbon dioxide (CO_2), it is central to efforts to reduce greenhouse gas emissions in the construction sector. Notable examples include Treet, the tallest pure timber residential building with 14 storeys, and Mjøstårnet, an 18-storey mixed-use timber building (Council on Tall Buildings and Urban Habitat, 2022).

While timber structures are environmentally advantageous, they face challenges at greater heights, particularly under dynamic loads (Smith & Coull, 1991). Timber's high strength-to-weight ratio results in lightweight structures prone to vibrations and sway, causing discomfort for occupants. Standard ISO 10137:2008 provides guidelines for acceptable movement, with stricter requirements for residential buildings than office spaces. This makes designing taller timber office buildings more feasible than residential buildings.

Hybrid solutions, combining timber with materials like concrete, address these challenges by increasing structural stiffness and weight. Adapting hybrid designs to high-rise office buildings introduces different challenges. The need for flexible, open floor plans in offices often conflict with structural requirements and the dynamic

behaviour caused by wind loads. Dynamic comfort remains a challenge, calling for creative solutions.

As urbanization and sustainability goals intensify, hybrid timber-concrete systems for high-rise office buildings emerge as a critical area for research and development.

1.2 Problem Description

Timber structures offer significant environmental benefits, but at greater heights, their low mass and stiffness pose challenges. These properties lead to increased wind-induced accelerations, potentially resulting in occupant discomfort.

Previous research by Dahlén and Niemi-Impola (2023) investigated how hybrid timber–concrete systems can be adapted to meet serviceability requirements related to wind-induced accelerations.

Alkhateb and Kallmér (2024) extended the analysis to include both Serviceability Limit State (SLS) and Ultimate Limit State (ULS) performance. While their study covered both residential and office buildings, the scope for office configurations was narrow, and the conclusions were mainly drawn from residential layouts. Their findings confirmed that wind-induced acceleration typically governed the design.

Office buildings, while subject to slightly less strict acceleration limits than residential ones, often require open floor plans, which reduce structural stiffness and increase susceptibility to dynamic effects. As a result, meeting both SLS and ULS criteria can be challenging.

There is currently a lack of standardized design approaches for hybrid high-rise office buildings, making it difficult to balance structural performance with environmental goals.

1.3 Aim and objectives

The aim of this thesis is to investigate how hybrid timber–concrete systems can be efficiently designed for high-rise office buildings. Through a parametric study, the influence of key parameters such as building height, concrete core thickness and layout, and the number and thickness of top storey concrete slab(s) is examined. The objective is to evaluate structural performance with respect to both SLS and ULS under dynamic wind loading, and to identify material-efficient configurations that meet comfort and strength requirements.

1.4 Research Questions

These questions aim to guide the study and explore important elements of hybrid structural systems in high-rise office buildings:

- How do different slab and core configurations (layout, thickness, placement) affect stiffness, acceleration, and the balance between SLS and ULS performance in hybrid timber-concrete office buildings?
- Which design factor ultimately limits building height— SLS or ULS?
- Which core and slab design configurations result in the most efficient use of concrete?

1.5 Method

The methodological approach of this thesis comprised the following steps:

Literature Review
A comprehensive review of standards, guidelines, and previous studies on the structural behaviour of high-rise timber buildings, with a particular focus on hybrid timber-concrete systems, was performed. Key parameters influencing structural performance, dynamic behaviour, and wind load resistance were identified. Insights into current practices and challenges were also gained through consultation with industry experts.

Analysis of Existing Structures
Existing high-rise office buildings that incorporate timber and hybrid structural systems were analysed. This review provided an understanding of current design practices, material selection, and structural configurations, forming a foundation for identifying critical parameters to be optimised in the parametric study.

Parametric Analysis
A structured parametric study was carried out to evaluate the influence of key design parameters—such as core thickness, core placement, and the number and thickness of concrete slabs—on the structural behaviour of the building. Eigenfrequencies were extracted using finite element modelling, and these values were used to manually calculate equivalent mass and wind-induced accelerations in accordance with ISO 10137:2008. The results were compared to comfort thresholds to assess SLS performance. The same structural models were also used to apply wind loads and evaluate ULS criteria.

Optimisation of Material Combinations
The timber–concrete material combinations were optimised for varying building heights. Different configurations were evaluated to achieve an efficient balance between structural strength, stiffness, and dynamic performance under wind loads.

Validation and Documentation
Simulation results were validated with hand calculations to ensure accuracy and reliability. All steps, methods, and results were thoroughly documented in the report

to ensure that the methodology is transparent and reproducible for others with sufficient technical background.

1.6 Limitations

The study is limited to a single building geometry, representative of a high-rise hybrid timber structure using a beam-column system with a concrete core. Two core configurations, one central and one dual-core layout are investigated. Wind loads are based on conditions in the Gothenburg region and are assessed using terrain category III, in accordance with Eurocode (EC) and the Swedish Annex, EKS 12. Seismic loads are not considered. Although torsional vibration modes are evaluated during the study, they are not treated explicitly in the design process. Instead, the analysis focuses on the first bending mode in the principal direction, which aligns with EC's wind action provisions, which do not account for torsional effects or contributions from higher vibration modes.

Vibration analysis and diaphragm action for the slabs were considered outside the scope of this study. Additionally, other SLS requirements such as deflection have not been addressed in the analysis.

1.7 Ethical, ecological and social aspects

The environmental footprint of the construction sector is substantial, with cement and steel production accounting for a significant share of global CO_2 emissions. In contrast, timber is a renewable and carbon-storing material, making it an attractive alternative for structural applications. By integrating engineered timber in high-rise buildings, it is possible to reduce CO_2 emissions while maintaining structural performance.

From a social perspective, high-rise buildings play an important role in enabling urban densification, which allows cities to grow without consuming additional land. Densification can reduce dependency on private vehicles, improve the efficiency of public transport and utilities, and help preserve green and agricultural areas outside urban zones. These effects contribute not only to lower per capita emissions, but also to more active, accessible, and walkable city centers.

This thesis investigates hybrid structural systems as a means to contribute to a more climate-conscious building sector. The work supports both national and international climate objectives, including Sweden's target of net-zero greenhouse gas emissions by 2045. From an ethical standpoint, contributing to lower emissions in one of the most resource-intensive industries is both a responsibility and an opportunity for engineers and planners.

2

Theory

This chapter begins with a brief overview of structural systems and materials commonly used in tall buildings, with a focus on hybrid solutions combining engineered timber and concrete elements. The chapter then outlines the theoretical framework for assessing wind effects and comfort criteria based on EC and ISO standards. It introduces key factors like topography, turbulence, and aerodynamic coefficients, and explains how they affect wind pressure and structural response. The section also includes how wind loads and comfort thresholds are calculated for use in structural analysis.

2.1 Timber

Timber is one of the oldest and most widely used building materials in the world, known for its low density and high strength-to-weight ratio. This section introduces the properties of wood, its challenges and limitations, and its applications in modern construction.

2.1.1 Properties of Timber

Mechanical Properties
Timber is an anisotropic material, meaning its mechanical properties vary depending on the direction of the load relative to the grain (Swedish Wood, 2022a). Timber shows high strength and stiffness parallel to the grain but significantly weaker properties perpendicular to the grain. Additionally, size effects impact the strength of timber: larger elements tend to have lower average strength due to the increased likelihood of defects like knots and cracks.

Environmental Influences on Structural Performance
Timber's long-term performance is influenced by sustained loading, temperature, and moisture. Creep can affect structural elements, especially under continuous load. Heat reduces strength, with degradation starting near 95 °C; temperatures above 65 °C should be avoided for durability. Moisture changes cause swelling or shrinkage, leading to cracks and strength loss around the fiber saturation point (27–33%).

2.1.2 Challenges and Limitations of Timber Structures

Despite its many advantages, wood as a building material faces certain challenges and limitations that affect its use, especially in tall and complex buildings.

Stiffness and Load-Bearing Capacity
Timber has a lower modulus of elasticity than steel and concrete, making it more flexible and prone to deformation, sway, and vibrations, especially in tall buildings exposed to wind loads (Swedish Wood, 2022a). It also has lower density and load-bearing capacity, requiring larger dimensions to achieve the same performance as steel and concrete, which can limit design possibilities. To address these challenges, reinforcements such as hybrid systems or damping solutions can be used to improve stability and strength.

Moisture and Biological Degradation
As a hygroscopic material[1], timber is largely affected by environmental humidity (Swedish Wood, 2022a). High moisture levels can lead to decay, swelling, and deformation, while dry conditions may cause shrinkage and cracking. These factors not only reduce the structural strength of wood but also shorten its lifespan.

Fire Resistance
Timber is a combustible material, which has been a challenge in the construction of tall buildings (Swedish Wood, 2022a). While timber develops a charred outer layer that slows combustion and temporarily preserves load-bearing capacity, it still requires additional protection to meet safety standards. To ensure structural integrity, fire design methods such as the reduced cross-section method in SS-EN 1995-1-1 help timber structures meet strict safety standards.

Metal fasteners in timber structures lose strength quickly in a fire, particularly unprotected steel-to-timber connections. Increasing timber thickness and edge distances can improve fire resistance. Additional protective measures, such as gypsum boards, stone wool, and fire-retardant treatments, enhance fire safety, while sprinkler systems can provide extra protection.

Strength at Joints and Connections
Connections concentrate stresses, making them the most vulnerable parts of a structure and the greatest risk for failure (Swedish Wood, 2016). As a natural material, wood has quality variations, such as knots, cracks, and grain direction, which can weaken joints. Brittle failures, such as cracking, occur particularly under loads perpendicular to the grain and when fasteners are poorly placed. Semi-rigid joints require precise calculations to ensure stability, as they often represent weak points in the structure.

[1] A hygroscopic material absorbs and retains moisture from the surrounding air, often leading to changes in its physical properties such as expansion or contraction.

Acoustics
Due to its low density, timber has lower damping properties for sound waves compared to heavier materials like concrete. This can cause certain sounds, particularly low-frequency noises like footsteps, to propagate more easily through the structure, leading to disturbances (Swedish Wood, 2022a). Techniques such as sound-insulating floor systems, acoustic membranes, and floating floors[2] are often employed to minimize these issues.

2.1.3 Timber Products

To meet the demands of building standards for timber construction, a range of timber products is used. This thesis specifically focuses on Cross-Laminated Timber (CLT) and glulam, as these are the primary materials used in the structural analysis.

Engineered Wood Products
Engineered wood products are created by combining multiple layers of wood, wood chips, or veneer with adhesives and compression (Swedish Wood, 2022a). These products are designed to overcome the natural limitations of solid wood, such as defects and variable properties, and provide improved strength, stiffness, and durability.

Cross-Laminated Timber (CLT):
CLT is a solid timber panel made by gluing together several layers of boards, where each layer is perpendicular to the previous layer, see Figure 2.1. This layout gives the panel strength and stiffness in both directions. CLT usually has 3, 5, or 7 layers, with each layer about 20–45 mm thick. The total thickness starts around 60 mm and can go up to 500 mm. Panels can be up to 3 meters wide and 24 meters long, depending on the manufacturer. CLT panels are often made in the factory with high precision, including cut-outs for windows, doors, and spaces for electrical systems. CLT panels are labeled by layups like 3s-120 or 5s-200, where the first number indicates the number of layers and the second shows the total thickness in millimeters. These labels give a quick idea of panel structure, but strength values vary depending on the manufacturer.

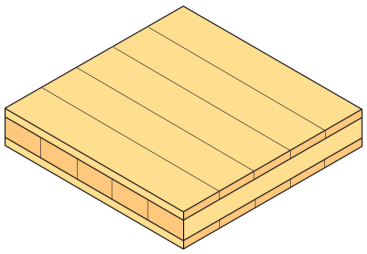

Figure 2.1: CLT panel with three layers (Swedish Wood, 2022a)

[2]Floating floors are floors that rest on a cushioning layer without being fixed to the subfloor with screws, nails, or glue, reducing impact noise and vibrations.

Glulam Timber:
Glulam is manufactured by gluing together several layers of sawn timber with their grain aligned in the same direction. These laminations are typically 18–45 mm thick and can be joined using finger joints to achieve longer lengths. Layers are often up to 215 mm wide, and wider beams can be produced by bonding multiple glulam units side by side. Beams can be straight or curved depending on design needs.

Glulam production is highly automated, involving drying the boards to a uniform moisture content (typically between 6–15%), grading for strength, finger-jointing, gluing, pressing, and finishing. The final product may also be waxed to improve moisture resistance.

Glulam beams can be made either as uniform (homogeneous) sections or as combined sections, where stronger boards are placed on the outside to handle higher tensile and compressive stresses, see Figure 2.2 a. Homogeneous sections are labeled as GLxxh, and combined ones as GLxxc, where "xx" represents the characteristic bending strength in MPa (e.g., 30 for 30 MPa). Glulam's main benefit over solid timber is its more predictable performance, thanks to the even distribution of natural defects like knots. In practice, its average strength may not be much higher than solid timber, but its consistency is superior, see Figure 2.2 b.

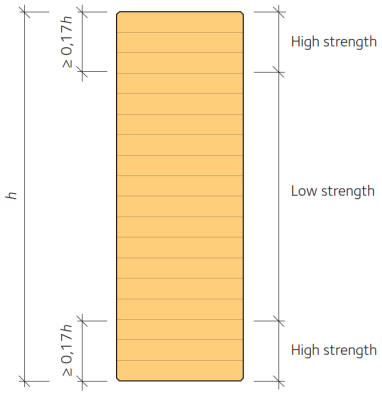

(a) The lay-up for a combined glulam beam

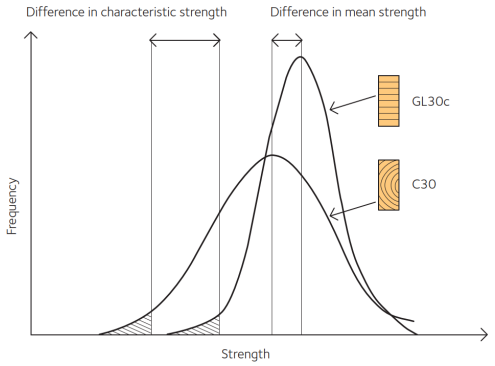

(b) Distribution function for the strength of glulam beams and structural timber

Figure 2.2: Comparison of glulam and its strength .

2.1.4 Environmental and Sustainability Aspects

Timber is essential for reducing environmental impact by storing CO_2. Trees naturally sequester 1.8 tonnes of CO_2 per dry tonne of timber. Sustainable forestry practices, such as selective harvesting and replanting, enhance carbon absorption during peak growth years (10–30 years for softwood) (Timber NSW, 2023).

In construction, timber serves as a long-term carbon reservoir, where a single timber-framed house storing 7.5 tonnes CO_2 of carbon, compared to steel-framed houses, which emit 2.9 tonnes of CO_2 (Timber NSW, 2023). Reusing and recycling timber further extends its storage capacity, while wood waste can be repurposed as bioenergy (International Timber, 2023). Producing timber is energy-efficient, requiring only about 5% of the energy needed for steel production (Mortlock Timber Group, 2023).

Adopting circular construction practices, such as disassembly and reuse, significantly enhances timber's sustainability by reducing waste and minimizing environmental impact (Research Institutes of Sweden (RISE), 2023). When timber residues and old construction timber can't be reused for building, they can be used to produce renewable energy. This helps avoid waste and shows how timber supports a sustainable economy while reducing environmental impact (Mortlock Timber Group, 2023).

2.2 Concrete

Concrete is a widely used construction material known for its compressive strength. It is made from three primary components: cement, aggregates, and water. Cement binds the mixture, while aggregates like sand, gravel, or crushed stone add bulk and strength (Al-Emrani et al., 2013). Water activates the cement and hardens the mixture. Additional additives or admixtures can be included to enhance properties like workability, durability, or chemical resistance. Concrete can be shaped into almost any form, making it suitable for many different structural and design purposes.

2.2.1 Properties of Concrete

Concrete has high compressive strength, making it ideal for supporting heavy loads. However, its low tensile strength requires reinforcement in many applications h(Al-Emrani et al., 2013). Its durability allows it to resist weathering, water, and chemical exposure, ensuring long service life in demanding conditions.

To address its tensile weakness, concrete is often reinforced with steel bars to handle tensile stresses and to enhance structural strength (Al-Emrani et al., 2013). Prestressing further improves performance by tensioning high-strength steel tendons before or after pouring, enabling longer spans, thinner sections, reducing cracking, and ensuring efficient material use.

2.2.2 Environmental and Sustainability Aspects

While concrete is known for its durability and versatility, its production poses significant environmental impact due to the energy-intensive cement production, which contributes 7–8% of global CO_2 emissions (Andrew, 2019). Timber, by comparison, has up to 75% lower emissions, as it stores CO_2 during growth and emits very little during processing (Blaß & Sandhaas, 2017). Concrete also stores CO_2 over time through carbonation. Reusing concrete directly in its original structural form (like beams or columns) is more complex and less common due to difficulties in ensuring its strength and integrity. Concrete can, however, be recycled by crushing old concrete and repurposing it for road bases, pavements, or as a substitute for natural aggregates in new mixes.

2.3 Structural System

The structural system of a building plays a critical role in ensuring the stability and functionality. This chapter presents the most common structural systems used to handle both vertical and horizontal loads in high-rise buildings. The focus is on systems utilized in timber and hybrid constructions.

2.3.1 Column-Beam System

The column-beam system is a common solution where columns carry vertical loads while beams support horizontal forces and transfer the loads to the columns. In timber buildings, these elements are often made of glulam or CLT as illustrated in Figure 2.3.

- **Advantages:** Flexibility in floor plans and simplicity in construction.
- **Limitations:** Limited resistance to lateral loads unless stabilizing units are used.

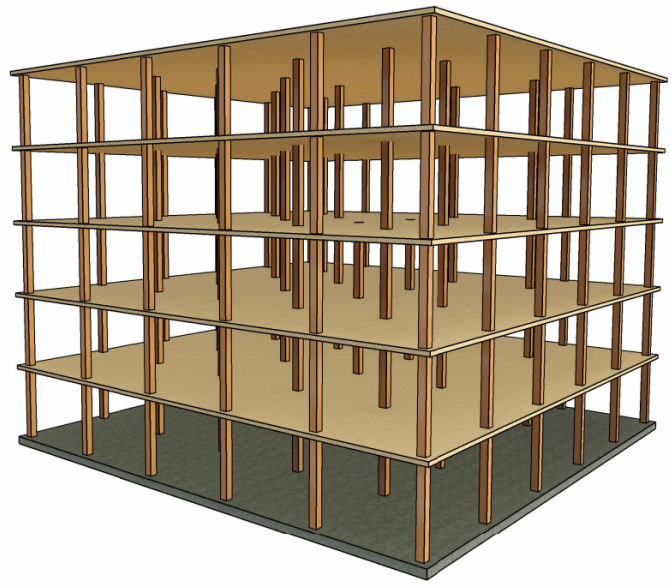

Figure 2.3: Illustration of a column-beam system, commonly used for its flexibility in design.

2.3.2 Load Bearing Walls

Load-bearing walls support both vertical and horizontal loads. In tall buildings, they reduce sway, enhance rigidity, and can serve as fire compartments as shown in Figure 2.4.

- **Advantages:** Strong lateral load resistance, high overall structural stiffness
- **Limitations:** Less flexibility in floor plans compared to column-beam systems as walls define fixed layouts and cannot be repurposed.

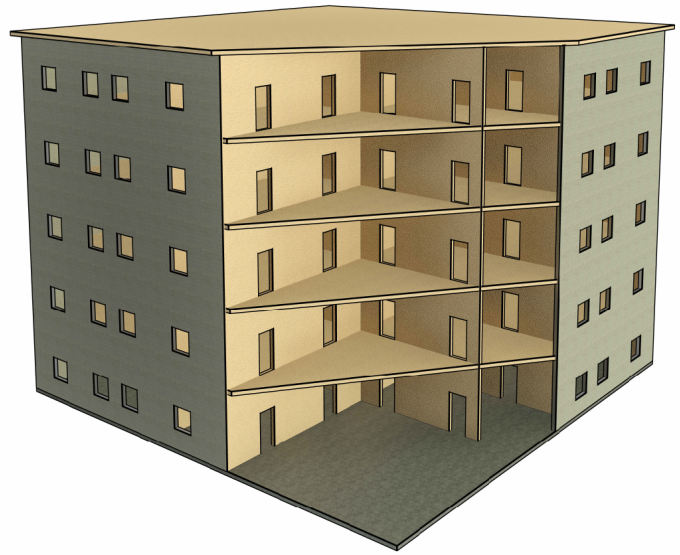

Figure 2.4: Illustration of load-bearing wall systems, efficient and resistant against lateral forces.

2.3.3 Core System

A core system involves the use of a central element to provide stability against lateral loads and torsion. The core is typically made of CLT panels or concrete for staircases and elevators as shown in Figure 2.5.

- **Advantages:** High stability, particularly in tall buildings.
- **Limitations:** Requires careful integration with other systems to avoid inefficient material usage.

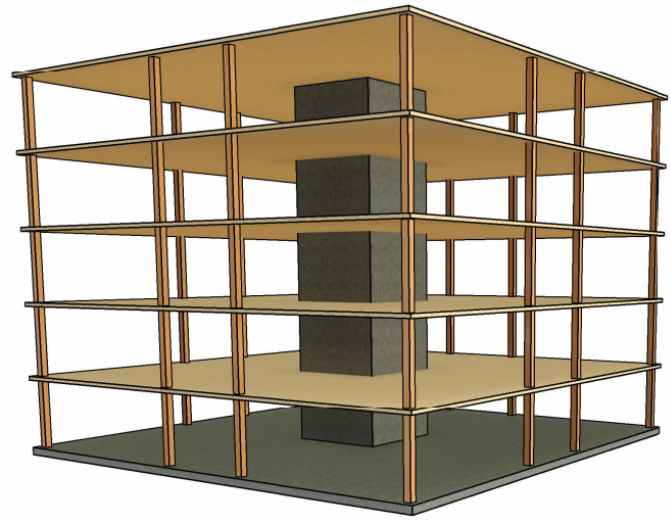

Figure 2.5: Core system providing stability against lateral loads and torsion

2.3.4 Hybrid Solutions

Hybrid structures can be designed in various ways to optimise both strength and dynamic performance. The choice of configuration depends on factors such as building height, load distribution, and construction purpose. Common strategies include:

- **Concrete cores with timber floors (Figure 2.6a):** Provides high lateral stiffness while keeping the structure lightweight.
- **Timber structures on concrete base (Figure 2.6b):** Lower concrete floors provide a solid base for structural integrity and enhanced resistance to uplift forces.
- **Different slabs (Figure 2.6c-d):** Combining CLT with concrete layers to enhance mass and stiffness, improving vibration performance.

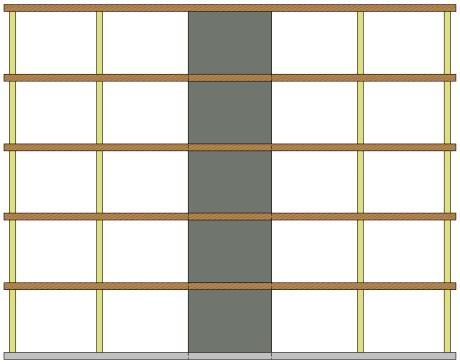

(a) Column-beam system in timber with CLT slabs and a concrete core

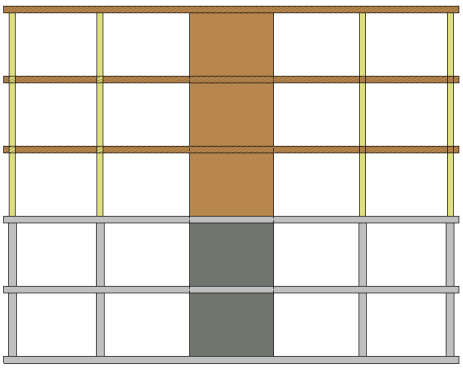

(b) A pure timber structure on top of a concrete structure

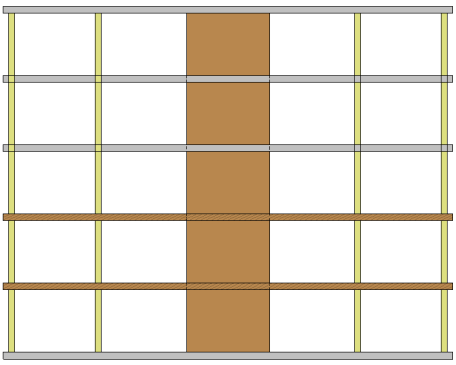

(c) Column-beam system in timber with a CLT core with top slabs in concrete

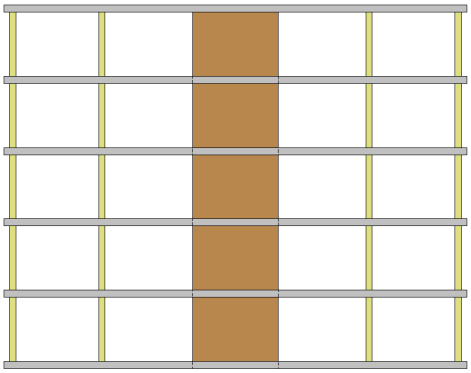

(d) Column-beam system in timber with a CLT core with concrete slabs

Figure 2.6: Hybrid systems combining timber and concrete in different ways to improve performance in buildings.

2.3.5 Horizontal Stability

To resist lateral forces, structures rely on bracing systems that distribute loads and prevent excessive deformation. Stability can be ensured through diagonal bracing, shear walls, or rigid frames.

Diagonal Bracing
Diagonal bracing utilizes inclined members, often of timber or steel. The diagonal bracing is arranged in a triangular pattern within the structural frame to efficiently transfer horizontal loads to the foundation through truss action, see Figure 2.7a. The design of diagonal bracing varies according to load requirements and may include X-bracing, K-bracing, or single diagonal configurations.

Shear Walls
Shear walls resist lateral forces through in-plane shear strength and are typically made of CLT or reinforced concrete, providing rigidity and stability in structures where diagonal bracing is not sufficient, see Figure 2.7b.

Rigid Frame Bracing
Rigid frame bracing uses moment-resisting connections at beam-column joints to create a stable frame without additional bracing elements, see Figure 2.7c. However, making these connections in timber is difficult due to the material's limited strength at joints. While effective for open spaces like warehouses, its use in tall buildings is impractical due to limited capacity.

Horizontal Diaphragms
Floors and roofs keep buildings stable by distributing sideways forces to walls and other supports. They are often made of plywood, CLT, or concrete floors and are attached to beams and walls for load transfer. In multi-storey buildings, they help prevent parts from shifting independently and work with walls and bracing to maintain stability.

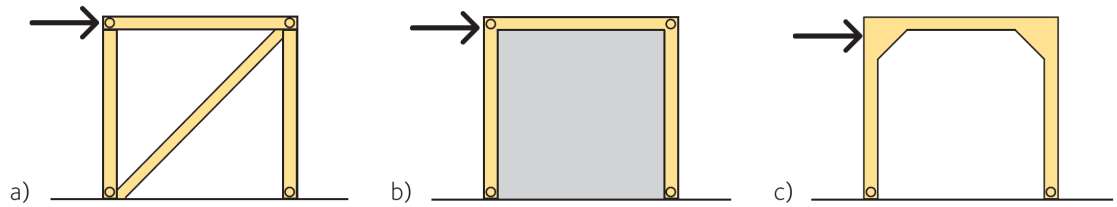

Figure 2.7: a) Diagonal bracing, b) shear wall, c) rigid joints. (Swedish Wood, 2022a)

2.3.6 Structural Response to Lateral Loads

When lateral forces act on a building, the structural response can be categorized into translational deformation and rotational deformation (Engström, 1999). If the center of lateral loads aligns with the rotational center, only translational deformation occurs. However, if misalignment exists, both translational and rotational deformations will act simultaneously. The rotational center is determined by the stiffness and placement of the bracing system and can be calculated using the following equation:

$$x_t = \frac{\sum(a_i S_{yi})}{\sum S_{yi}}, \quad y_t = \frac{\sum(b_i S_{xi})}{\sum S_{xi}} \tag{2.1}$$

- S_{xi} and S_{yi} are the stiffness of the bracing members in the x- and y-directions, respectively,
- a_i and b_i define the position of the bracing members.

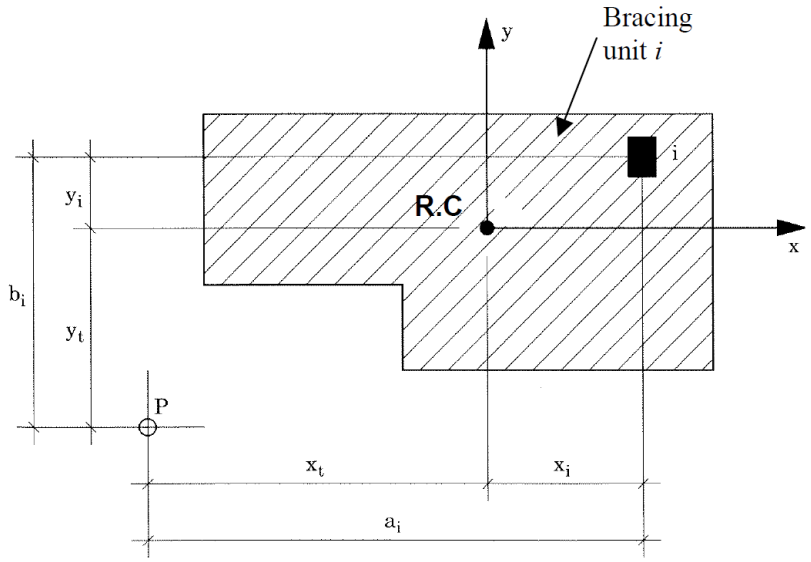

Figure 2.8: Coordinates of rotation centre and bracing units, from Engström, 1999.

The lateral loads distributed to each bracing element due to translation are given by:

$$H_{xi} = H_x \frac{S_{xi}}{\sum S_{xi}}, \quad H_{yi} = H_y \frac{S_{yi}}{\sum S_{yi}} \tag{2.2}$$

Torsional Effects
If the resultant lateral load does not act through the rotational center, an additional *torsional moment* is introduced, calculated as:

$$T = H \cdot e \tag{2.3}$$

- H is the total lateral force,
- e is the eccentricity, which represents the distance between the resultant force and the rotational center.

The lateral loads distributed to each bracing element due to *torsional moment* are given by:

$$H_{i,C} = T\frac{S_i r_i}{\sum(S_i r_i^2)} = T\frac{S_i r_i}{S_T} \tag{2.4}$$

- S_T is the global torsional stiffness,
- r_i is the radial distance from the rotation center.

The **global torsional stiffness** is determined using:

$$S_T = \sum(S_i \cdot r_i^2) = \sum(S_{xi} \cdot y_i^2) + \sum(S_{yi} \cdot x_i^2) \tag{2.5}$$

The contribution depending on both translation and rotation is:

$$H_{xi} = H_x\frac{S_{xi}}{\sum S_{xi}} + T\frac{S_{xi} \cdot y_i}{S_T}, \quad H_{yi} = H_y\frac{S_{yi}}{\sum S_{yi}} + T\frac{S_{yi} \cdot x_i}{S_T} \tag{2.6}$$

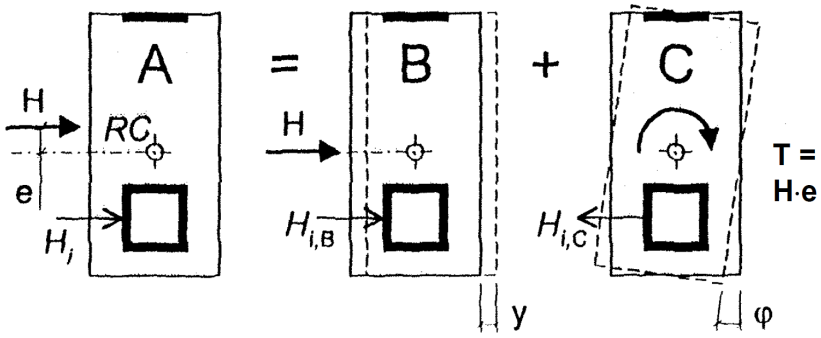

Figure 2.9: Load case A with resultant acting besides the rotation center can be divided in two load cases, B with pure translation and C with pure rotation, from Engström, 1999.

Bracing Systems and Stiffness Considerations
The overall lateral stiffness of the structure is determined by combining the shear stiffness and bending stiffness of the bracing elements (Engström, 1999). The total stiffness of a bracing wall is calculated as:

$$\frac{1}{S_i} = \frac{1}{S_{si}} + \frac{1}{S_{bi}} \tag{2.7}$$

Where:

- S_{si} is the shear stiffness,
- S_{bi} is the bending stiffness.

For a shear wall [3], these stiffness components are defined as:

$$S_{si} = k_s \frac{E_i A_i}{l_i}, \quad S_{bi} = k_b \frac{E_i I_i}{l_i^3} \tag{2.8}$$

Where:

- k_s and k_b are load case-dependent factors,
- E_i is the modulus of elasticity,
- A_i is the cross-sectional area,
- I_i is the moment of inertia,
- l_i is the wall length.

[3]Note that for truss structures, bracing stiffness is complex to determine analytically, as it depends on connections, load distribution, and geometry. Therefore, FEM-analysis is typically required for accurate evaluation.

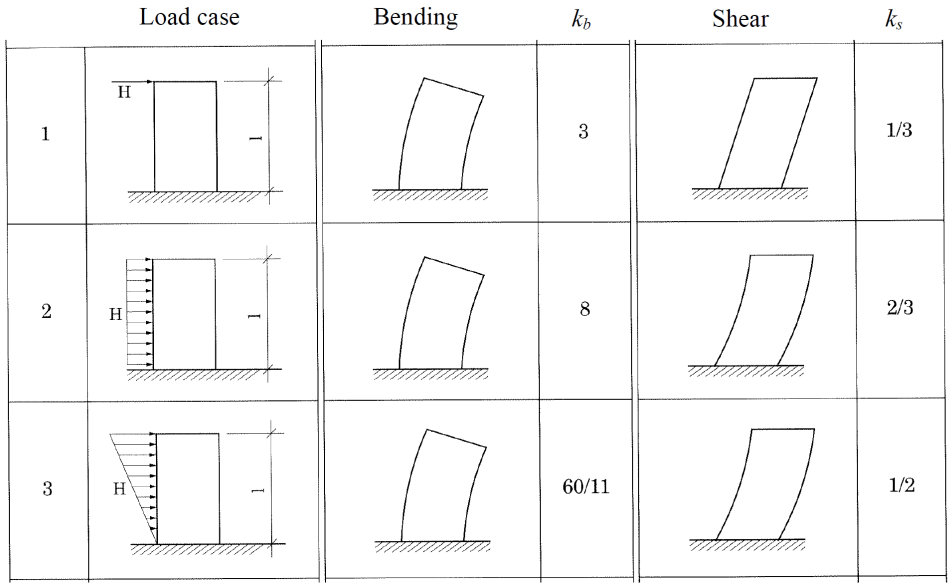

Figure 2.10: Stiffness coefficients for various load cases on shear walls (Engström, 1999).

2.4 Wind Dynamics

The interaction between wind and buildings is influenced by turbulence, wind speed variations, and terrain characteristics. Understanding these factors is essential for designing and stabilizing tall buildings, especially timber structures.

2.4.1 Wind Characteristics

Turbulence and its Impact on Buildings
Turbulence arises when wind flows break into a complex pattern of vortices and fluctuations in wind speed and direction (Mendis et al., 2007). These variations can cause uneven loading on buildings, leading to dynamic effects such as vibrations and oscillations. Turbulence levels depend on factors such as terrain roughness, the shape and height of the building, and atmospheric conditions.

In the lower layers of the atmosphere, where wind interacts with the ground surface and buildings, turbulence is more pronounced. This is because airflows are affected by obstacles like trees, houses, and structures, creating localized variations in wind speed and pressure. In higher layers, above the so-called boundary layer height, turbulence decreases, and the wind becomes more stable and uniform.

Difference Between Mean Wind and Gusty Wind Wind can be divided into two main components: mean wind and gusty wind (Mendis et al., 2007).

- **Mean wind** refers to the average wind speed over a specific time period, often measured over 10 minutes or longer. This stable component of wind is used in design standards and calculations for structural stability.
- **Gusty wind** represents short-term, sudden variations in wind speed caused by turbulence. Gusty winds can generate increased loads on buildings and result in short-term, intense forces that must be considered in the design.

Mean wind tends to increase with height, while the gustiness tends to decrease. Gusty winds can cause vibrations, which occupants of the building may perceive as uncomfortable, making SLS a critical design parameter.

Terrain Influence on Wind Speed and Gradient Height

Terrain characteristics significantly influence wind speed and its variation with height. This variation is often described using the logarithmic wind profile, which models how wind velocity increases with height due to reduced surface friction. The profile follows the equation:

$$v_2 = v_1 \frac{\ln(h_2/z_0)}{\ln(h_1/z_0)} \tag{2.9}$$

where:

- v_1 is the wind speed at reference height h_1,
- v_2 is the wind speed at height h_2,
- z_0 is the roughness length, which depends on terrain type.

According to EC, terrain is classified into five roughness categories, ranging from open sea (with low roughness) to dense urban areas (with high roughness). This classification influences wind speed distribution, with higher roughness leading to a slower increase in wind speed with height. The gradient height is the altitude at which wind reaches its full speed is shown in Figure 2.11

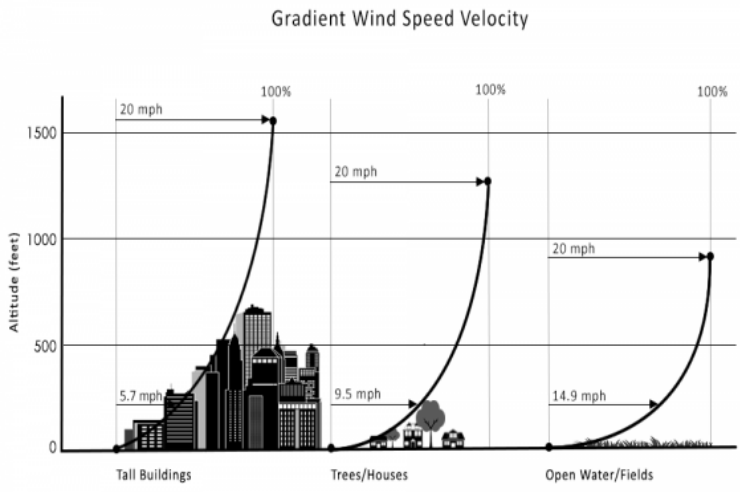

Figure 2.11: The gradient height is shown in relation to terrain types and wind speed.

2.4.2 Wind Effects on Buildings

Different wind phenomena affecting tall buildings include buffeting, vortex shedding, galloping, and flutter. These dynamic effects can influence both structural stability and occupant comfort.

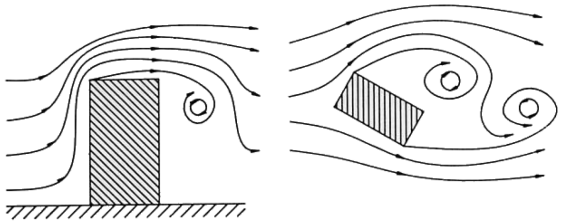

Figure 2.12: Illustration of eddies.

Buffeting
Buffeting occurs when turbulent wind causes uneven and random variations in the load acting on the building (Mendis et al., 2007). These loads are generated by large vortices in the wind that interact with the building's surfaces. Buffeting often results in vibrations and deformations that are frequent and irregular. This phenomenon is most pronounced in the wind direction but can also cause effects in the cross-wind direction.

Vortex Shedding
Vortex shedding is a phenomenon where the wind creates regular vortices as it flows around the building (Mendis et al., 2007). These vortices generate alternating pressure forces that can cause transverse oscillations in the building, particularly if the frequency of the vortices matches the building's natural frequency. This resonance phenomenon can lead to significant movements and potential damage if not properly managed. To minimize the effects of vortex shedding, design solutions such as aerodynamic modifications to break up the vortices and damping systems can be implemented.

Galloping and Flutter
Galloping and flutter are two forms of instability that can occur in structures, although they are less common in buildings and more often observed in slender structures such as towers or bridges.

- **Galloping** occurs when wind-induced forces amplify the building's movements, leading to increasing oscillations. This phenomenon is more common in flexible structures with an asymmetric shape.
- **Flutter** is a combined bending and torsional instability that can occur at high wind speeds. Flutter is particularly dangerous as it can lead to sudden and catastrophic failure if left uncontrolled.

2.4.3 Simulations & Wind Tunnel Tests

Wind tunnel testing has proven to be an invaluable tool for accurately assessing wind effects on tall buildings, especially when simplified code provisions fall short (Mendis et al., 2007) [4]. The process involves placing a scaled model of a building in a boundary-layer wind tunnel, where controlled wind conditions simulate real-world airflow, see Figure 2.13. This allows engineers to measure dynamic loads, identify wind-induced vibrations, and optimise structural design.

Computational Fluid Dynamic (CFD) simulations offer an advanced method for predicting wind effects on tall buildings, complementing traditional wind tunnel tests. CFD allows for early-stage analysis of aerodynamic phenomena such as turbulence and crosswind forces. While effective, CFD results should be validated against experimental data to ensure reliability. This approach enables designers to optimise the structural response and mitigate wind-induced vibrations in structures.

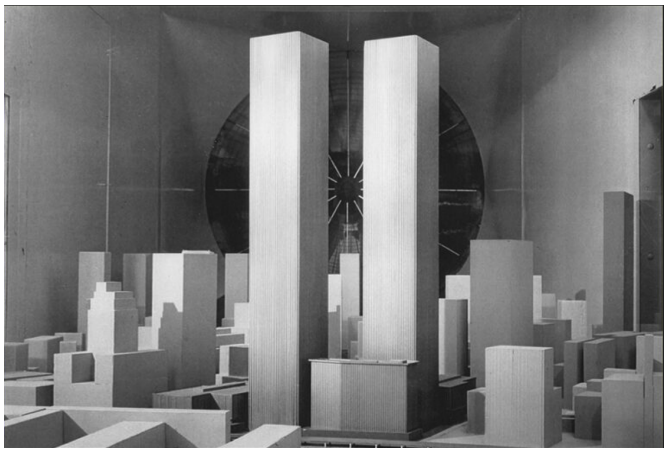

Figure 2.13: Historical image of the wind tunnel test of the Twin Towers.

2.4.4 Human Perception and Comfort Considerations

Building motion due to wind loads can significantly impact occupant comfort. Several psychological and physiological factors influence how individuals perceive and tolerate movement, including age, gender, body orientation, and activity level (Sæmundsson, 2007). Saemundsson highlights that excessive building sway can cause dizziness, motion sickness, and, in severe cases, vertigo, leading to potential issues for long-term occupancy.

No universal standard exists for comfort criteria in tall buildings, but Smith and Coull, 1991 present a framework for assessing human sensitivity to motion and

[4] According to EKS 12, wind tunnel tests or CFD simulations should be used to determine the impact of large nearby buildings on the design wind loads.

vibration in tall buildings, within the low-frequency range of 0-1 Hz, Table 2.1. This research provides insights into human sensitivity to building movement, focusing on acceleration thresholds that influence discomfort levels. The study determines the conditions under which occupants may experience mild discomfort, challenges in performing tasks, or even loss of balance, reinforcing the importance of serviceability criteria in structural design.

Table 2.1: Human perception levels. Peak acceleration, 5 year return wind (0-1 Hz)

LEVEL	**ACCELERATION** $(\mathbf{m/s^2})$	**EFFECT**
1	< 0.05	Humans cannot perceive motion.
2	0.05 - 0.1	Sensitive people can perceive motion. Hanging objects may move slightly.
3	0.1 - 0.25	Majority of people will perceive motion. Level of motion may affect desk work. Long-term exposure may produce motion sickness.
4	0.25 - 0.4	Desk work becomes difficult or almost impossible. Ambulation still possible.
5	0.4 - 0.5	People strongly perceive motion. Difficult to walk naturally. Standing people may lose balance.
6	0.5 - 0.6	Most people cannot tolerate motion and are unable to walk naturally.
7	0.6 - 0.7	People cannot walk or tolerate motion.
8	> 0.85	Objects begin to fall and people may be injured.

2.5 Natural Frequencies of Structural Systems

This chapter provides the main analytical formulas and parameters for estimating the natural vibration frequencies of structures, along with a summary of numerical modal analysis using the finite element method (FEM). The focus is on how material properties, geometry, boundary conditions, and cross-sectional shape affect structural frequencies in practice. Simple, established formulas are presented for bending and torsional modes, with notes on when different beam theories are applicable.

2.5.1 Fundamentals of Natural Frequencies

A structure's natural frequencies are the rates at which it vibrates freely after a small disturbance. These frequencies depend on the distribution of mass and stiffness, and each vibration mode has its own natural frequency. Resonance can occur if external loads coincide with these frequencies, potentially causing large oscillations. Predicting natural frequencies is therefore important to ensure structural safety and avoid resonance problems. Several classical beam theories provide practical formulas for estimating these frequencies under different assumptions:

- **Euler–Bernoulli beam theory:** Assumes deflection is due only to bending, with plane cross-sections remaining perpendicular to the neutral axis (no shear deformation or rotary inertia). Suitable for slender beams where shear effects are negligible, but tends to overestimate frequencies for short or deep members.

- **Timoshenko beam theory:** Accounts for both shear deformation and rotary inertia, making it more accurate for short or deep beams. The theory captures lower frequencies than Euler–Bernoulli for such cases, but leads to more complex equations that usually require numerical or FE solutions. Timoshenko beam elements are standard in most FE software.

- **Saint–Venant torsion theory:** Describes torsional vibrations by assuming uniform twist and neglecting warping. Appropriate for solid or closed sections subjected mainly to torsion. Provides direct formulas for torsional natural frequencies using the cross-section's torsional rigidity.

In modern FE software, the appropriate beam or shell theory is selected automatically based on the chosen element type. For example, most beam elements are based on Timoshenko theory to account for both bending and shear effects, while torsional modes are typically captured using Saint–Venant's theory for closed or solid sections. However, real structures often exhibit coupled bending and torsion, and torsional modes may involve significant cross-sectional warping especially in open or thin-walled sections. In such cases, more advanced formulations, such as Vlasov beam theory, are required to accurately capture warping effects and the interaction between torsion and bending. FE analysis allows these complexities to be included as needed, providing reliable frequency predictions even for cases where pure analytical formulas are insufficient.

2.5.2 Bending Modes: Euler–Bernoulli Beam Theory

Under the Euler–Bernoulli assumptions, the natural frequencies of a uniform beam in bending can be estimated using a simple analytical formula. The nth bending mode frequency is given by

$$f_{EB,n} = \frac{\beta_n^2}{2\pi L^2}\sqrt{\frac{EI}{\rho A}} \tag{2.10}$$

Parameters:

- E: Young's modulus (Pa)
- ρ: Material density (kg/m^3)
- A: Cross-sectional area (m^2)
- I: Second moment of area (m^4)
- L: Beam length (m)
- β_n: Dimensionless wavenumber (depends on support conditions and mode number)

The values of β_n are determined by the boundary conditions of the beam and are obtained by solving the corresponding characteristic equation. Table 2.2 lists the most common support conditions together with the equations for β_n and the first few roots.

Table 2.2: Boundary conditions and $\beta_n L$ roots for Euler–Bernoulli bending modes

End Conditions	**Characteristic Equation**	**First roots $\beta_n L$**
Fixed–Free	$\cosh(\beta L)\cos(\beta L) + 1 = 0$	1.87, 4.69, 7.85
Fixed–Fixed	$\sin(\beta L) = 0$	$n\pi,\ n = 1, 2, \ldots$
Pinned–Pinned	$\sin(\beta L) = 0$	$n\pi,\ n = 1, 2, \ldots$
Fixed–Pinned	$\cosh(\beta L)\sin(\beta L) - \sinh(\beta L)\cos(\beta L) = 0$	3.93, 7.07, 10.21

2.5.3 Bending Modes: Timoshenko Beam Theory

Timoshenko beam theory extends Euler–Bernoulli by including both shear deformation and rotary inertia. This makes it more accurate for short or deep beams, or when shear effects are significant. The theory introduces a shear correction factor κ (typically $\kappa = 5/6$ for rectangular sections) to account for non-uniform shear distribution across the section.

The nth Timoshenko bending frequency is given by

$$f_{T,n} = \frac{\beta_n^2}{2\pi L^2}\sqrt{\frac{EI}{\rho A(1+\phi_n)}} \tag{2.11}$$

where

$$\phi_n = \frac{\beta_n^2 EI}{\kappa GAL^2} \tag{2.12}$$

Additional parameters:

- G: Shear modulus (Pa)
- κ: Shear correction factor (typically 5/6 for rectangular sections)
- ϕ_n: Shear parameter (depends on geometry and stiffness)

The β_n values for Timoshenko beams generally require numerical calculation, as the governing equations are transcendental. In a finite-element solution, the β_n values are implicitly obtained from the eigenvalue problem, rather than explicitly calculated. In practice, these frequencies are typically computed using FE software or numerical routines. In this work, a Timoshenko beam model with $\kappa = 5/6$ was used for comparison with analytical results.

2.5.4 Torsional Modes: Saint–Venant Theory

Saint–Venant's theory describes the natural frequencies for torsional (twisting) vibration of prismatic members, assuming uniform twist and neglecting warping. This approach is accurate for solid or closed sections.

The nth torsional frequency is given by

$$f_{\mathrm{SV},n} = \frac{\alpha_n}{2\pi L}\sqrt{\frac{GJ_t}{\rho I_p}} \tag{2.13}$$

Additional parameters:

- J_t: Torsional constant (m^4)
- I_p: Polar mass moment of inertia per unit length (kg·m)
- α_n: Dimensionless frequency factor (depends on support conditions)

The values of α_n are determined by the boundary conditions of the member. Table 2.3 lists characteristic root conditions and the first few values for standard support types.

Table 2.3: Boundary conditions and $\alpha_n L$ roots for torsional modes

End Conditions	**Root Condition**	**First roots $\alpha_n L$**
Fixed–Free	$\alpha L = (2n-1)\frac{\pi}{2}$	1.571, 4.712, 7.854
Fixed–Fixed	$\alpha L = n\pi$	3.142, 6.283, 9.425
Free–Free	$\alpha L = n\pi$	3.142, 6.283, 9.425
Pinned–Pinned	$\alpha L = n\pi$	3.142, 6.283, 9.425

With the appropriate value of α_n, the above formula provides a direct estimate of the torsional frequencies for typical shaft or beam configurations.

2.5.5 Numerical Modal Analysis (FEM)

Numerical modal analysis using the finite element method (FEM) provides a flexible framework for determining natural frequencies and mode shapes in structural systems where analytical solutions may be impractical. In the context of beam dynamics, the Timoshenko beam theory is commonly implemented, capturing both shear deformation and rotary inertia effects.

The beam is discretized into finite elements, each characterized by nodal degrees of freedom: typically, transverse displacement and rotation. For each element, stiffness and mass matrices are formulated based on material and geometric properties. The shear correction factor, κ, accounts for the non-uniform distribution of shear stresses (with $\kappa = 5/6$ for rectangular sections), and rotary inertia is included for accuracy in higher modes.

After assembly, the global stiffness (K) and mass (M) matrices define the discretized dynamic system. Appropriate boundary conditions are applied by constraining selected nodal degrees of freedom according to the support configuration (e.g., fixed base for cantilever beams).

The eigenfrequencies and mode shapes are then found by solving the generalized eigenvalue problem,

$$(K - \omega^2 M)\varphi = 0,$$

where the eigenvalues ω_n yield the natural frequencies, $f_n = \omega_n/2\pi$, and the eigenvectors φ_n correspond to the mode shapes. Both lumped and consistent mass matrix formulations are possible; for lower modes, the choice typically has little effect on the results.

This numerical approach can be readily extended to more complex geometries, boundary conditions, or non-uniform beams, offering a powerful complement to analytical theory.

2.6 Design Standards

The Eurocodes are a set of European design standards used in the construction industry to ensure safe structures. Since 2011, the ECs have been a regulatory requirement in Sweden (Swedish Standard, 2025). SS-EN 1991-1-4 provides wind load guidelines for buildings and bridges up to 200 meters, considering their fundamental vibration mode. It does not apply to specific structures such as cable-supported bridges, guyed masts, braced masts and braced chimneys.

For timber structures, these regulations are primarily governed by SS-EN 1991 (actions on structures) and SS-EN 1995 (design of timber structures), and for concrete structures, SS-EN 1992 (design of concrete structures) applies. These provide methods for calculating loads, structural capacity, and stability. In Sweden, the ECs are supplemented by Boverket's Construction Regulations, EKS 12, which adapt and refine the European standards to Swedish conditions. EKS 12 includes national application rules and safety factors that account for climate, material properties, and local construction practices.

2.6.1 Wind Pressure

Wind pressure consists of external and internal pressure. Only external wind pressure affects global structural stability and behaviour. Internal pressure is regarded as a localized effect and is primarily taken into account when designing individual components. The external wind pressure is calculated considering shape factors, dynamic behaviour of the building, and velocity pressure.

External wind pressure F_w on buildings
According to SS-EN 1991-1-4:2005, the external wind pressure is calculated using the following expression:

$$F_w = c_s c_d \cdot c_f \cdot q_p(z) \tag{2.14}$$

Structural Factor $c_s c_d$
The structural factor $c_s c_d$ accounts for both shape-related and dynamic effects of wind on a structure, modifying the wind pressure to reflect the structure's response to turbulence and aerodynamic loading.

$$c_s c_d = \frac{1 + 2 \cdot k_p \cdot I_v(z_s)\sqrt{B^2 + R^2}}{1 + 6 \cdot I_v(z_s)} \tag{2.15}$$

The structural factor $c_s c_d$ is set to 1 for:

- Buildings with a height of less than 15 m.

- Façade and roof elements with a natural frequency greater than 5 Hz.
- Framed buildings with structural walls that are less than 100 m high and have a height to depth (in wind direction) ratio less than 4.

Peak Factor k_p
The peak factor k_p quantifies turbulence intensity.

$$k_p = \begin{cases} \sqrt{2\ln(\nu T)} + \frac{0.6}{\sqrt{2\ln(\nu T)}}, & \text{for dynamically sensitive structures} \\ 3.0, & \text{for static structures} \end{cases} \tag{2.16}$$

Where T is the return period for wind load (600 seconds).

Cross-up frequency ν
The cross-up frequency ν defines the transition between background turbulence effects and resonant vibrations based on the structure's dynamics.

$$\nu = n_{1,x} \cdot \frac{R}{\sqrt{B^2 + R^2}} \tag{2.17}$$

Where $n_{1,x}$ is the natural frequency in the first mode.

Response factors B^2 & R^2
The background response factor B^2 represents low-frequency turbulence, while the resonance response factor R^2 describes dynamic amplification that occurs when wind turbulence coincides with the structure's natural frequency.

$$B^2 = \exp\left[-0.05\left(\frac{h}{h_{\text{ref}}}\right) + \left(1 - \frac{b}{h}\right)\left(0.04 + 0.01\left(\frac{h}{h_{\text{ref}}}\right)\right)\right] \tag{2.18}$$

$$R^2 = \frac{2\pi \cdot F \cdot \Phi_b \cdot \Phi_h}{\delta_s + \delta_a} \tag{2.19}$$

Wind energy spectrum F Describes the distribution of wind energy across different frequencies.

$$F = \frac{4 \cdot y_C}{(1 + 70.8 \cdot y_C^2)^{5/6}} \tag{2.20}$$

Frequency factor y_C
Relates the building's natural frequency to wind velocity.

$$y_C = \frac{150 \cdot n_{1,x}}{v_m(h)} \tag{2.21}$$

Reduction factors Φ_h & Φ_b
Reduce dynamic response based on height and width effects.

$$\Phi_h = \frac{1}{1 + 2 \cdot n_{1,x} \cdot h / v_m(\bar{h})} \tag{2.22}$$

$$\Phi_b = \frac{1}{1 + 3.2 \cdot n_{1,x} \cdot b / v_m(\bar{h})} \tag{2.23}$$

Damping δ_s & δ_a
Structural damping δ_s and aerodynamic damping δ_a at the lowest eigenfrequency.

δ_s is expressed in Table F.2 SS-EN 1991-1-4:2005

$$\delta_a = \frac{c_f \cdot \rho \cdot b \cdot v_m(z_s)}{2 \cdot n_1 \cdot m_e} \tag{2.24}$$

Mean wind speed at height z $v_m(z)$
Defines wind speed considering terrain roughness and topographic effects.

$$v_m(z) = c_r(z) \cdot c_0(z) \cdot v_b \tag{2.25}$$

Roughness Factor $c_r(z)$
Adjusts wind velocity based on height and terrain, following a logarithmic profile where z_0 and $z_{\min}$ depend on terrain type.

$$c_r(z) = \begin{cases} k_r \cdot \ln\left(\frac{z}{z_0}\right), & z_{\min} \leq z \leq z_{\max} \\ c_r(z_{\min}), & z < z_{\min} \end{cases} \tag{2.26}$$

Terrain Factor k_r
Describes how the roughness length z_0 affects the wind velocity profile at a given height.

$$k_r = 0.19 \cdot \left(\frac{z_0}{z_{0,\mathrm{II}}}\right)^{0.07} \tag{2.27}$$

Table 2.4: Terrain types and terrain parameters (Table 4.1 in SS-EN 1991-1-4:2005).

Terrain Type	**Description**	z_0 **(m)**	$z_{\min}$ **(m)**
0	Sea or coastal area exposed to open sea.	0.003	1
I	Lake or flat, horizontal area with negligible vegetation and no obstacles.	0.01	1
II	Area with low vegetation such as grass and isolated obstacles (trees, buildings) with minimum spacing equal to 20 times the obstacle height.	0.05	2
III	Area covered with vegetation or buildings or with isolated obstacles with maximum spacing equal to 20 times the obstacle height (e.g., villages, suburbs, and forests).	0.3	5
IV	Area where at least 15% of the area is built-up, and the average building height is $> 15\,\text{m}$.	1.0	10

Topographic Factor $c_0(z)$
Accounts for increased wind velocity over isolated hills and slopes. Depends on wind speed at the base of the slope and should be considered in specific cases. For flat terrain, $c_0(z) = 1$. The detailed methodology for calculating $c_0(z)$ is provided in Annex A of SS-EN 1991-1-4:2005.

Turbulence Intensity $I_v(z)$
Describes the relative fluctuations in wind speed due to atmospheric turbulence, depending on height and terrain roughness.

$$I_v(z) = \frac{1}{c_0(z) \cdot \ln\left(\frac{z}{z_0}\right)} \tag{2.28}$$

Force Coefficient c_f
Describes wind-induced pressure and suction on surfaces, considering shape, edge conditions, and flow effects.

$$c_f = c_{f,0} \cdot \psi_r \cdot \psi_\lambda \tag{2.29}$$

Force Coefficient $c_{f,0}$
Figure 2.14 illustrate how $c_{f,0}$ varies with the aspect ratio d/b, showing higher values for thinner sections and a decrease as the section becomes more square.

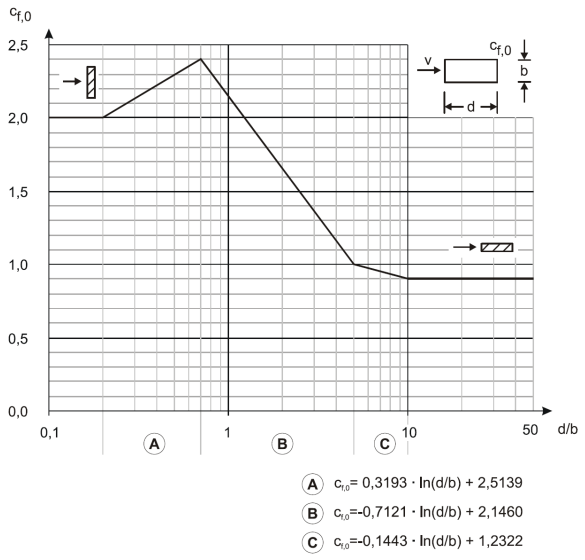

Figure 2.14: Force coefficient $c_{f,0}$ for a structural component with a rectangular cross-section with sharp edges and negligible flow over the ends (Figure 7.23, EN 1991-1-4:2005).

Reduction factor ψ_r

Figure 2.15 illustrate the reduction factor ψ_r for rounded edges, demonstrating how aerodynamic effects reduce the force coefficient compared to sharp-edged sections.

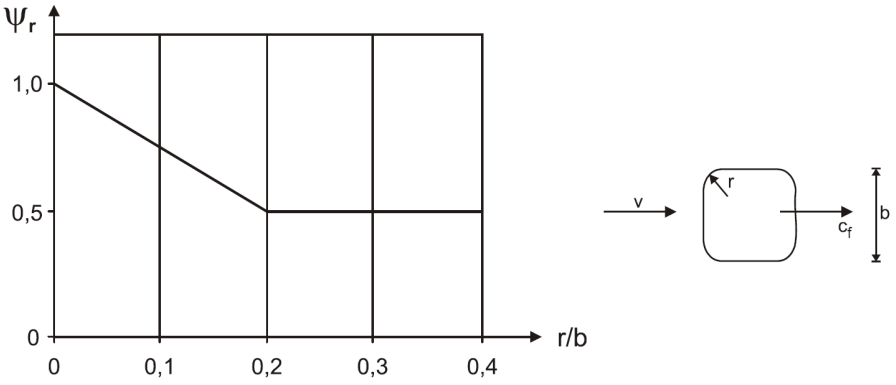

Figure 2.15: Reduction factor Ψ_r for square cross-sections with rounded edges (Figure 7.24, EN 1991-1-4:2005).

Reduction factor ψ_λ

The reduction factor Ψ_λ accounts for the reduced flow resistance due to airflow over the ends of the structural component, depending on effective slenderness λ and the fill ratio φ, defined in Figure 2.16.

The effective slenderness λ is determined by component dimensions and wind direction. Recommended values for λ are provided in Table 2.5.

For given values of λ and φ, the reduction factor Ψ_λ can be determined graphically from Figure 2.16 or interpolated linearly between given data.

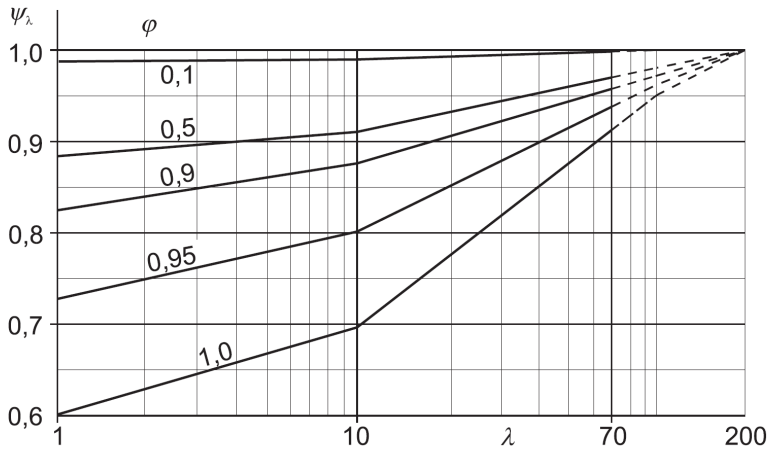

Figure 2.16: Reduction factor Ψ_λ as a function of effective slenderness λ and fill ratio φ (Figure 7.36, EN 1991-1-4:2005).

Peak Velocity Pressure
Peak velocity pressure at height z, including mean and short-term velocity fluctuations and according to EKS 12, this is expressed as:

$$q_p(z) = [1 + 2 \cdot k_p \cdot I_v(z)] \cdot \left[k_r \cdot \ln\left(\frac{z}{z_0}\right) \cdot c_0(z)\right]^2 \cdot q_b \tag{2.30}$$

Reference Velocity Pressure q_b
The reference velocity pressure q_b is calculated as:

$$q_b = \frac{1}{2} \cdot \rho \cdot v_b^2 \tag{2.31}$$

Where:

- ρ: Air density (Recommended value: $1.25\,\mathrm{kg/m^3}$).
- v_b: Reference wind velocity.

Reference Wind Velocity v_b
The reference wind velocity v_b is determined from EKS 12. Figure 2.17 shows average reference wind velocity values in different regions of Sweden, expressed in meters per second (m/s). These values vary based on geographical location and are derived from extreme wind speed statistics with a return period of 50 years.

Table 2.5: Recommended λ-values for cylinders, structural components with polygonal, rectangular, or sharp-edged cross-sections, and trusses. Reproduced from Table 7.16, EN 1991-1-4:2005.

No.	Position of the structure, wind normal to the plane of the page	Effective slenderness λ
1	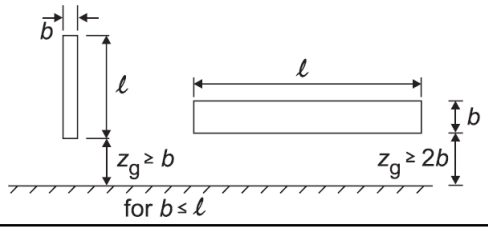	For polygonal, rectangular and sharp edged sections and lattice structures: for $\ell \geq 50$ m, $\lambda = 1{,}4\ \ell/b$ or $\lambda = 70$, whichever is smaller for $\ell < 15$ m, $\lambda = 2\ \ell/b$ or $\lambda = 70$, whichever is smaller For circular cylinders: for $\ell \geq 50$, $\lambda = 0{,}7\ \ell/b$ or $\lambda = 70$, whichever is smaller for $\ell < 15$ m, $\lambda = \ell/b$ or $\lambda = 70$, whichever is smaller For intermediate values of ℓ, linear interpolation should be used
2	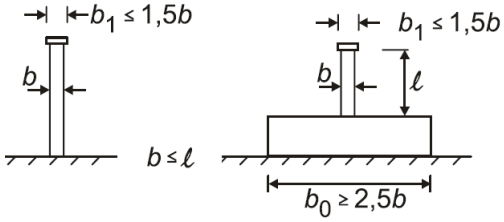	
3	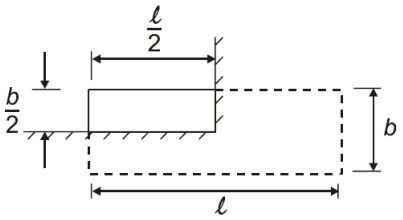	
4	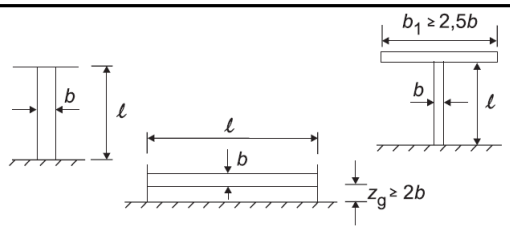	for $\ell \geq 50$ m, $\lambda = 0{,}7\ \ell/b$ or $\lambda = 70$, whichever is larger for $\ell < 15$ m, $\lambda = \ell/b$ or $\lambda = 70$, whichever is larger For intermediate values of ℓ, linear interpolation should be used

2.6.2 Comfort Requirements Regarding Acceleration in Buildings

SS-ISO 10137:2008 defines acceleration thresholds for occupant comfort by limiting peak acceleration in the along-wind, cross-wind, and torsional directions, using a one-year return period wind load, illustrated in Figure 2.18. However, in Europe, a one-year return period is not typically used and cannot be derived with Equation 2.25. According to ISO 6897 EN, acceleration values calculated by using a five-year return period should be multiplied by 0.72 to correspond with the one-year return period wind load used in Figure 2.18.

Peak acceleration
Defines the maximum acceleration response of the structure due to wind.

$$\ddot{X}_{\max}(z) = k_p \sigma_{\ddot{x}}(z) \tag{2.32}$$

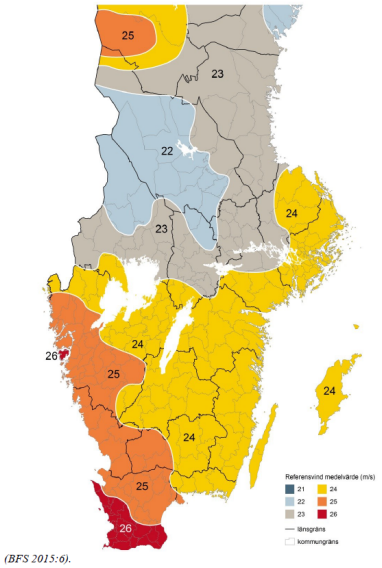

Figure 2.17: Reference wind velocity in southern Sweden according to EKS 12 (Boverket, 2022).

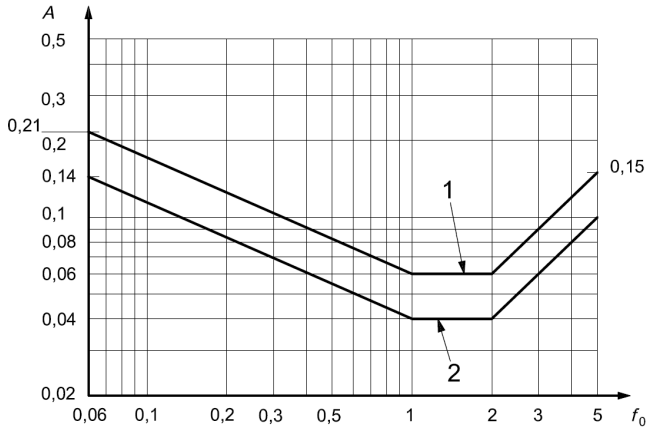

Key

A peak acceleration, m/s^2

f_0 first natural frequency in a structural direction of a building and in torsion, Hz

1 offices

2 residences

Figure 2.18: Comfort requirement curves for wind-induced vibrations for a 1-year wind (Figure D.1, SS-ISO 10137:2008).

Multiplied by 0.72 if five-year return period is used.

Standard deviation of the acceleration

Represents the variability in acceleration response, influenced by turbulence inten-

sity, resonance effects, force coefficient, and mode shape.

$$\sigma_{\ddot{x}}(z) = \frac{3 \cdot I_v(h) \cdot R \cdot q_m(h) \cdot b \cdot c_f \cdot \phi_{1,x}(z)}{m_e} \tag{2.33}$$

Mode shape
Describes the deformation pattern of the structure in its fundamental mode.

$$\phi_{1,x}(z) = \left(\frac{z}{h}\right)^{\zeta} \tag{2.34}$$

where the exponent ζ depends on the structural system. For buildings with a central reinforced concrete core, the recommended value is $\zeta = 1.5$.

Mean Velocity Pressure at height h $q_m(h)$
The reference mean velocity pressure $q_m(h)$ at height h is calculated as:

$$q_m(h) = \frac{1}{2} \cdot \rho \cdot v_m(h)^2 \tag{2.35}$$

To determine the mean velocity pressure $q_m(h)$, the wind speed v_b in equation 2.25 should be replaced with v_{T_a}, corresponding to the selected return period. Resulting $v_m(h)$ is then used.

Wind speed for a given return period
Estimates wind speed corresponding to a specific return period, considering statistical wind speed distributions.

$$v_{T_a} = 0.75 v_{50} \sqrt{1 - 0.2 \ln\left(-\ln\left(1 - \frac{1}{T_a}\right)\right)} \tag{2.36}$$

Where T_a is the return period in years (usually 5 years[5]).

Equivalent mass
Represents the mass distribution of the structure, considering its mode shape.

$$m_e = \frac{\int_0^\ell m(s) \cdot \phi_1^2(s)\, ds}{\int_0^\ell \phi_1^2(s)\, ds} \tag{2.37}$$

[5] $T_a = 1$ results in ln(0) which is undefined

2.7 Case Studies: Tallest Hybrid Buildings

In recent years, an increasing number of tall timber buildings have been constructed due to advances in engineered wood products, sustainability goals, and architectural ambition. Both realised and conceptual projects provide valuable insights into how structural strategies can overcome challenges related to horizontal stability. This section highlights case studies and summarises technical principles in three areas: mass distribution, structural design, and damping systems.

2.7.1 Realised Projects

Ascent MKE (USA, 2022, 86.6 m)

- 25-storey hybrid tower
- 6-storey concrete podium
- 19 timber floors above podium
- Dual concrete cores for stability
- CLT floors with gypsum topping

Figure 2.19: Ascent MKE.
Source: (Thornton Tomasetti, 2022).

Mjøstårnet (Norway, 2019, 85.4 m)

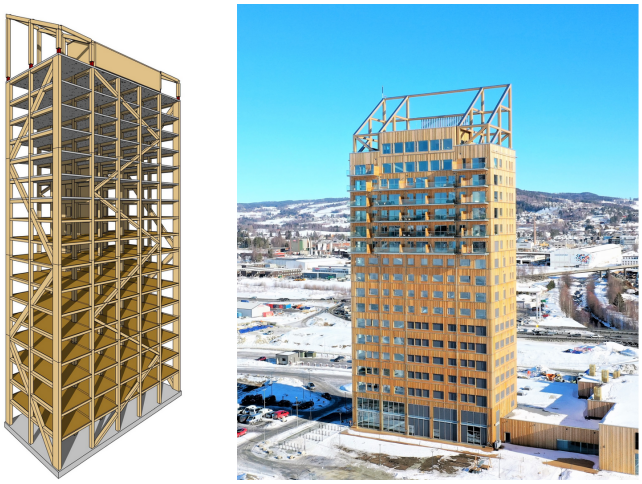

- 18-storey timber tower
- External glulam diagonals for stability
- Core is not stabilizing
- CLT shafts for elevators/stairs
- Concrete slabs for damping (top 7 floors)
- Deep-piled foundation

Figure 2.20: Mjøstårnet.
Sources: (Byggnadsarbetaren, 2021; Metsä Wood, 2019; Swedish Wood, 2022b; Woodsafe Timber Protection, 2020).

Sara Kulturhus (Sweden, 2021, 80 m)

- 20-storey timber tower
- Dual CLT cores for stability
- Concrete slabs for damping (top 3 floors)
- Steel trusses for wide open spaces

Figure 2.21: Sara Kulturhus.
Sources: (Byggindustrin, 2021; Martinsons, 2021; Sara Kulturhus, 2025).

HoHo Wien (Austria, 84 m)

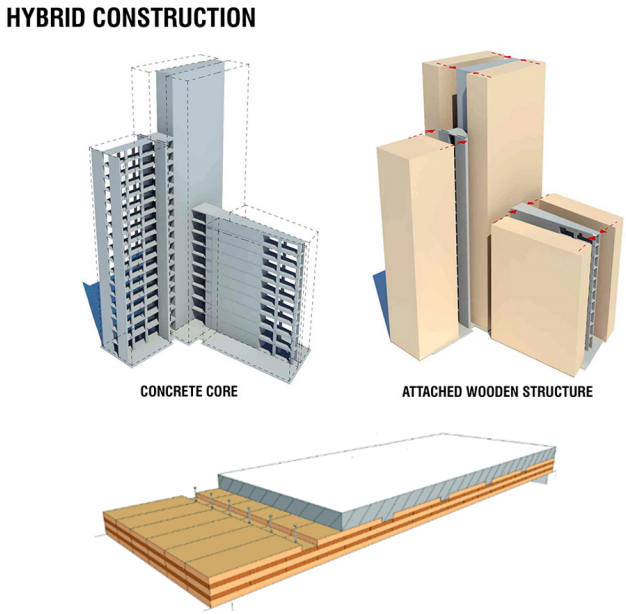

- 24-storey hybrid structure
- Central concrete core
- Timber-steel structural frame
- Timber-concrete composite floors
- Approx. 75% timber volume

Figure 2.22: HoHo Wien.
Sources: (BIG SEE, 2022; University of Melbourne, 2021).

2.7.2 Conceptual Projects

- **W350** (Japan, 350 m) – Hybrid mega-tower with timber and steel. Uses braced external frames, integrated dampers, and passive damping through strategic mass distribution for seismic and wind resilience (Harada et al., 2021).
- **Oakwood Tower** (UK, 300 m) – Spiral-core concept of interlocked timber towers enhancing stiffness, aerodynamic behaviour, and considering economical active damping systems like Tuned Mass Dampers (Foster & Ramage, 2016).
- **River Beech Tower** (USA, ∼244 m) – Twin towers connected by bracing and atrium trusses, emphasizing diagrid structural systems and designed with significant wind tunnel validation (Sanner et al., 2017).

2.7.3 Technical Strategies

Mass Distribution
Proper mass distribution significantly influences the dynamic response of tall timber structures, reducing sway and enhancing occupant comfort. Strategies include:

- **Top-heavy floors**: Heavy concrete slabs placed at higher floors to lower the natural frequency, thus minimizing sway due to wind-induced vibrations (e.g., Mjøstårnet, Sara Kulturhus).
- **Mass anchoring**: Utilizing substantial concrete podium structures as mass anchors to reduce horizontal movements and enhance stability (e.g., Ascent MKE).
- **Distributed mass**: Even distribution of mass throughout the building height help to reduce torsional effects and improve the building's dynamic behaviour under wind and seismic loads (e.g., proposed for W350) (Botis & Cerbu, 2020).

Structural Design
The structural design approach for tall timber structures aims at maximizing lateral stiffness, strength, and minimizing deformation:

- **Wide and interconnected cores**: Strategic use of multiple cores or linked volumes to increase the overall building footprint, enhancing resistance to torsion and providing improved lateral stiffness (e.g., River Beech Tower).
- **Tapering**: Gradually reducing building cross-section toward higher floors to lower wind loads and reduce the structural demand in taller structures (e.g., Oakwood Tower).

- **Diagrid and outrigger systems**: Incorporating diagonal framing systems (diagrids) and outriggers that connect external columns to internal cores, significantly enhancing lateral stiffness and reducing drift under lateral loads (e.g., River Beech Tower).

Damping Systems

Another approach to controlling building motion is the use of damping systems (Irwin & Breukelman, 2001). While optimal geometry and strategic mass placement can provide inherent damping, supplemental devices are sometimes required. Two of the most commonly used systems are:

- **Tuned Mass Dampers (TMDs)**: Secondary masses tuned to the structure's natural frequency, oscillating out-of-phase to reduce sway and absorb vibrational energy.
- **Viscous Dampers**: Hydraulic devices that dissipate motion by converting kinetic energy into heat through fluid resistance.

3

Modelling

This chapter introduces the finite element model developed for the structural analysis carried out in this thesis. The modelling approach includes an overview of the structural layouts, boundary condition assumptions, and mesh refinement strategy. Key material parameters and modelling choices are presented, followed by verification steps to ensure the reliability of the model.

3.1 Building geometry

The model analysed in this thesis represents a multi-storey office building with a structural system consisting of a column-beam system with a stabilizing concrete core and bracing. Inspired by the office building Habitat 7 in Gothenburg, it has a rectangular shape (54 × 18 m). The first floor has a height of 4.5 m, while the remaining floors are 3.5 m. Two different layouts for the concrete core and bracing, presented in Figure 3.1-3.4, will be tested and compared. The roof is flat with a 3-degree slope for drainage.

Layout 1: One core in the center of the building and frame bracing at the short sides.

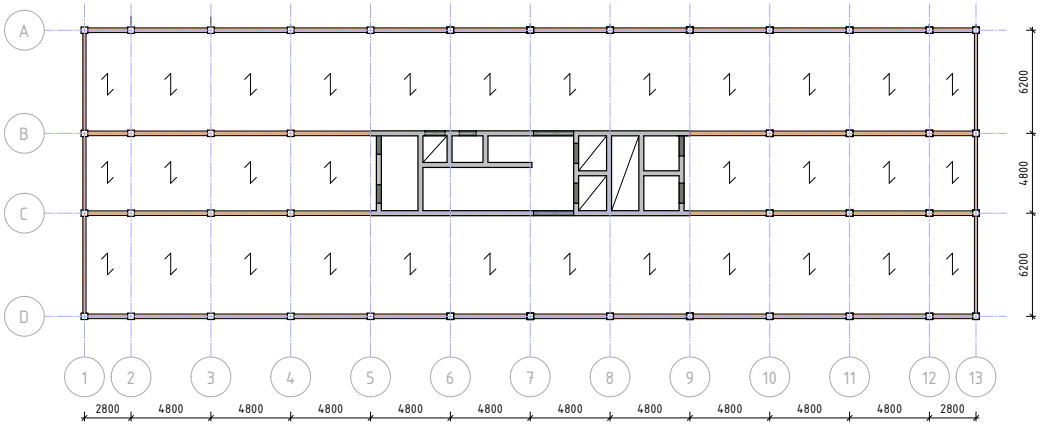

Figure 3.1: Schematic view of floor plan, Layout 1 .

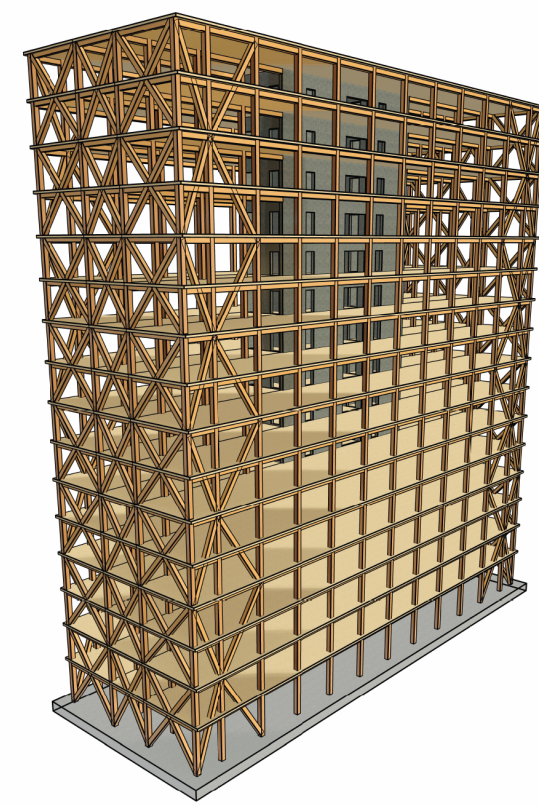

Figure 3.2: 3D-view, Layout 1

Layout 2: Two smaller cores at a smaller distance from the short sides, no bracing.

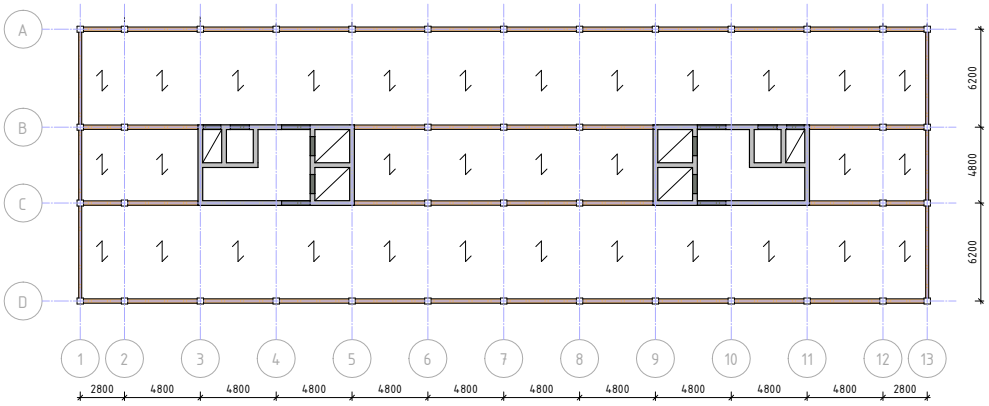

Figure 3.3: Schematic view of floor plan, Layout 2

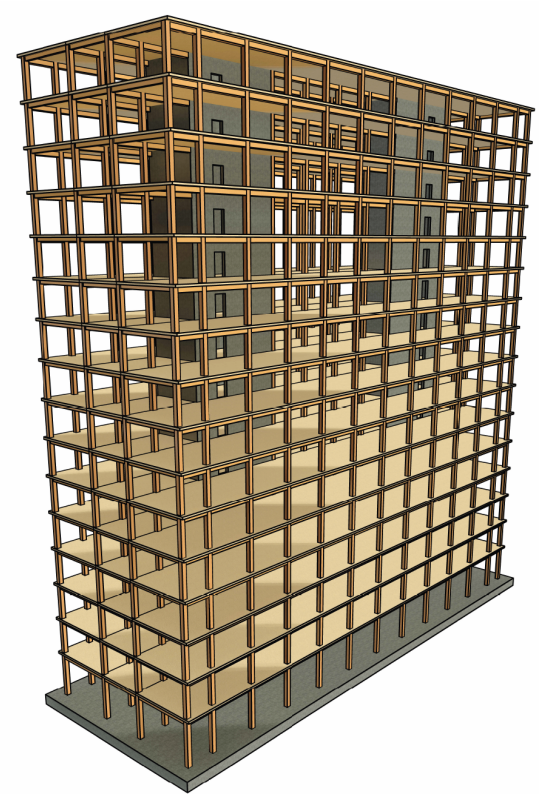

Figure 3.4: 3D-view, Layout 2

Table 3.1 summarises the structure.

Table 3.1: Building properties

Property	**Value**
Width	54 [m]
Length	18 [m]
Beam span	4.8 and 2.8 [m]
Floor span	6.2 and 4.8 [m]
Height of first storey	4.5 [m]
Height of other storeys	3.5 [m]
Number of columns per floor	Layout 1 = 42 Layout 2 = 40

3.2 Loads

The following sections provide an overview of the considered loads and their associated factors. The building is designed for self weight along with additional permanent and variable loads, including live, wind and snow load.

3.2.1 Vertical Loads

Vertical loads that act on the structure include the self-weight of structural elements (Dead Load), superimposed dead loads (SDL), imposed live loads (LL), and snow loads. These loads are determined according to SS-EN 1991-1-1, with the building classified as an office building (Category B). The following sections outline the assumptions and calculations for each type of vertical load.

Self Weight
The self-weight of the building is determined based on the primary materials used in the structure, including concrete, CLT, and glulam. The specific material densities and resulting self-weight values are presented in Table 3.3.

Table 3.3: Self-weight of main construction materials

Material	**Self-weight** $\left[\frac{\text{kg}}{\text{m}^3}\right]$
Concrete	2550
CLT	402.5
Glulam GL30c	430
Glulam GL30h	480

Superimposed Dead Load
In addition to the self-weight of the structure, SDLs account for permanent non-structural elements that contribute to the overall load. These include non-load-bearing walls, fixed installations, façade elements [1] etc. The assumed SDL values are presented in Table 3.5.

Table 3.5: Superimposed Dead Loads (SDL)

Component	**Load**
Non-load-bearing walls, installations	0.5 $\left[\frac{\text{kN}}{\text{m}^2}\right]$
Façade	1.5 $\left[\frac{\text{kN}}{\text{m}}\right]$

[1] The self weight of the façade is applied on the beams along the facades as a line load.

Live Load
The building is classified as an office building, Category B. The characteristic live load in the core/stairs (Category C3) and in offices (Category B) according to EKS 12 is presented in Table 3.7.

Table 3.7: Characteristic Live Loads

Component	Load
Core/Stairs	3.0 $\left[\frac{\text{kN}}{\text{m}^2}\right]$
Office	2.5 $\left[\frac{\text{kN}}{\text{m}^2}\right]$

Snow Load
According to SS-EN 1991-1-3, the characteristic snow load on the roof is given by:

$$s = \mu_i \, C_e \, C_t \, s_k \tag{3.1}$$

Where:

- μ_i is the snow load shape coefficient (see Section 5.3 and Annex B)
- s_k is the characteristic value of snow load on the ground
- C_e is the exposure coefficient
- C_t is the thermal coefficient

In this thesis, the values used are:

- $\mu_i = 0.8$ (Roof slope of 3 degrees)
- $s_k = 1.5\,\text{kN/m}^2$ (for Gothenburg)
- $C_e = 1.0$, $C_t = 1.0$

Thus, the characteristic snow load on the roof is:

$$s = 1.2 \left[\frac{\text{kN}}{\text{m}^2}\right]$$

3.2.2 Lateral Loads

Lateral loads act horizontally on the structure and primarily consist of wind loads and unintended inclination. Seismic loads are disregarded due to the low seismic activity in the building's location.

Wind Load
The wind load can be applied using different methods, each offering varying levels of accuracy:

1. **Uniform Wind Load (Default in FE-Design)**

   The software automatically applies a uniform peak wind pressure along the building height, simplifying the load application, overestimating wind effects at lower levels.

2. **Section-Based Wind Load**

   According to SS-EN 1991-1-4, Figure 7.2, wind pressure $q_p(z)$ varies with height. This method divides the building into sections based on the aspect ratio h/b and assigns a uniform load within each section, using its upper height as the reference. This provides a more precise wind load distribution than a fully uniform approach.

3. **Logarithmic Wind Profile**

   By following the methodology in Chapter 2.5 - Design Standards, a continuously varying wind load can be derived using a logarithmic wind profile. This method offers the highest precision and generally results in slightly lower total wind loads than the section-based approach. As stated in EKS 12, Section 7.2.2(1), Note 1, this procedure is permitted, allowing $q_p(z)$ to vary smoothly along the building height.

In this project, the wind pressure was calculated at the top and bottom of each storey, and linear interpolation was used to capture the continuous variation along the facade. The wind load is transferred from the facade to the slabs, which then distribute it to the core and bracing. Since the wind load does not induce a bending moment in the facade columns, it can be applied as pressure on one side without dividing it into pressure and suction on two sides.

Figure 3.5 illustrates how wind pressure varies with height in a 25-storey building. It highlights the influence of the dynamic factor $c_s\, c_d$, and compares the Section-Based Wind Load with the Logarithmic Wind Profile method.

Unintended Inclination
According to SS-EN 1992-1-1:2005, imperfections in structures may be represented by an unintended inclination, θ, given by:

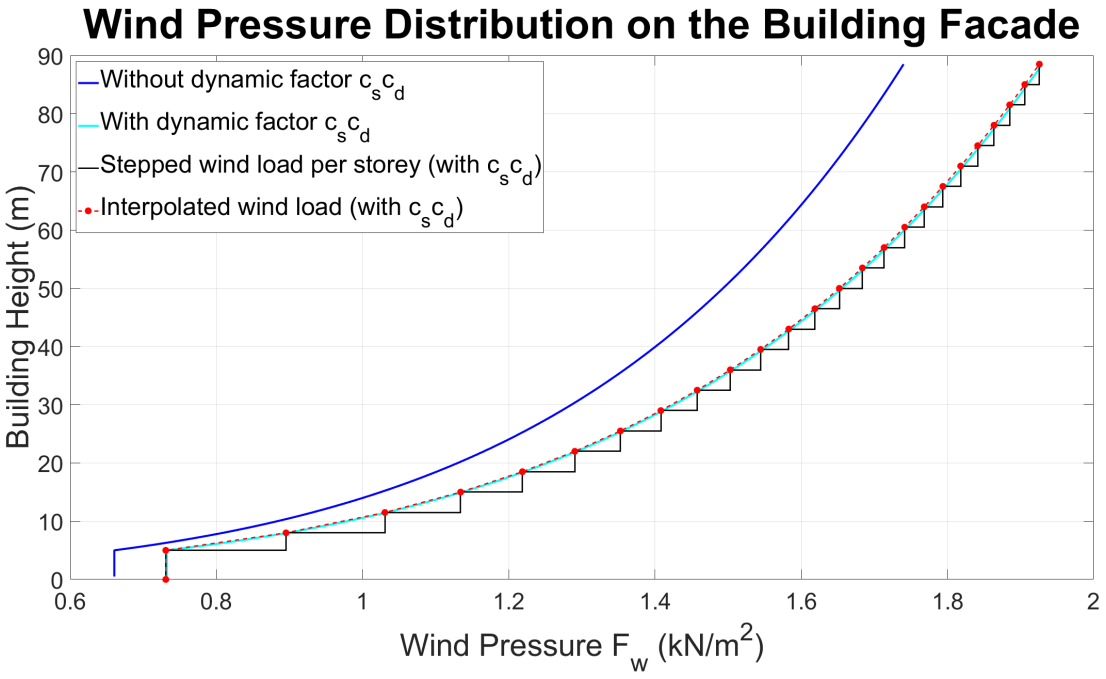

Figure 3.5: Illustrating the logarithmic wind profile with and without the dynamic factor $c_s c_d$, an interpolated wind load per storey, and a stepped uniform wind load per storey.

$$\theta = \theta_0 \cdot \alpha_h \cdot \alpha_m \tag{3.2}$$

Where:

- θ_0 is the base value. Recommended value: $\theta_0 = 1/200$
- α_h is the reduction factor for length or height: $\alpha_h = \frac{2}{\sqrt{l}}, \quad \frac{2}{3} \leq \alpha_h \leq 1$
- α_m is the reduction factor for number of members: $\alpha_m = \sqrt{0.5\left(1 + \frac{1}{m}\right)}$
- l is the length or height [m].
- m is the number of vertical members contributing to the total effect.

The parameters l and m in the expression depend on the structural effect under consideration:

- For an **isolated member**: l is the actual member length, and $m = 1$.
- For a **bracing system**: l is the total building height, and m is the number of vertical elements resisting lateral loads.
- For **floor or roof diaphragms**: l corresponds to the storey height, and m is the number of vertical elements resisting lateral loads.

These factors ensure that the structural design accounts for imperfections that may influence stability and load distribution. Geometric imperfections in structural members and systems are illustrated in Figure 3.6.

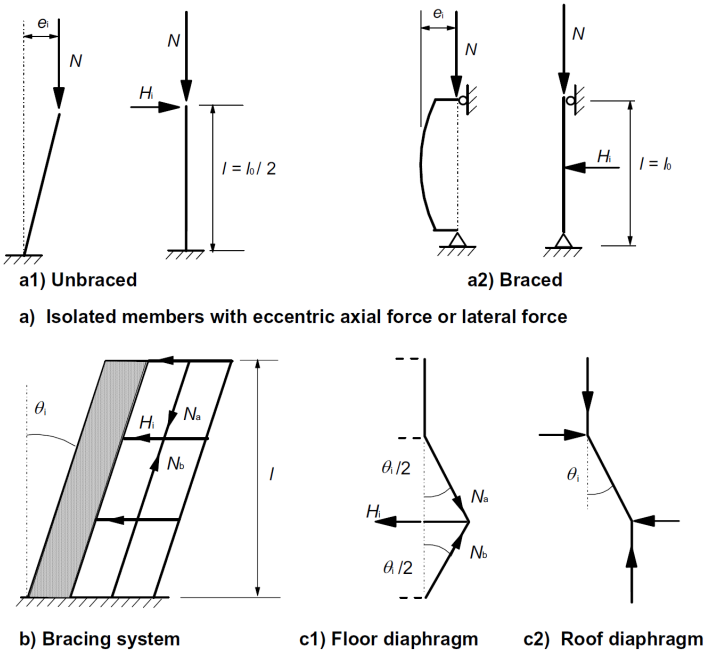

Figure 3.6: Illustration of geometric imperfections in structural systems. From SS-EN 1992-1-1:2005, Figure 5.1.

3.2.3 Design Factors and Load Combinations

Ψ-Factors
In SS-EN 1990, Chapter 6.5.3, Ψ-factors reflect the probability and duration of simultaneous variable loads. Specified in EKS 12 paragrapf A1.2.2(1).

- Ψ_0 – Characteristic combination. Accounts for the reduced likelihood of simultaneous occurrence of multiple variable loads, typically for irreversible conditions.
- Ψ_1 – Frequent combination. Represents load levels frequently exceeded, typically for reversible conditions.
- Ψ_2 – Quasi-permanent combination. Reflects load levels acting continuously or over extended periods, addressing long-term effects and appearance considerations.

These three Ψ-factors ensure that the structure is realistically designed, considering the varying probabilities of simultaneous and long-term variable loads according to EC principles.

Table 3.9: Ψ-Factors for Different Load Types According to EKS 12

Load Type	Ψ_0	Ψ_1	Ψ_2
Imposed load (Category B)	0.7	0.5	0.3
Snow load	0.6	0.3	0.1
Wind load	0.3	0.2	0.0

Reduction Factor for Imposed Load in Multi-Storey Buildings
In multi-storey buildings, the imposed load on structural members supporting several floors can be reduced by applying two different reduction factors in accordance with SS-EN 1991-1-1 and EKS 12:

- α_n, which accounts for the reduced probability that all floors are fully loaded simultaneously, and
- α_A, which considers the reduced likelihood that large areas within a single floor are subjected to maximum loading.

These reductions reflect the statistical improbability that every floor or every square metre of a building will experience the full characteristic imposed load simultaneously.

Reduction for Number of Loaded Floors - α_n
The reduction factor α_n is applied when calculating the total imposed load from several floors acting on common structural elements, such as columns or walls. It is given by:

$$\alpha_n = \frac{2 + (n-2)\Psi_0}{n} \tag{3.3}$$

Reduction for Large Floor Areas - α_A
In addition, the reduction factor α_A may be applied for large floor areas in categories A to D, as defined in Table 6.2 of SS-EN 1991-1-1. The recommended value is:

$$\alpha_A = \frac{5}{7} \cdot \Psi_0 + \frac{A_0}{A} \leq 1.0 \tag{3.4}$$

Where:

- A is the loaded area
- $A_0 = 10\,\mathrm{m}^2$ is the reference area

For load categories C and D, $\alpha_A \geq 0.6$

Load Combinations
The governing load combinations used according to SS-EN 1990, (Equation 6.10b) for ULS and (Equation 6.12b) the quasi-permanent load combination for SLS are presented below:

$$Q_{ULS} = 1.35G_k + 1.50Q_{k1} + 1.5\sum_{i>1}\psi_{0,i}Q_{ki} \tag{3.5}$$

$$Q_{SLS} = 1.0G_k + \psi_{2,i}Q_{ki} \tag{3.6}$$

3.3 Member Sizing

The sizing of the structural elements was carried out to meet both ULS and SLS requirements, ensuring enough strength and stiffness throughout the building. CLT floor slabs were selected based on span tables provided by Martinsons, 2022, while vibration analysis and diaphragm action for the slabs is considered outside the scope of this study.

The trusses were designed uniformly throughout the height of the structure, following the design philosophy used in Habitat 7. This contributes to global stiffness, particularly in torsional resistance and also supports a more unified architectural appearance.

To balance structural efficiency with constructability and material usage, columns were grouped and designed in five-storey intervals. Larger cross-sections are applied at lower levels to accommodate the increasing axial loads from the accumulating weight of the superstructure.

An overview of the selected cross-sections for beams, trusses and columns, distributed by storey level, is presented in Table 3.11 and Figure 3.7.

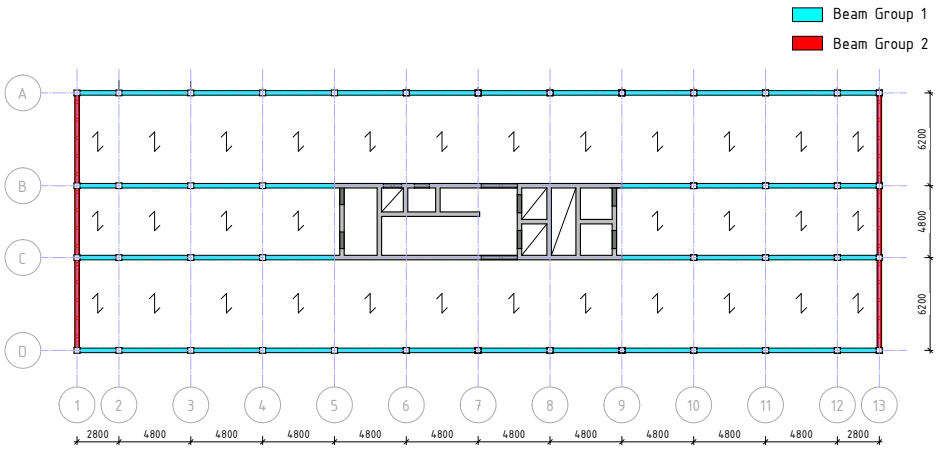

Figure 3.7: Beam groups based on load conditions.

Table 3.11: Beam, Truss and Column Dimensions

Element Group	Cross-section [mm]	Material
Beam Group 1	380 × 360	GL30c
Beam Group 2	570 × 585	GL30c
Trusses	380 × 360	GL30h

Storeys (From top down)	Cross-section [mm]	Material
1–5	380 × 360	GL30h
6–10	430 × 405	GL30h
11–15	570 × 585	GL30h
16–20	645 × 720	GL30h
21–25	760 × 765	GL30h

3.4 Finite Element Model

The structural analysis was performed using the software *FEM-Design* (StruSoft), enabling detailed modelling and analysis of multi-storey buildings. The finite element (FE) model was developed to accurately represent the global structural behaviour, with particular focus on the dynamic response under wind and serviceability loads.

Two main FE types were used in the model:

- **1D Line Elements:** Used for beams, columns, and trusses. These Timoshenko -type elements feature six degrees of freedom per node—three translations and three rotations—allowing for accurate representation of axial, bending, shear, and torsional behaviour.
- **2D Shell Elements:** Used for slabs and walls, including the concrete core and floor diaphragms. Shell elements also have six degrees of freedom per node, capturing both in-plane and out-of-plane deformations as well as rotational effects, consistent with Reissner-Mindlin plate theory.

The mesh consists of 2-node line elements for beams and columns, and both 6-node triangular and 9-node quadrilateral shell elements for walls and slabs, see Figure 3.8. The selection of mesh size was based on a convergence study (see Section 3.4.2), ensuring accurate results with reasonable computational effort.

Figure 3.8: Finite element types used in the model: 2-node line element (left), 6-node triangular shell element (middle), and 9-node quadrilateral shell element (right).

All materials were modeled as linear elastic. Concrete was assumed to remain in *Stadium I* (uncracked), since the cores are designed to remain uncracked under service load conditions. An overview of the finite element model is presented in Figure 3.9, illustrating the overall layout.

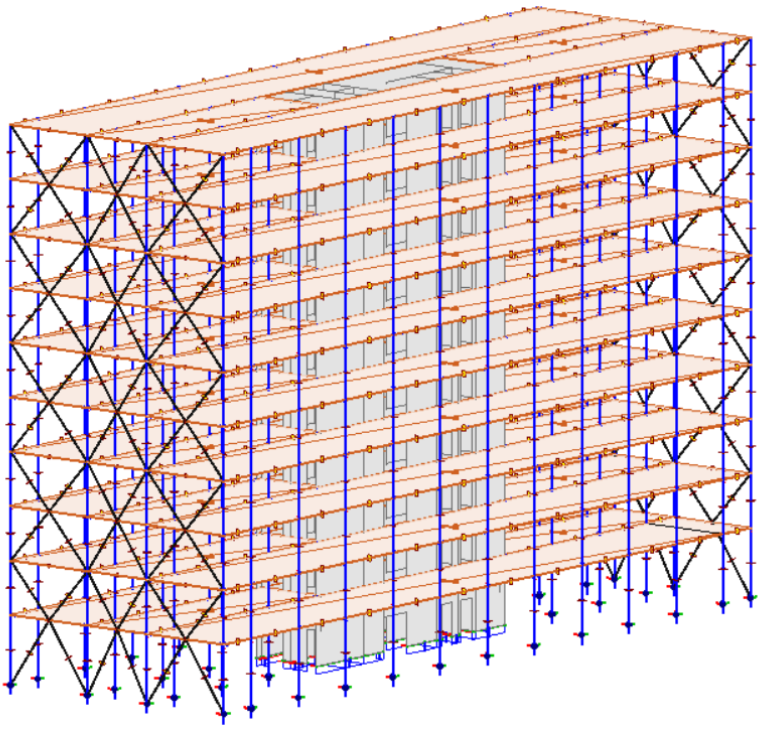

Figure 3.9: Overview of the FE-model in FEM-Design, showing a 10-Storey building

3.4.1 Boundary Conditions

In the FE model, three types of boundary conditions can be applied:

- **Pinned** (Hinged): Allow rotation but prevent translation, no moment transfer.
- **Rigid** (Fixed): Restrict both rotation and translation, ensuring full moment transfer.
- **Semi-Rigid** (Partially Restrained): Allow limited rotation and moment transfer, depending on the stiffness.

In this study, all connections are assumed to be pinned. However, since real-world connections typically exhibit partial restraint, a separate sensitivity study is conducted to investigate how different boundary condition assumptions influence the overall dynamic behaviour of the structure. Four boundary condition schemes were tested by progressively introducing fixed connections into the system as described in Section 5.2.4. Table 3.14 summarises the connection types used in the model, showing where fixed or pinned conditions were applied and later varied in the sensitivity study.

Table 3.14: Boundary Condition Assignments

Connection Type	Condition
Foundation - Core	Pinned or fixed
Foundation - Column	Pinned or fixed
Core - Core[1]	Fixed
Beam - Beam	Pinned
Column - Column	Pinned or fixed
Beam - Column	Pinned or fixed
Beam - Core	Pinned or fixed
Frame bracing	Pinned

[1] "Core - Core" refers to the connection between wall elements on different floors. This connection is considered fixed, as the core is assumed to be cast in place, resulting in cantilever-like behaviour.

3.4.2 Convergence Study

A convergence study was performed to determine the optimal mesh size that balances accuracy and computational efficiency. The mesh density has a direct impact on both the reliability of structural response predictions and the total analysis time. To identify a suitable mesh, average element sizes of 1.5 m, 1.0 m, 0.8 m, 0.6 m, 0.5 m, 0.4 m, and 0.3 m were evaluated. For each mesh, the following structural response parameters were analysed:

- Fundamental frequency of the building
- Maximum deflection and maximum moment in a representative beam
- Maximum moment and shear force in a representative CLT slab
- Maximum compression force in the concrete core wall

These parameters were chosen to capture both global (dynamic) and local (force and deformation) behaviour, ensuring that the selected mesh size would be sufficiently refined for all critical aspects of the analysis.

Figure 3.10 presents the results of the convergence study, showing that all response parameters stabilize as the mesh is refined. Improvements diminish rapidly beyond a mesh size of 0.6 m, and further refinement has minimal effect on results while substantially increasing computational effort. Therefore, a mesh size of 0.6 m was selected for all analyses as it offers a reliable balance between computational efficiency and solution accuracy. Detailed results are presented in Appendix D.

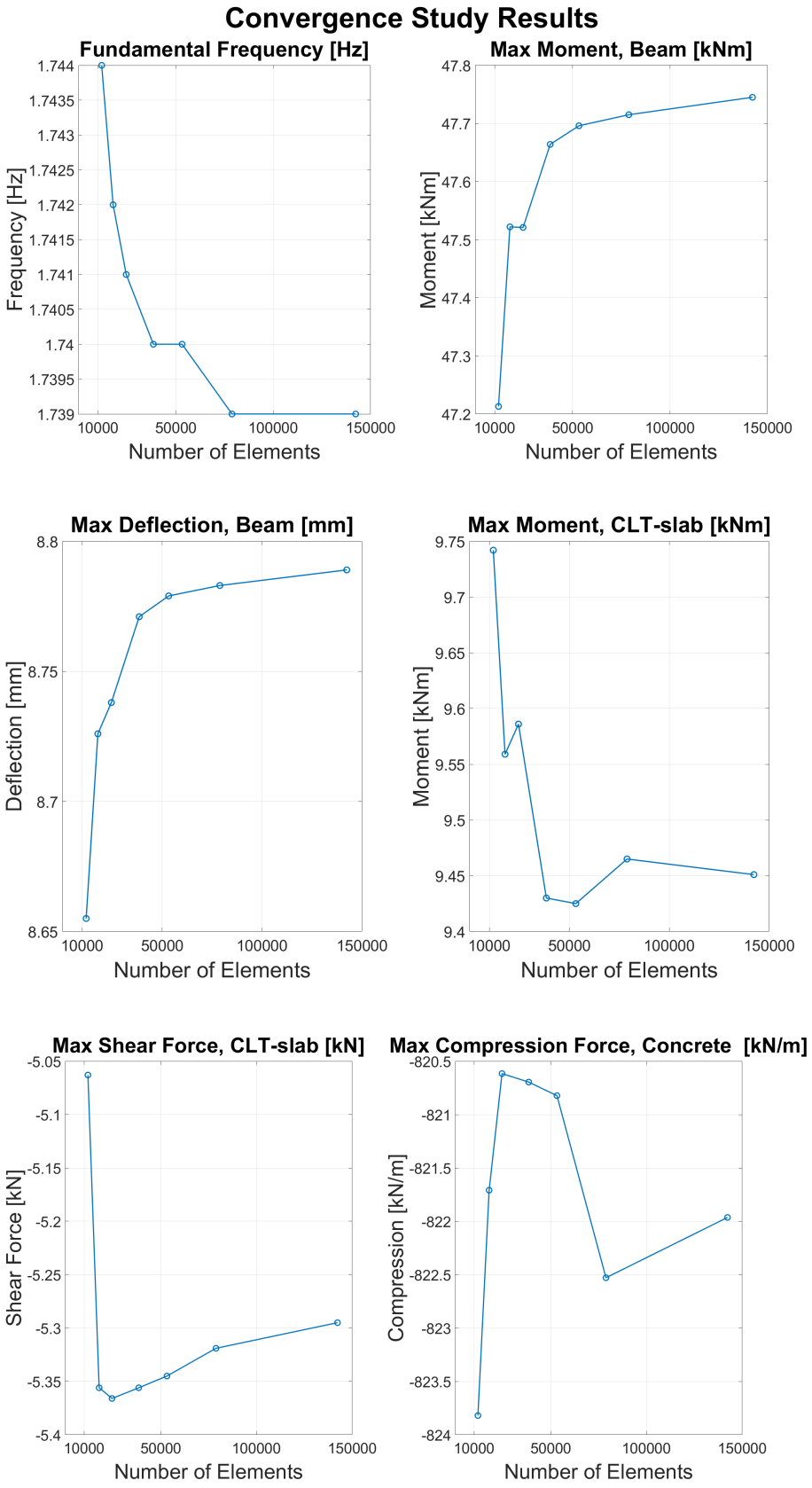

Figure 3.10: Convergence study results showing the variation in structural response parameters with increasing number of finite elements.

3.5 Verification of the Finite Element Model

This section presents the methodology used to verify the FE models developed in this project. Several verification steps were conducted to ensure the reliability of the structural modelling, including mass checks, ULS verification, and dynamic analysis.

3.5.1 Mass Verification

To validate the basic accuracy of the models, the total structural mass of the FE models was compared to corresponding hand calculations. This check was carried out for all structural models as part of the process of computing equivalent mass for dynamic analysis. The deviations were consistently small, typically below 0.1% indicating strong numerical agreement. Table 3.16 presents a selection of 20 storey, 1-Core models as examples.

Table 3.16: Comparison of Total Structural Mass

Configuration	Hand Calculation	FEM-Design	Difference
300 mm core, 0 slabs	9 638 [ton]	9 633 [ton]	0.05 [%]
400 mm core, 1 × 300 slab	11 550 [ton]	11 543 [ton]	0.06 [%]
500 mm core, 3 × 400 slabs	14 724 [ton]	14 714 [ton]	0.07 [%]

3.5.2 Verification in Ultimate Limit State

To verify the ULS, two representative columns and beams were analysed. Utilization ratios were compared between FEM-Design and hand calculations, as shown in Table 3.18 and 3.20. For the columns, the differences were minor, with deviations below 2%. The beam verifications showed significantly larger discrepancies, ranging from 20% to over 100%.

This variation stems from how load paths are modeled in FEM-Design. The relative stiffness between structural elements allows the CLT slabs to transfer a larger share of the vertical loads directly to the columns, bypassing the beams. In reality, vertical loads are expected to pass from slab to beam and then to the column. Hand calculations that account for this distribution pattern provide a more realistic basis for beam design.

Importantly, this discrepancy in vertical load path representation does not affect the global stiffness of the structure. Therefore, the FEM results remain valid for evaluating global structural behaviour, such as dynamic performance and overall

deformation. In addition, the beams were checked for Lateral Torsional Buckling (LTB) in both FEM-Design and manual calculations. The results confirmed that LTB is not a governing factor, and thus the bending utilization ratio remains unaffected. Detailed calculations are presented in Appendices A, B and C.

Table 3.18: Comparison of Utilisation Ratios [%] – Columns

Check	Hand calculation	FEM-Design	Difference
Axial compression	31.5	32	1.9
Flexural buckling	31.6	32	1.5

Table 3.20: Comparison of Utilisation Ratios [%] – Beams

Check	Hand calculation	FEM-Design	Difference
Bending	78.2	38	105.8
Lateral Torsional Buckling	78.2	38	105.8
Shear	68.6	57	20.4

3.5.3 Mode shapes

Before analysing eigenfrequencies, it's essential to check the mode shapes. This reveals whether the structure behaves globally or locally in its initial modes.

Global modes involve the entire building moving, while local modes affect only parts, which might indicate modeling issues like overly stiff elements or lack of connection.

The first three mode shapes for the 20-storey building shown in Figure 3.11 include two translational modes (x- and y-direction) and one torsional mode. Displacements increase from ground to roof for the translational modes and with the first mode in the x-direction which suggest lower stiffness in that direction.

While these models show global behaviour, it is worth noting that all other models also display global mode shapes from the beginning, reinforcing the consistency and reliability of the FE-models across different configurations.

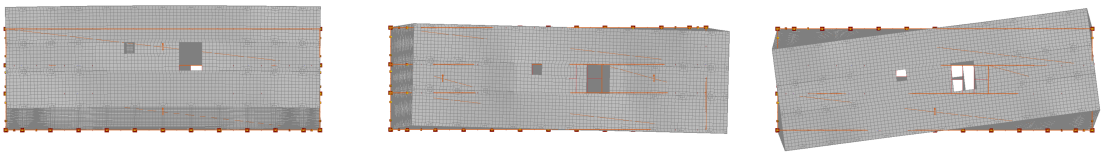

(a) 1st mode shape **(b)** 2nd mode shape **(c)** 3rd mode shape

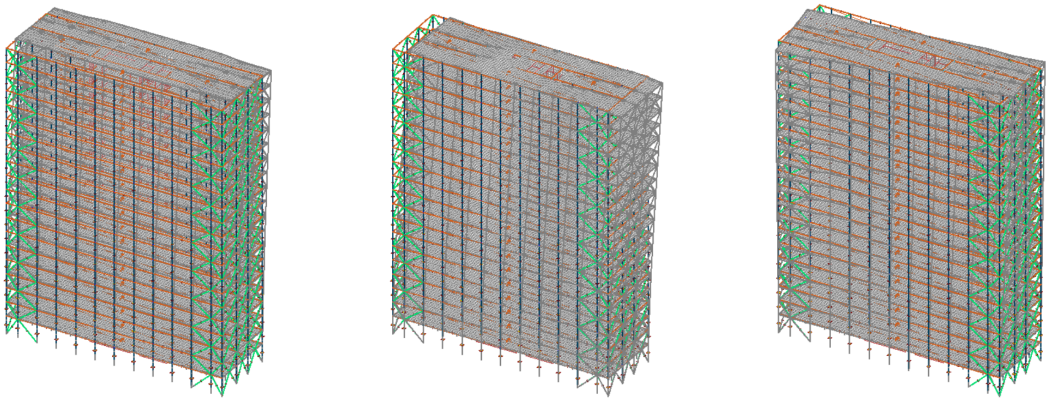

(d) 1st Bending Mode, X-direction **(e)** 1st Bending Mode, Y-direction **(f)** 1st Torsional Mode

Figure 3.11: Illustration of the first global vibration mode shapes.

3.5.4 Verification of Dynamic Properties

To verify the dynamic properties of the FE models, eigenfrequency verification was performed with gradually increasing model complexity. The first bending and torsional modes were studied using structural elements as summarised in Table 3.22.

Table 3.22: Simplified Structural Models Used in Eigenfrequency Verification

Structural Type	Size [mm]	Height/Length [m]	Material	Element Type
Glulam Beam	140×140	10.0	GL30c	Beam Element
Steel Tube Profile	450×250	10.0	S355	Shell Element
Concrete Core	19 200×4 800	88.5	C30/37	Shell Element

These simplified models enabled direct comparison with analytical hand calculations based on Euler–Bernoulli and Saint-Venant theory. For consistency, the same Timoshenko beam approach used by FEM-Design was adopted in the hand calculations, resulting in excellent agreement for the beam element.

For the shell elements, FEM-Design uses Mindlin–Love plate theory, which better accounts for shear deformation in thick plates. This was especially evident for the concrete core, where analytical models neglecting shear deformations introduced greater deviations.

Overall, the results for the beam and steel tube showed very small differences, confirming that the implemented boundary conditions and mass/stiffness distributions were correct. For the concrete core, larger deviations were expected due to model simplifications and the complexity of torsional modes. Tables 3.24–3.26 summarise the calculated eigenfrequencies. For full details of the MATLAB scripts and calculations, see Appendix I.

Table 3.24: Calculated eigenfrequencies (Hz) for beam element. Comparison of the first bending modes using analytical and numerical methods.

Mode	FEM-Design	Analytical	Numerical
Bending 1	1.242	1.244	1.242
Bending 2	7.736	7.793	7.728
Bending 3	21.462	21.820	21.422

Table 3.25: Calculated eigenfrequencies (Hz) for tubular profile. Comparison of the first bending and torsional modes using analytical and numerical methods.

Mode	FEM-Design	Analytical	Numerical
Bending 1	2.809	3.163	2.965
Bending 2	18.229	19.821	18.450
Bending 3	51.392	55.499	51.116
Torsion 1	67.816	63.817	68.750

Table 3.26: Calculated eigenfrequencies (Hz) for simplified concrete core. Comparison of the first global modes using numerical results and analytical estimations.

Mode	FEM-Design	Analytical	Numerical
Bending 1	0.535	0.575	0.516
Bending 2	2.611	3.609	3.145
Bending 3	4.339	10.106	8.453
Torsion 1	2.477	3.643	3.451

4

Analysis

This chapter presents the analytical framework used to evaluate the structural performance of the hybrid timber–concrete building. The analysis builds on the modelling strategies described in the previous chapter and aims to explore how parameters affect both SLS and ULS behaviour.

4.1 Parametric Study

The parametric study investigates how key design configurations impact the building's dynamic response and load-bearing capacity. The aim is to identify efficient combinations of material and geometry that satisfy both comfort and strength criteria.

The following parameters were systematically varied:

- Number of storeys (15, 20, and 25)
- Number of concrete slabs at the top levels (0, 1, 3, and 5 slabs)
- Concrete core thickness (300, 400, and 500 mm)
- Concrete slab thickness (200, 300, and 400 mm)
- Boundary conditions (fixed or pinned)
- Combinations of the above parameters

4.2 Analysis Procedure

The analysis process is divided into two main stages: SLS evaluation and ULS evaluation. In the SLS stage, eigenfrequency analyses were performed on a preliminary structural model to determine mode shapes and fundamental frequencies. Equivalent masses were calculated manually and used to manually calculate the maximum accelerations, which were compared against comfort limits defined in SS-ISO 10137.

In the ULS stage, wind loads were calculated using manually derived dynamic amplification factors based on the structure's eigenfrequency and equivalent mass. These amplified wind loads are applied in FEM-Design for structural verification. The

analysis focused on the load-bearing capacity to ensure that stress levels remained within acceptable limits.

A range of configurations was studied to assess how parameters such as core thickness, slab thickness, and number of slabs influence dynamic response and acceleration levels, and structural capacity. A flowchart summarising the analysis procedure is presented in Figure 4.1.

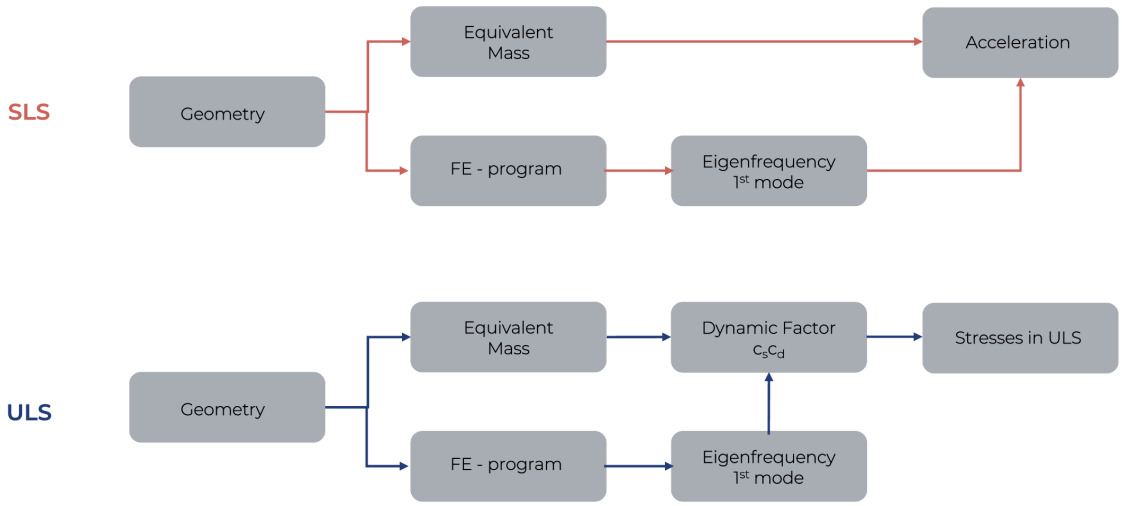

Figure 4.1: Flowchart summarising the analysis procedure.

4.3 Early findings

This chapter presents key observations from the initial analysis phase, focusing on the dynamic performance of the hybrid timber–concrete structure. The study initially aimed to assess the first translational mode in accordance with EC's guidelines, but early results revealed that torsional modes appeared earlier than anticipated. This prompted further investigation into how bracing configurations could increase the building's stiffness to raise the torsional mode.

Additionally, it became apparent that the 2-Core model demonstrated weaker torsional performance than the 1-Core model. To better understand this difference and enable fair comparisons, the 2-Core model was also evaluated using the same bracing configurations as the 1-Core model. These findings helped decide which core layout to continue using in the next steps of the study.

In addition, the strong (longitudinal) direction was reviewed as part of the SLS assessment. Since the results showed accelerations well below the comfort limits, no further analysis was deemed necessary in that direction.

4.3.1 Torsional Mode and Bracing Configurations

The tests in this section were conducted for the 1-Core model with bracing at the short ends as a reference case (Model 1 in Table 4.1). Six additional models, each with variations in bracing configurations and wall layouts, were analysed. To provide context for the analysis, each model is described and illustrated in Figure 4.2 & 4.3. A summary of the results is presented in Table 4.1, showing how each variation affected the torsional mode.

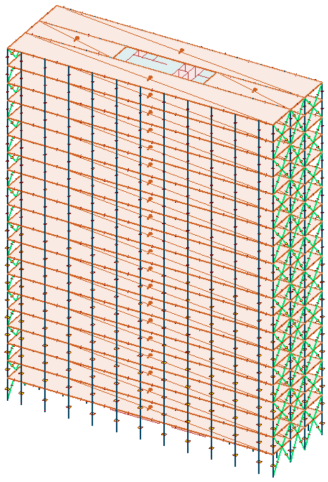

(a) Model 1 – Diagonal bracing along short façades.

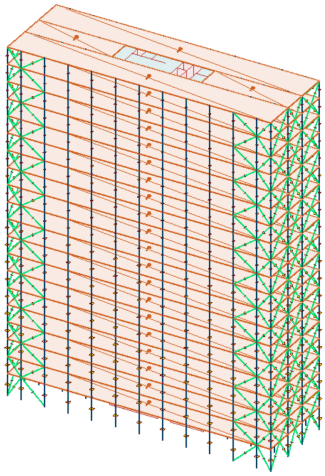

(b) Model 2 – Folded bracing on long façade.

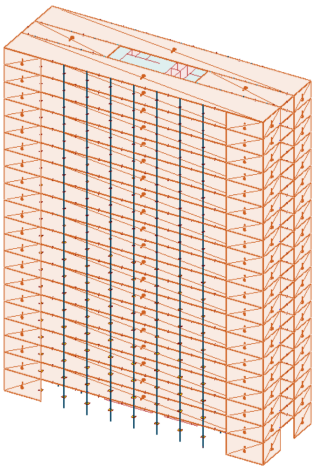

(c) Model 3 – 180 mm CLT walls, open at mid-span.

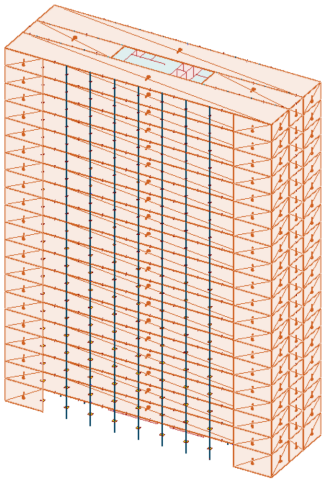

(d) Model 4 – 180 mm CLT walls across short side.

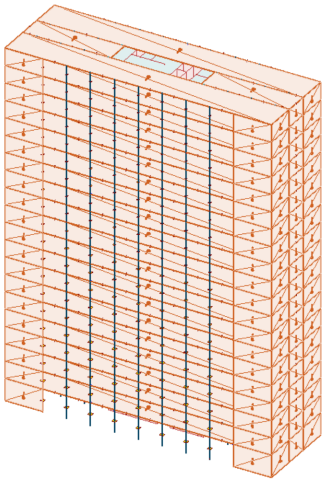

(e) Model 5 – 240 mm CLT walls across short side.

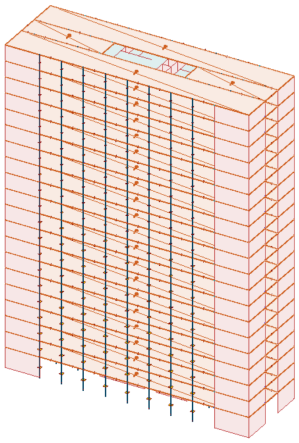

(f) Model 6 – 300 mm concrete walls, open at mid-span.

Figure 4.2: Structural modelling configurations (a)-(f).

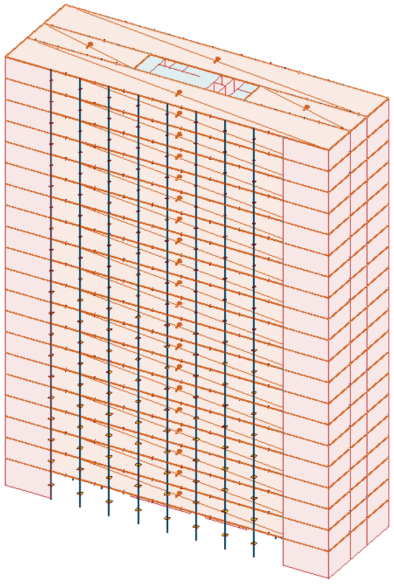

(g) Model 7 – 300 mm concrete walls across short side.

Figure 4.3: Structural modelling configuration (g).

Table 4.1: Eigenfrequencies, mass, equivalent mass and peak acceleration for single-core models. Asterisk (*) denotes the torsional mode.

Model	Mode 1 [Hz]	Mode 2 [Hz]	Mode 3 [Hz]	Mass [ton]	Eqv.Mass [ton/m]	Acc. [m/s^2]
Model 1	0.571	1.161*	1.219	9 578	134.9	0.106
Model 2	0.670	1.237	1.409*	9 633	135.7	0.088
Model 3	0.456	0.925*	1.232	9 443	133.0	0.135
Model 4	0.563	1.149*	1.237	9 492	133.7	0.108
Model 5	0.621	1.211	1.278*	9 676	136.3	0.096
Model 6	0.529	0.992*	1.182	12 157	171.2	0.092
Model 7	1.165	1.194	2.181*	12 645	178.1	0.036

Model 7, featuring full concrete walls along the short façades, is the only configuration that produced a notable improvement in torsional stiffness and mode separation. This solution involves extensive use of concrete and is therefore not considered an option for the intended design. For the other configurations, the torsional frequency was only marginally affected, demonstrating that the global stiffness is not easily increased without more substantial changes. One underlying reason is the building's geometry, with a large width-to-depth ratio that inherently lowers the rotational frequency. Among the remaining configurations, Model 2, featuring bracing at the short façades with extensions over the long side, offered the best improvement in

torsional stiffness without increasing concrete volume, and was therefore selected for further analysis.

4.3.2 Comparative Study: 1-Core vs. 2-Core

To further investigate the influence of core layout and bracing on dynamic performance, additional analyses were performed for both the 1-Core and 2-Core configurations (see Figure 3.1 and 3.3). Each layout was tested with three different bracing strategies:

- No bracing
- Regular bracing (along the short sides)
- Folded bracing (along the short sides and partially extended along the long façades)

Table 4.3 presents the dynamic properties for each setup, showing the first bending modes in the weak and strong directions as well as the first torsional mode. Although the 2-Core layout was initially expected to provide better torsional stiffness due to the spread of cores toward the short façades, results showed a very similar torsional performance between the two layouts when identical bracing configurations were used. This highlights the importance of applying the same bracing setup to ensure a fair comparison. While torsional behaviour was comparable, the 2-Core layout consistently showed lower stiffness in the strong direction. For instance, strong-axis frequencies ranged from 0.813 to 0.853 Hz for the 2-Core setup, compared to 1.219 to 1.237 Hz for the 1-Core model.

Based on these early findings, further torsional analysis was not pursued in this thesis. Although torsional modes appearing early may be a concern, more detailed studies would be needed to check if the structure meets the requirements of ISO 10137:2008.

Table 4.3: Dynamic properties for single-core and dual-core structures. Asterisk (*) denotes the torsional mode.

Core	Config.	Mode 1 [Hz]	Mode 2 [Hz]	Mode 3 [Hz]	Eqv. Mass [ton/m]	Acc. [m/s²]
1-Core	No Bracing	0.439	0.829*	1.219	133.9	0.140
	Regular B.	0.571	1.161*	1.219	134.9	0.106
	Folded B.	0.670	1.237	1.409*	135.7	0.088
2-Core	No Bracing	0.433	0.813	0.858*	140.0	0.136
	Regular B.	0.561	0.814	1.045*	140.4	0.104
	Folded B.	0.660	0.853	1.231*	141.8	0.086

4.3.3 Verification in the Longitudinal Direction

The strong (longitudinal) direction was also reviewed during early analysis for the most critical configuration, the 2-Core layout with a 300 mm core and no concrete slabs. As previously shown, the 2-Core layout consistently demonstrated lower stiffness in the strong direction compared to the 1-Core alternative.

Since higher natural frequencies correspond to lower permissible accelerations (for buildings with fundamental frequencies below 1 Hz), verifying this direction ensures that serviceability limits are met under wind excitation. Table 4.5 summarises the first three modes, total and equivalent mass, and both transverse (Acc.) and longitudinal (Acc_{long}) peak accelerations for heights from 15- to 25 storeys.

Table 4.5: Longitudinal-axis dynamic properties and accelerations for increasing building height. Asterisk (*) denotes the torsional mode.

Storeys	Mode 1 [Hz]	Mode 2 [Hz]	Mode 3 [Hz]	Mass [ton]	EqMass [ton/m]	Acc. [m/s²]	Acc_{long} [m/s²]
15	1.028	1.405	1.741*	7 335	142.79	0.051	0.013
20	0.664	0.854	1.236*	9 864	141.84	0.086	0.024
25	0.472	0.573	0.945*	12 432	141.46	0.125	0.036

Despite the lower stiffness observed in the longitudinal direction for the 2-core configuration, the resulting accelerations remained well below the ISO 10137:2008 comfort limits. This applied to both office use (0.06 m/s²) and residential use (0.04 m/s²), so no further consideration was deemed necessary for the longitudinal direction.

5

Results

This chapter presents the main parametric study, covering a range of building heights and structural configurations. The focus is on how various modelling choices, such as core wall thickness, number and thickness of top concrete slabs and connection conditions, affect the building's dynamic response under wind loading. The SLS is examined in detail, with particular attention to natural frequencies and peak accelerations relative to ISO 10137 comfort criteria. Additionally, selected cases are evaluated for the ULS to assess stress distribution and the risk of cracking in the concrete core. Figures, observations, and numerical data are presented throughout the chapter and the full results and calculation methods are provided in Appendices F, G, H & E.

5.1 Reference models

The analysis began with a set of reference models (Figure 5.1) featuring a 300 mm concrete core and no concrete slabs, developed for 15-, 20-, and 25-storey buildings There models serve as a benchmark for all variations and comparisons presented in Section 5.2. Figure 5.1 plots acceleration versus frequency for both 1-Core and 2-Core systems, including ISO 10137 comfort limits for office and residential buildings to guide performance evaluation.

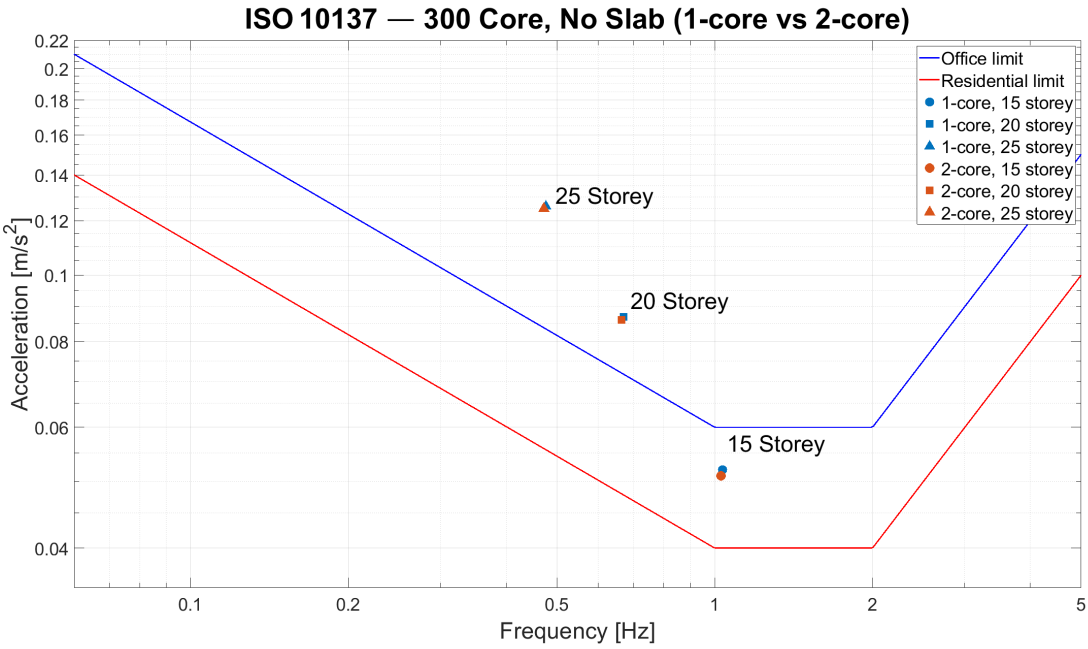

Figure 5.1: ISO 10137 comfort limits with base model results for 15-, 20-, 25-storeys.

5.2 Effect of Modelling Choices

This section presents how different modelling choices affect the building's dynamic response. To improve clarity, the results are presented in two types of graphs. The first graph builds on the ISO 10137 comfort diagram, showing how eigenfrequency and acceleration vary with changes in core configuration and slab arrangement. The second graph type relates acceleration utilization (relative to ISO limits) and frequency to concrete volume, highlighting trade-offs from a sustainability perspective. For this second graph type, results are presented separately for each building height: 15, 20, and 25 storeys.

Each subsection investigates a specific modelling parameter:

- Variation in core thickness
- Addition of concrete slabs
- Changes in slab thickness

Finally, Section 5.2.4 presents the influence of connection and support types. This part explores how different boundary conditions affect the building's eigenfrequencies and accelerations and gives an idea of how support choices impact the overall structure.

5.2.1 Different thickness of concrete core

To examine the impact of core wall thickness on structural performance, three different thicknesses, 300 mm, 400 mm, and 500 mm, were analysed for each building height (15, 20, and 25 storeys), see Figure 5.2-5.5. All models use CLT floor slabs, meaning no heavy concrete slabs have been included at this stage.

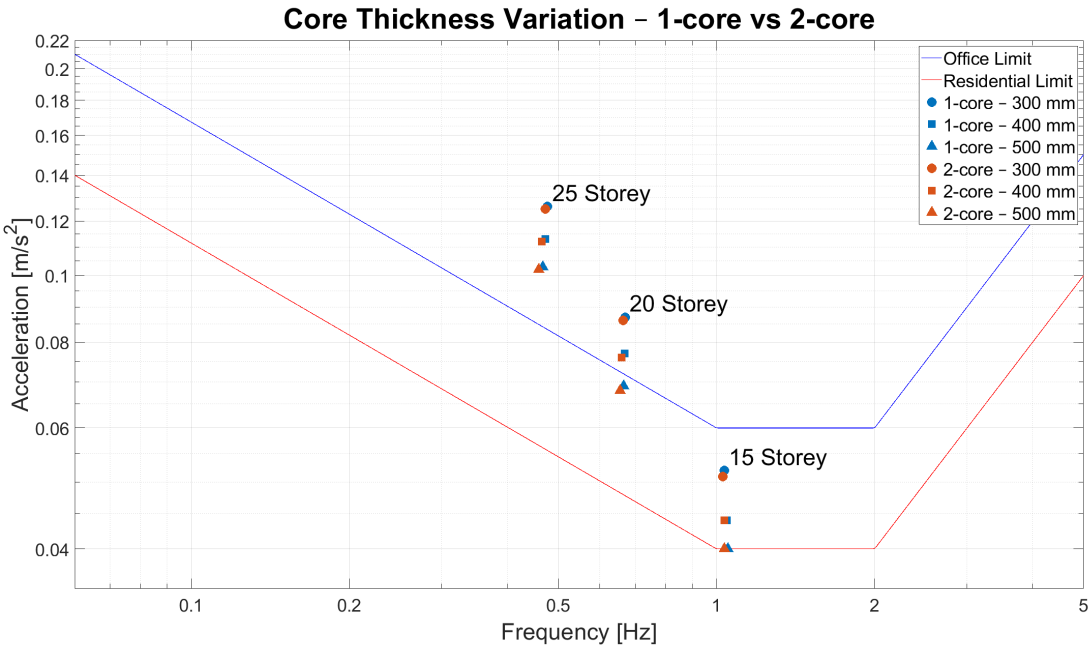

Figure 5.2: ISO 10137 comfort limits with results for varying core thickness (300, 400, 500 mm) for 1-Core and 2-Core layouts at 15, 20, and 25 storeys

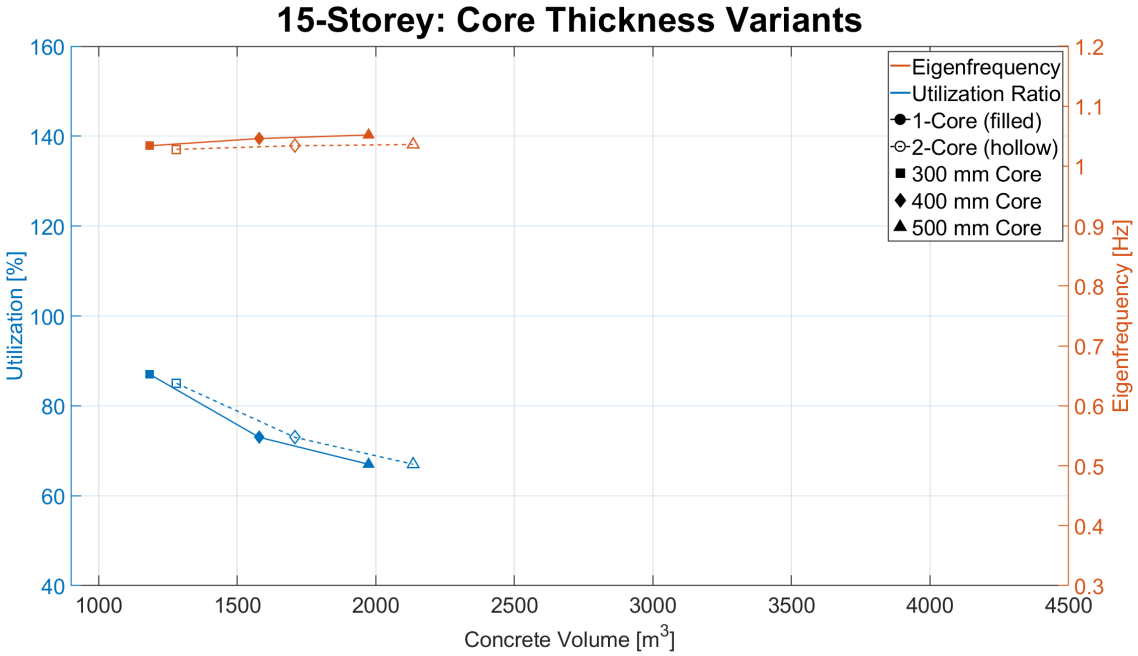

Figure 5.3: Utilization ratio and eigenfrequency for different core thicknesses in a 15-storey building.

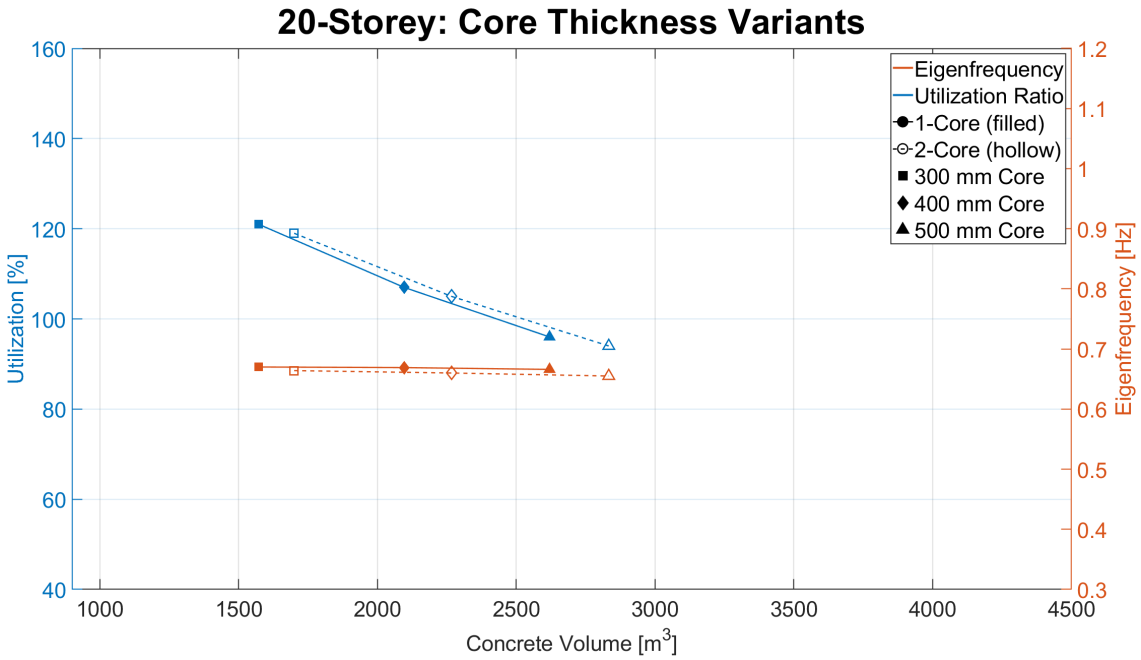

Figure 5.4: Utilization ratio and eigenfrequency for different core thicknesses in a 20-storey building.

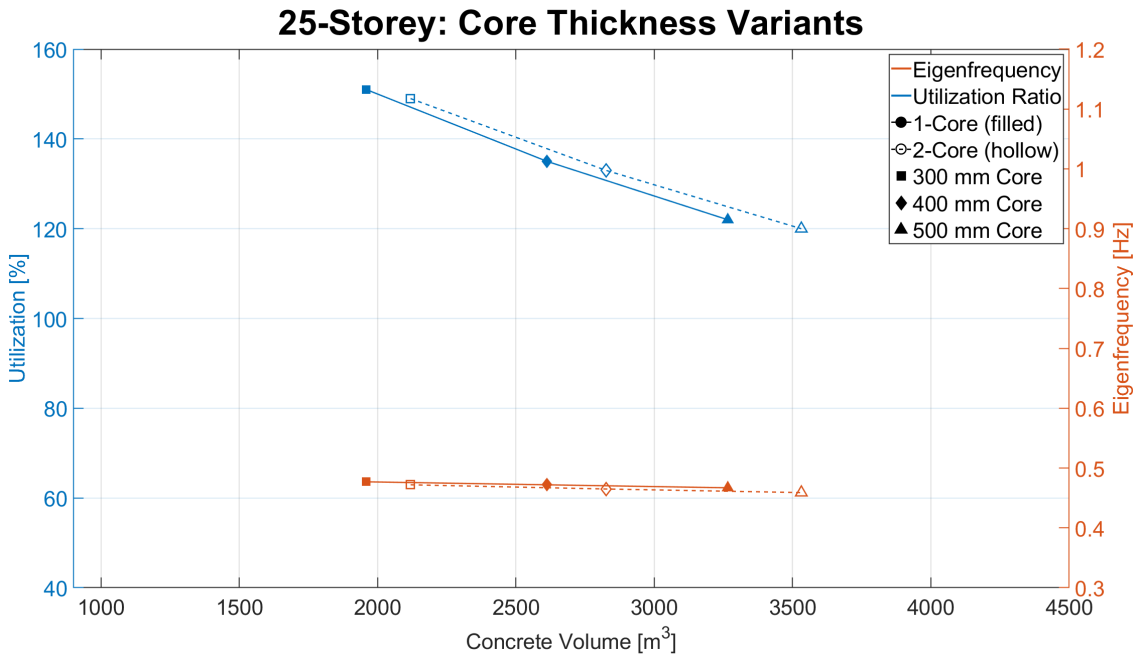

Figure 5.5: Utilization ratio and eigenfrequency for different core thicknesses in a 25-storey building.

The eigenfrequencies remain relatively constant across the different core thicknesses, indicating that increasing wall thickness alone has limited impact on the building's natural frequency. Likely due to the added stiffness being offset by increased mass. Thicker core walls do result in lower acceleration utilization, improving comfort performance, this comes at the cost of greater concrete volume.

5.2.2 Adding concrete slabs

To assess the impact of adding heavy concrete slabs at the top of the building, models with 15, 20, and 25 storeys were analysed using a constant core wall thickness of 300 mm. Each variant included 0, 1, 3, or 5 concrete slabs, each 300 mm thick, placed in the uppermost storeys and is presented in Figure 5.6-5.9.

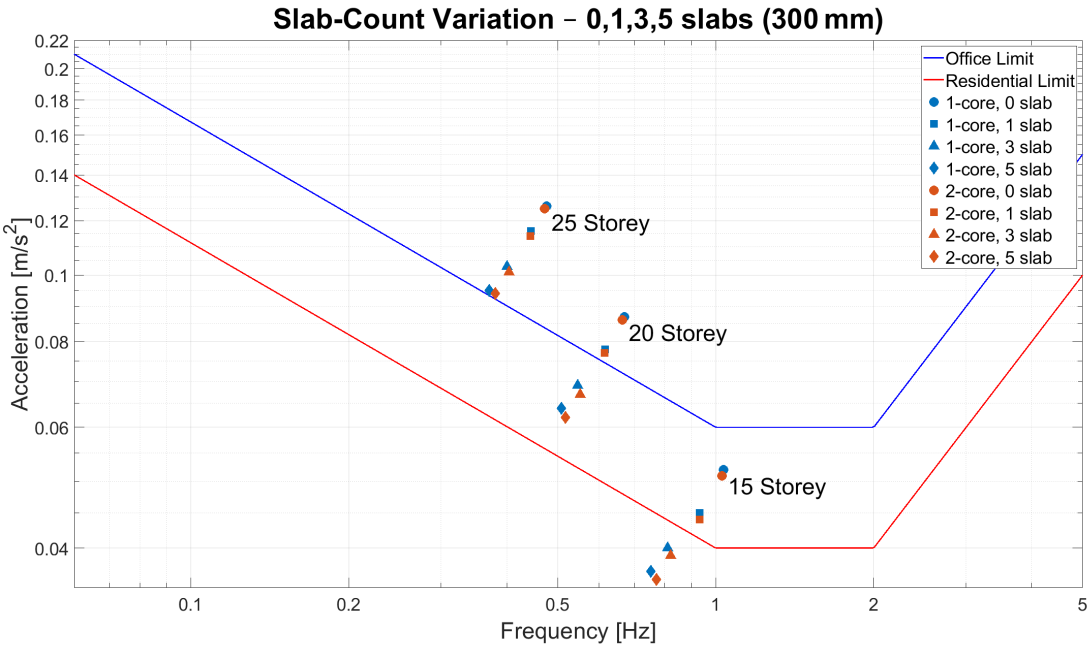

Figure 5.6: ISO 10137 comfort limits with results for varying number of concrete slabs (300 mm) for 1-Core and 2-Core layouts at 15, 20, and 25 storeys.

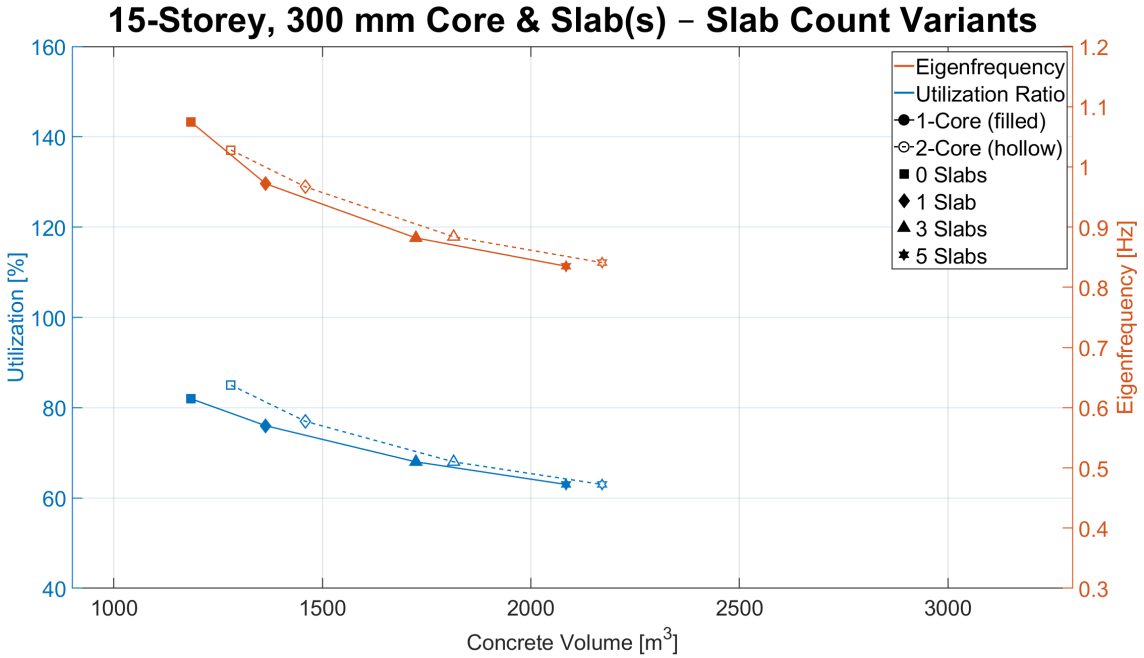

Utilization ratio and eigenfrequency for different number of concrete slabs (300 mm) in a 15-storey building.

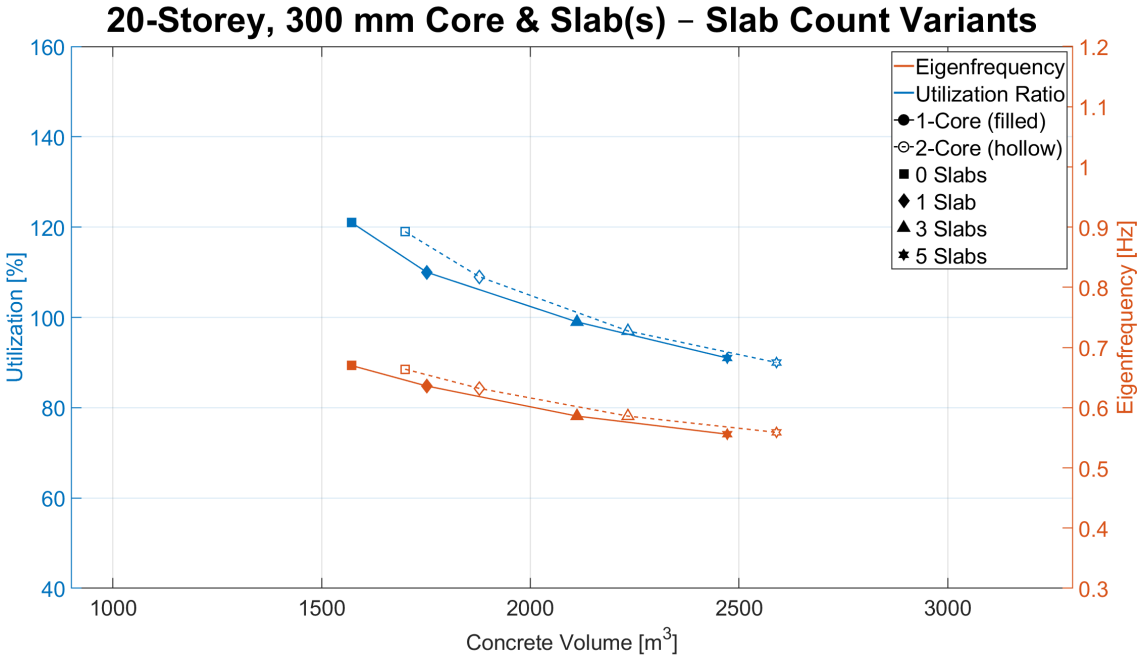

Figure 5.8: Utilization ratio and eigenfrequency for different number of concrete slabs (300 mm) in a 20-storey building.

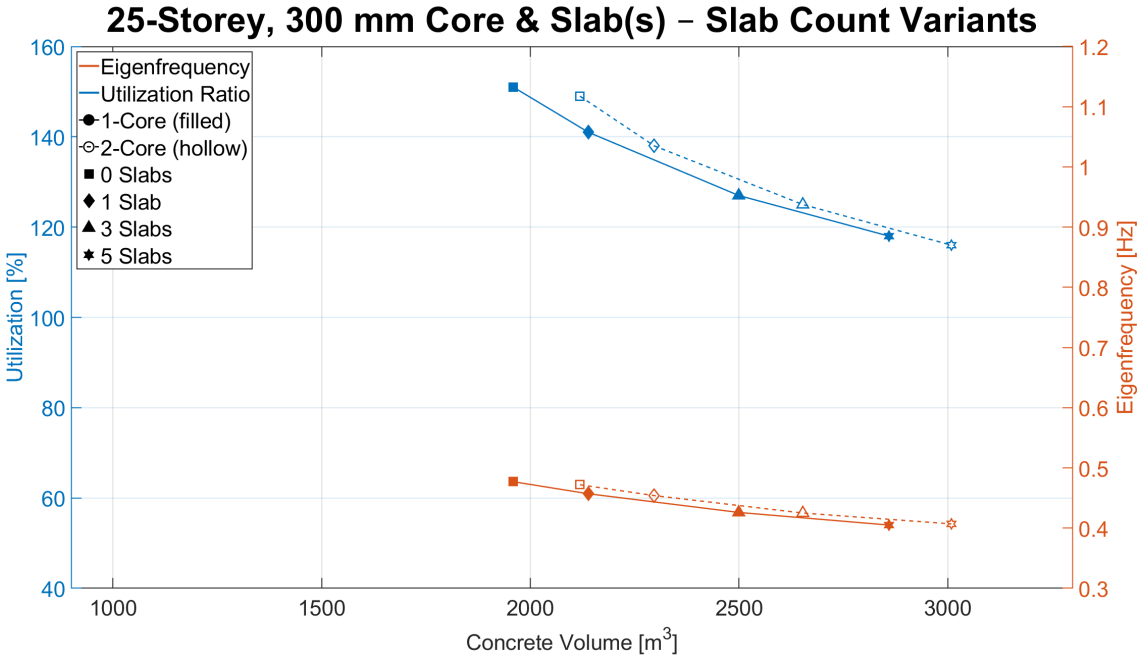

Figure 5.9: Utilization ratio and eigenfrequency for different number of concrete slabs (300 mm) in a 25-storey building.

Across all building heights, the addition of slabs led to a clear reduction in both acceleration levels and eigenfrequencies, indicating improved comfort performance. Unlike the core thickness study, the frequencies decreased more noticeably as more slabs were added. This outcome is expected, as placing additional mass at the top increases the structure's equivalent mass, thereby lowering its natural frequency.

5.2.3 Different thickness of concrete slab

To assess the impact of slab thickness on dynamic performance, models were analysed with varying top-slab thicknesses: 200 mm, 300 mm, and 400 mm, along with a baseline case with no slab. The slab was placed at the top storey and the core thickness remained fixed at 300 mm. Figure 5.10-5.13 shows these setups and the results.

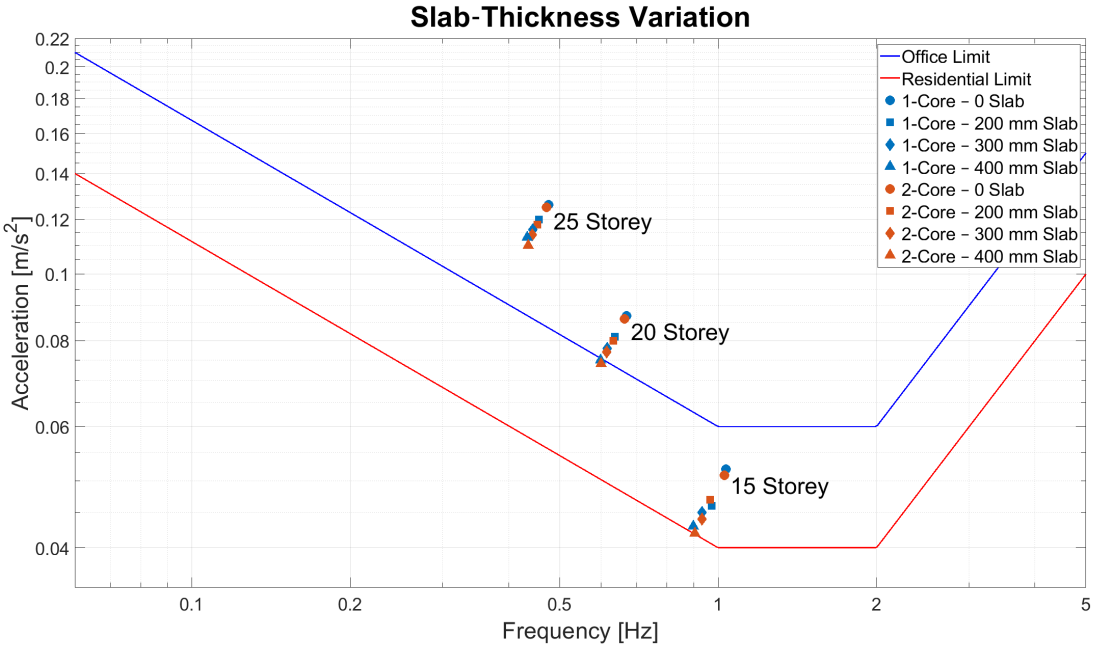

Figure 5.10: ISO 10137 comfort limits with results for varying slab thickness (200, 300, 400 mm) for 1-Core and 2-Core layouts at 15, 20, and 25 storeys.

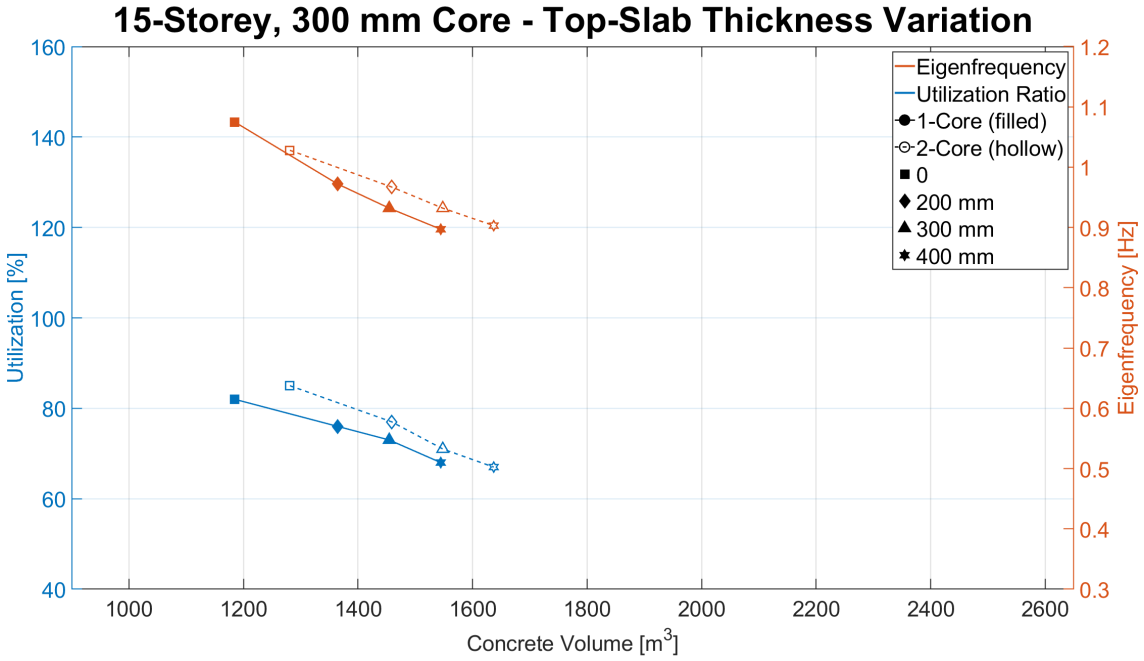

Figure 5.11: Utilization ratio and eigenfrequency for different thickness of top level concrete slab in a 15-storey building.

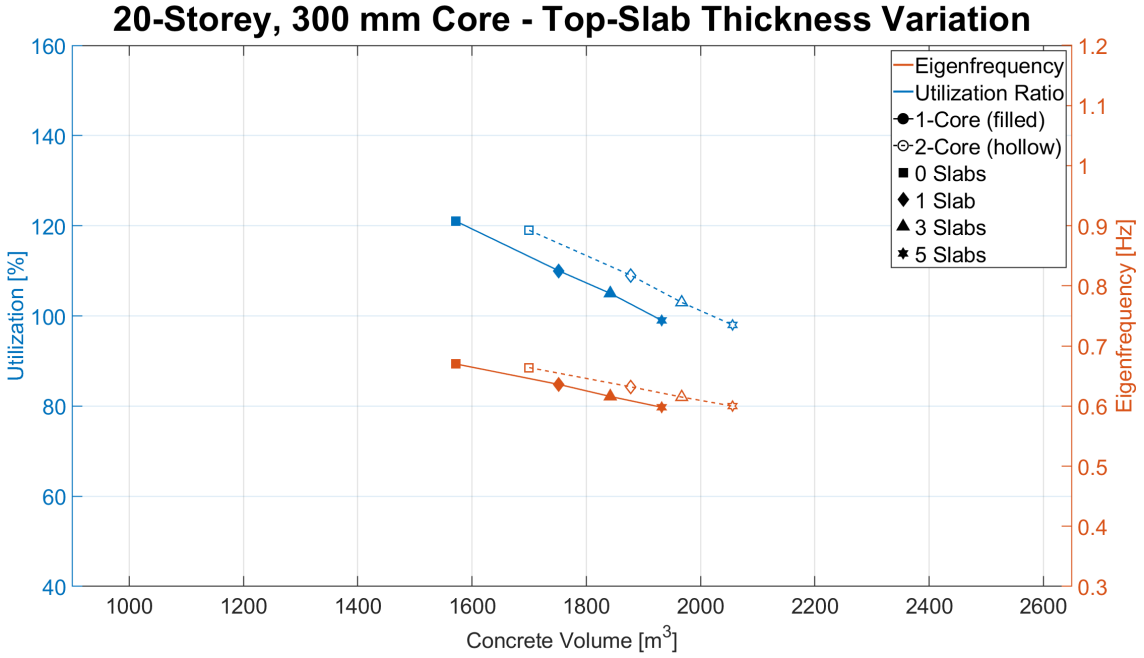

Figure 5.12: Utilization ratio and eigenfrequency for different thickness of top level concrete slab in a 20-storey building.

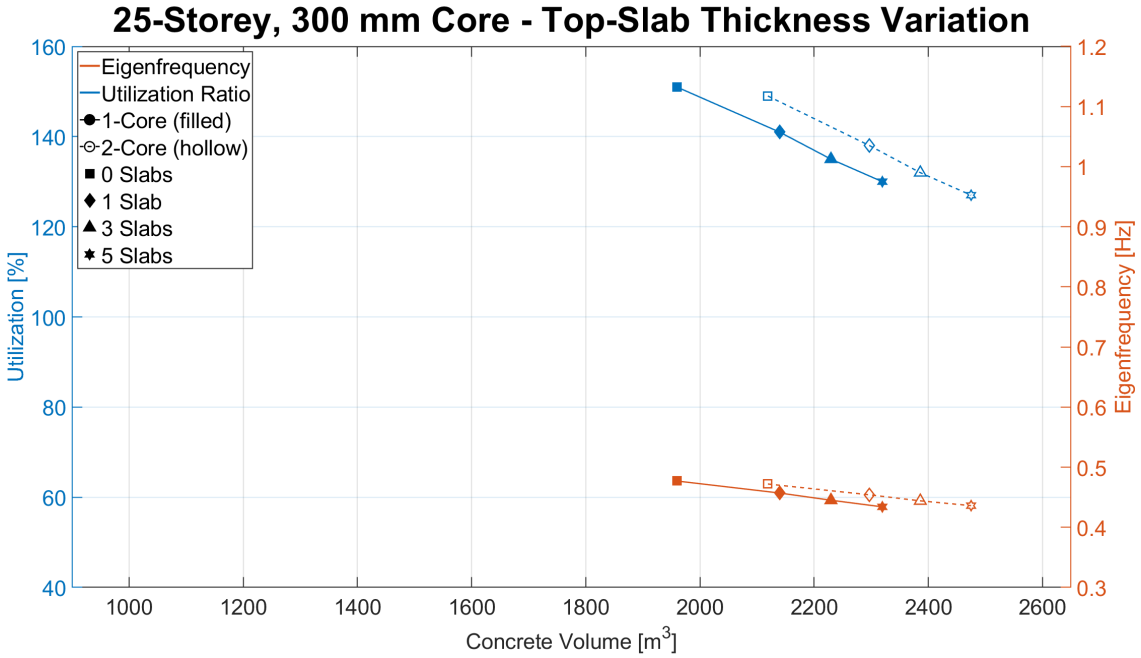

Figure 5.13: Utilization ratio and eigenfrequency for different thickness of top level concrete slab in a 25-storey building.

Across all building heights, increasing the slab thickness led to improved comfort performance. The results closely resemble those from adding multiple slabs, confirming that increased mass at the top enhances comfort, consistent with theoretical expectations.

5.2.4 Connection and support types

To evaluate how connection assumptions affect the global dynamic response, a 25-storey model with 3 x 300 mm concrete slabs was analysed under four different boundary condition schemes. In each successive case, additional elements were changed from hinged to fixed, increasing the overall stiffness of the structure.

- **Case 1:** All connections are hinged, except for a fixed connection between core segments (representing cast-in-situ concrete).
- **Case 2:** Fixed supports are added at the base of both the columns and the core.
- **Case 3:** Continuity is added to the columns, replacing hinge connections.
- **Case 4:** Continuity is added to the beams, and the beam-to-column connections are changed from hinged to fixed, creating a fully rigid frame.

Table 5.1 shows that Mode 1–3 frequencies and peak acceleration remain nearly unchanged across the cases, indicating that the global dynamic response is insensitive to the variation of the boundary condition.

Table 5.1: Global dynamic properties under different boundary conditions (25 storeys, 3 slabs). Asterisk (*) denotes the torsional mode.

Boundary Condition	**Mode 1 [Hz]**	**Mode 2 [Hz]**	**Mode 3 [Hz]**	**Mass [ton]**	**EqMass [ton/m]**	**Acc. [m/s^2]**
Case 1	0.380	0.667	0.812*	14 560.6	234.9	0.097
Case 2	0.381	0.677	0.814*	14 560.6	234.9	0.096
Case 3	0.381	0.677	0.814*	14 560.6	234.9	0.096
Case 4	0.383	0.692	0.824*	14 560.6	234.9	0.096

5.3 Summation

This section summarises the results of the parameter studies carried out to evaluate how different modeling choices affect the building's dynamic behaviour and material usage. The goal is to identify which combinations of core and slab configurations offer the most efficient balance between comfort performance (in terms of acceleration utilization) and concrete volume.

To maintain clarity, results are only shown for 1-Core configurations as they show similar results, and the presentation is divided into two parts. The first subchapter presents comparisons based on individual parameter groups, while the second provides a combined summary of all configurations.

5.3.1 Parameter-Based Summation

The following graphs present the results of the parameter-based comparison. The results are divided into two combinations:

- The first focusing on variations in core thickness (300 mm, 400 mm, and 500 mm), each combined with 0, 1, 3, and 5 concrete slabs of 300 mm thickness.
- The second focusing on variations in concrete slab thickness (200 mm, 300 mm, and 400 mm), combined with a fixed core thickness of 300 mm and 0, 1, 3, and 5 slabs.

This structure facilitates the interpretation of results and allows for clearer identification of how each parameter and their combinations influence the outcome.

5.3.2 Variations in core thickness combined with number of slabs

Graph 5.14-5.16 illustrate how changes in core thickness (300 mm, 400 mm, and 500 mm), combined with 0, 1, 3, and 5 concrete slabs of 300 mm thickness, influence dynamic performance across 15-, 20-, and 25-storey buildings. In all configurations, increasing the number of slabs corresponds with improved comfort performance, particularly with thinner cores. However, certain cases with five slabs exhibit higher utilization ratios compared to configurations with fewer slabs and thicker cores.

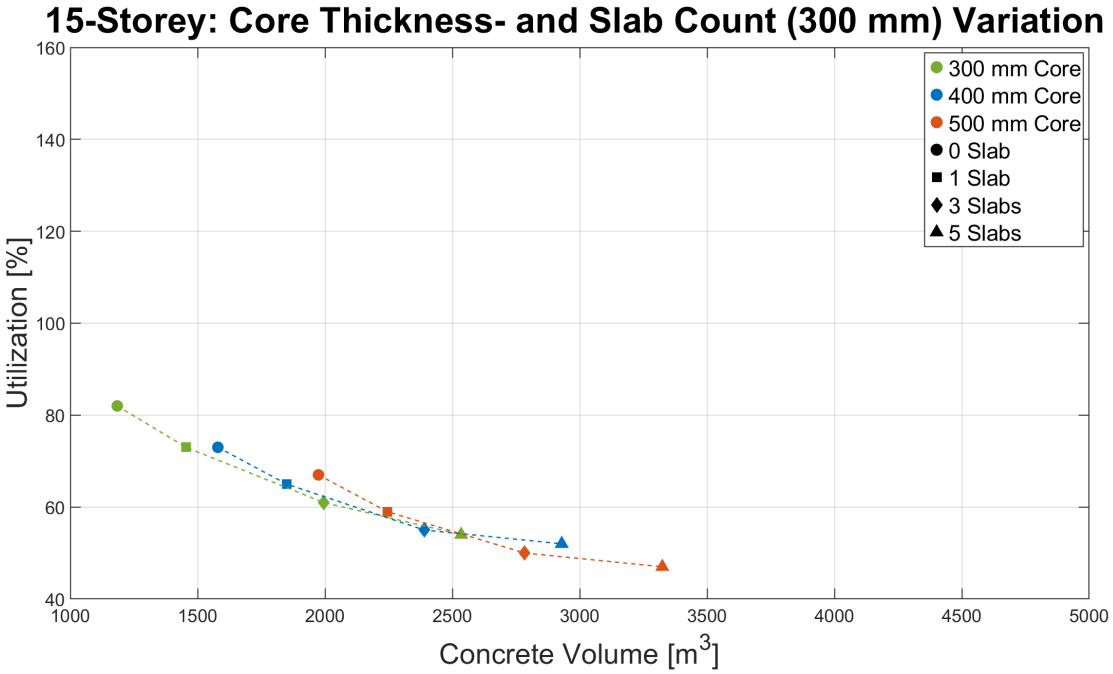

Figure 5.14: Utilization ratio versus concrete volume for different combinations of core thickness and number of 300 mm slabs in a 15-storey building.

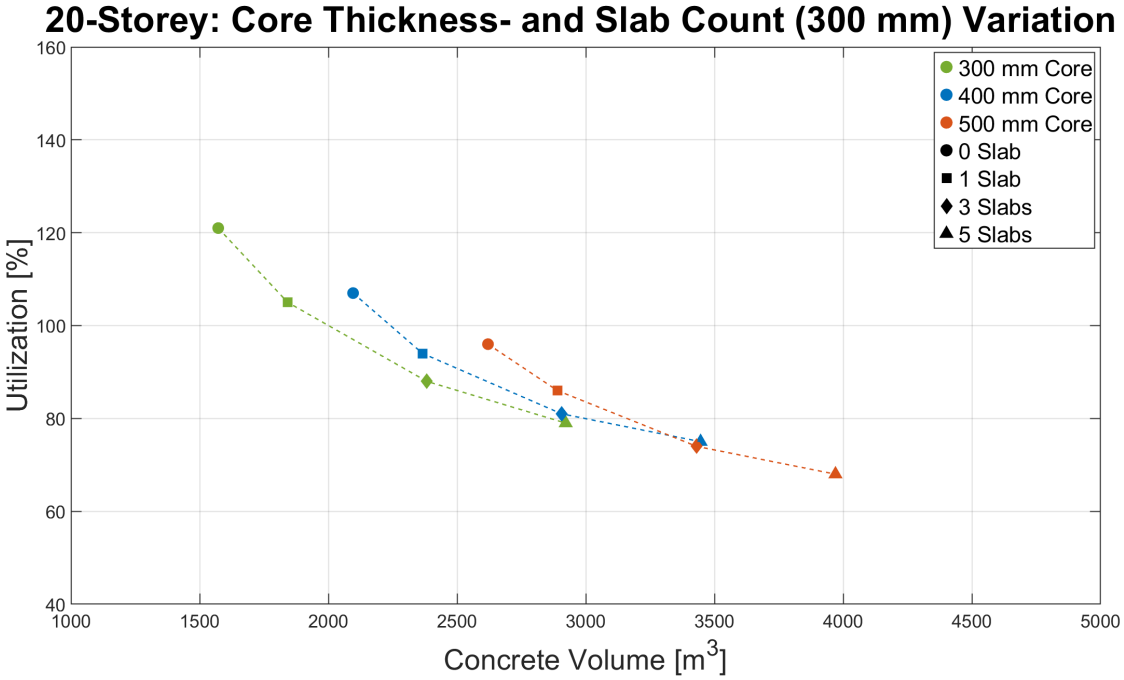

Utilization ratio versus concrete volume for different combinations of core thickness and number of 300 mm slabs in a 20-storey building.

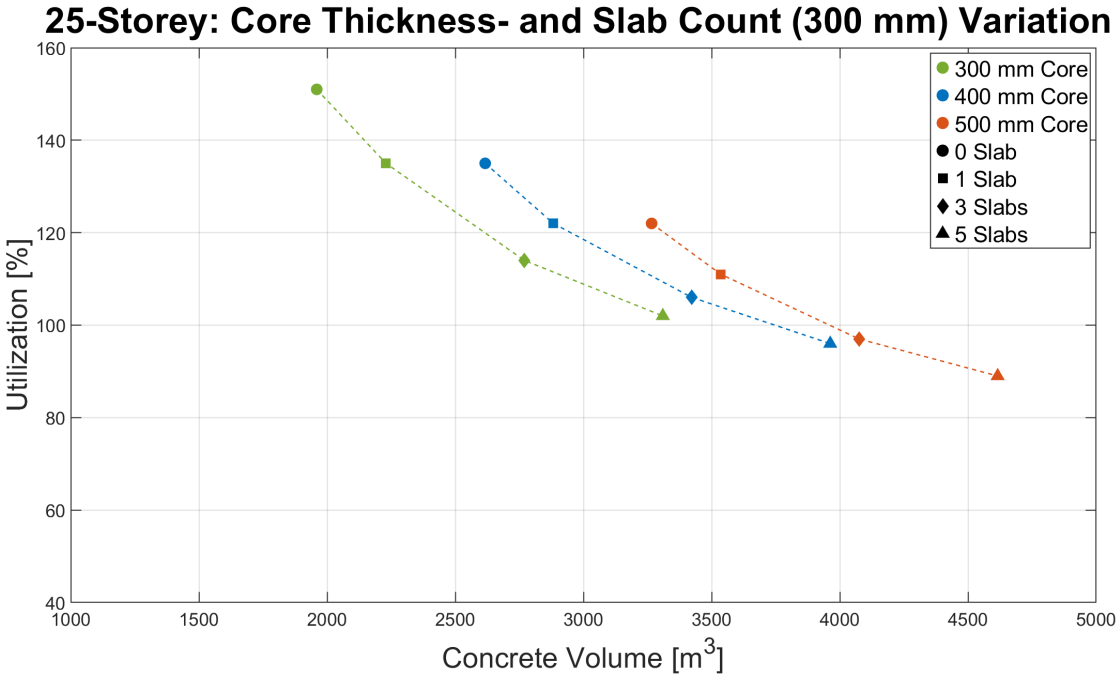

Figure 5.16: Utilization ratio versus concrete volume for different combinations of core thickness and number of 300 mm slabs in a 25-storey building.

5.3.3 Variations in concrete slab thickness combined with number of slabs

Graph 5.17-5.19 show how adding 0, 1, 3, and 5 concrete slabs of 300 mm thickness affects dynamic performance across 15-, 20-, and 25-storey buildings. As seen in the plots, both eigenfrequency and acceleration utilization decrease as more slabs are added. Compared to earlier results, the effect of slab thickness is more clearly visible here, with thicker slabs leading to greater improvements in comfort performance. Meaning that configurations with fewer but thicker slabs perform better than those with several thinner ones, offering a more material-efficient way to reduce accelerations and enhance occupant comfort.

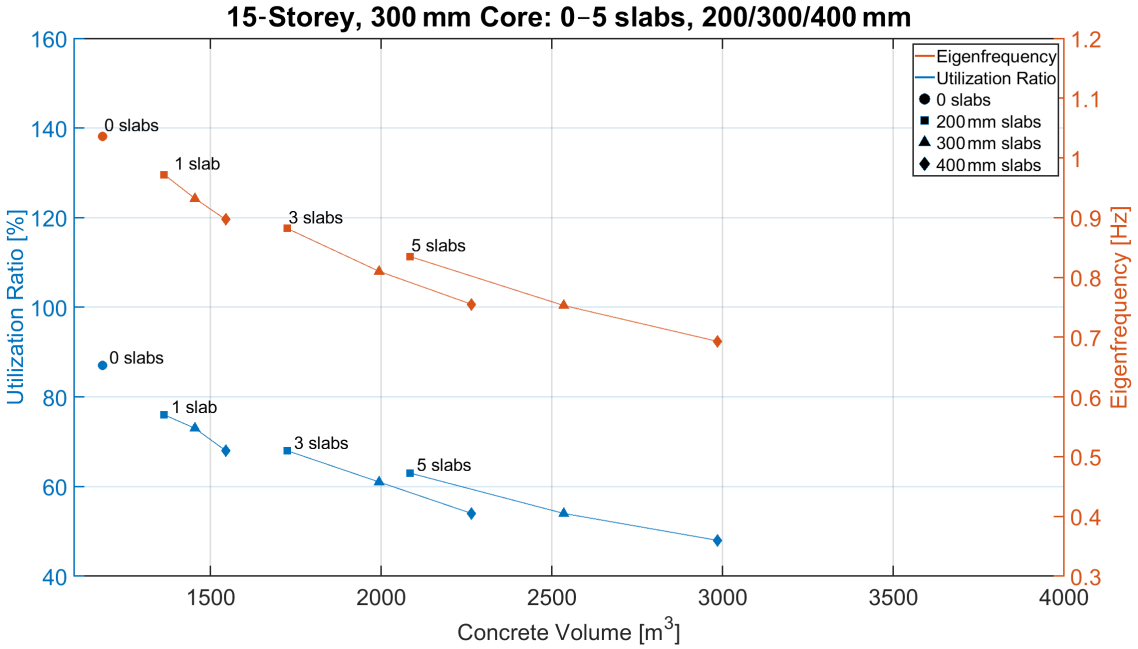

Figure 5.17: Utilization and eigenfrequency vs concrete volume for 15-storey building with 300 mm core. Results shown for 0–5 concrete slabs and varying slab thicknesses (200, 300, 400 mm).

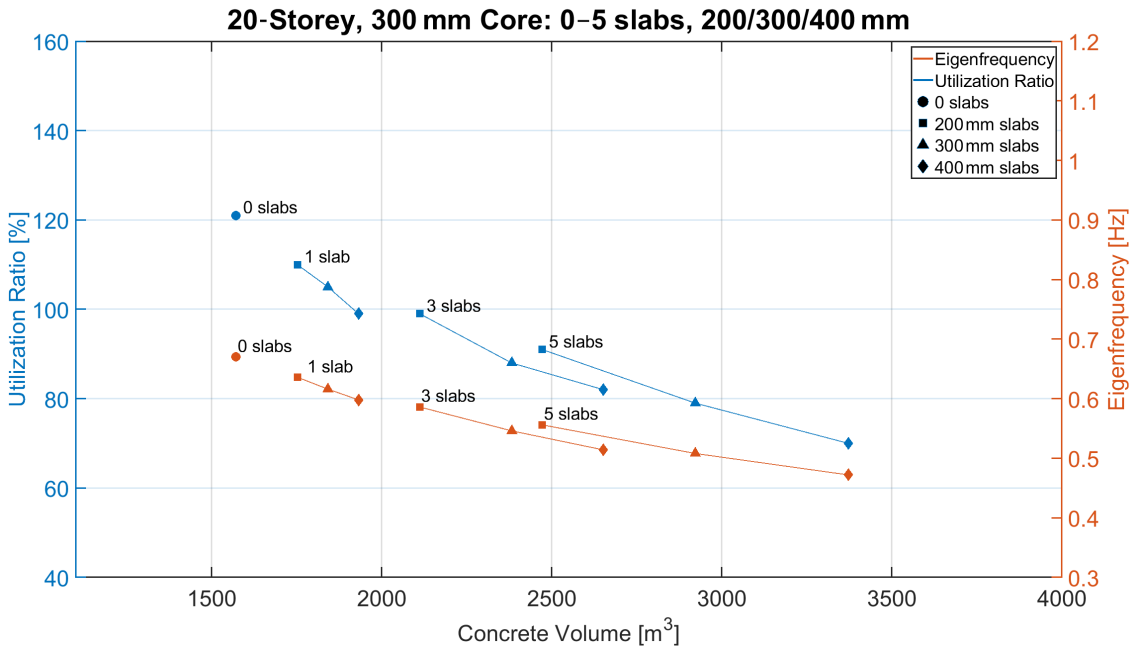

Figure 5.18: Utilization and eigenfrequency vs concrete volume for 20-storey building with 300 mm core. Results shown for 0–5 concrete slabs and varying slab thicknesses (200, 300, 400 mm).

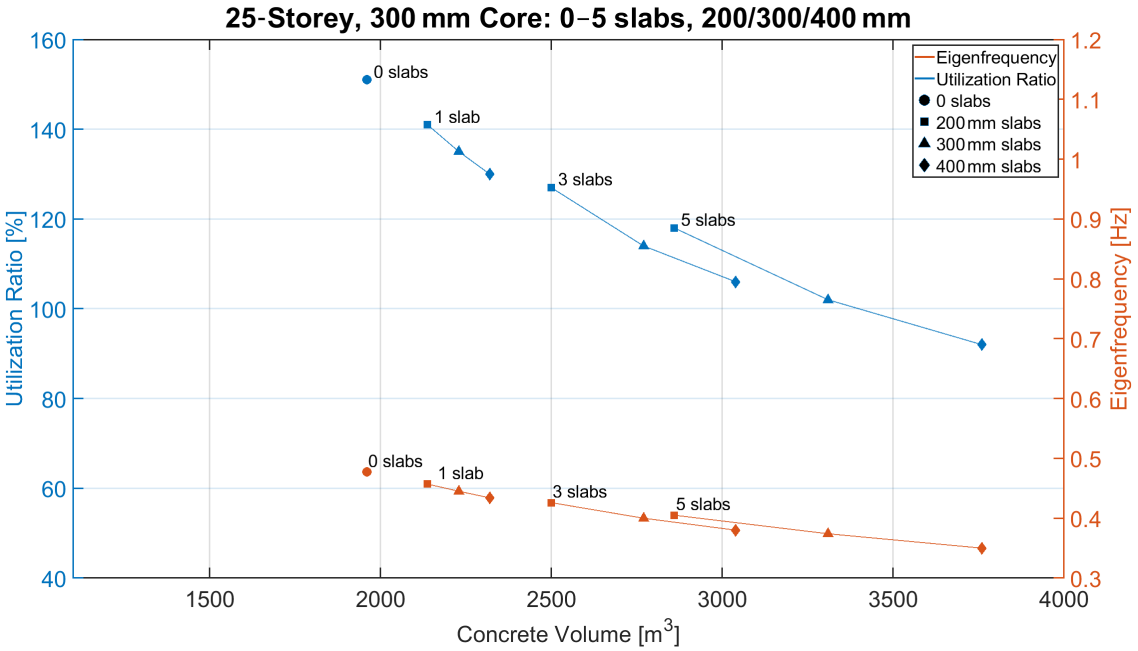

Figure 5.19: Utilization and eigenfrequency vs concrete volume for 25-storey building with 300 mm core. Results shown for 0–5 concrete slabs and varying slab thicknesses (200, 300, 400 mm).

5.3.4 Combined Summary

To conclude the analysis, Figure 5.20 presents a combined ISO 10137 diagram, illustrating the dynamic performance of all studied configurations across 15-, 20-, and 25-storey buildings. The figure provides a comprehensive overview of how different combinations of core thicknesses and slab arrangements influence acceleration and frequency in relation to the comfort limits for office and residential buildings.

This is followed by Figures 5.21–5.23, which show acceleration utilization (relative to ISO limits) as a function of concrete volume for each building height. Eigenfrequency values are excluded from these graphs to enhance clarity and focus attention on material efficiency.

As seen in the results, certain configurations achieve lower utilization levels while using less concrete than others. Highlighting that efficient dynamic behaviour does not necessarily require increased material volume. This insight is especially relevant from a sustainability perspective when optimising structural mass versus comfort performance.

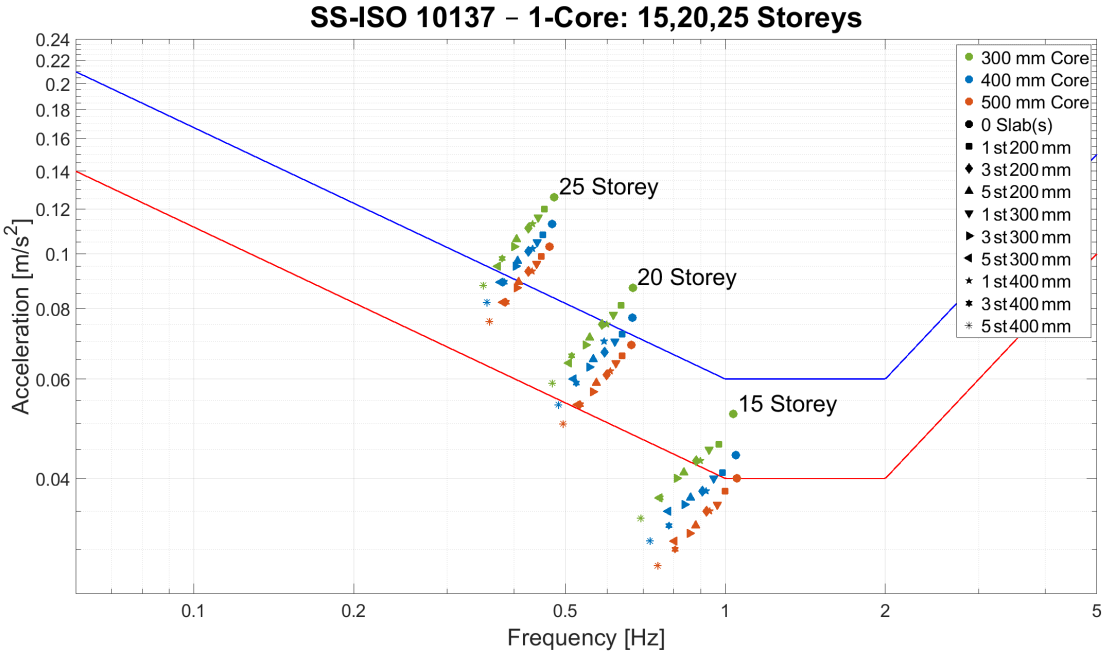

Figure 5.20: ISO 10137 comfort diagram showing the combined impact of core thickness and slab configuration on acceleration and eigenfrequency for 1-Core configurations at 15, 20, and 25 storeys.

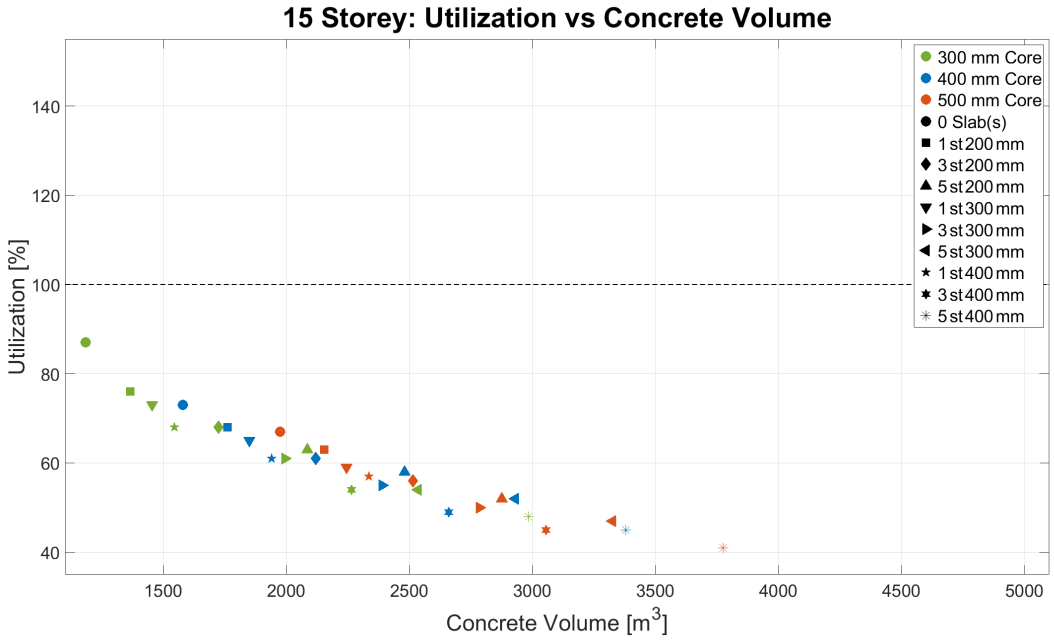

Figure 5.21: Utilization versus concrete volume for 15-storey buildings with varying combinations of core thickness and number/thickness of top concrete slabs (1-Core configuration).

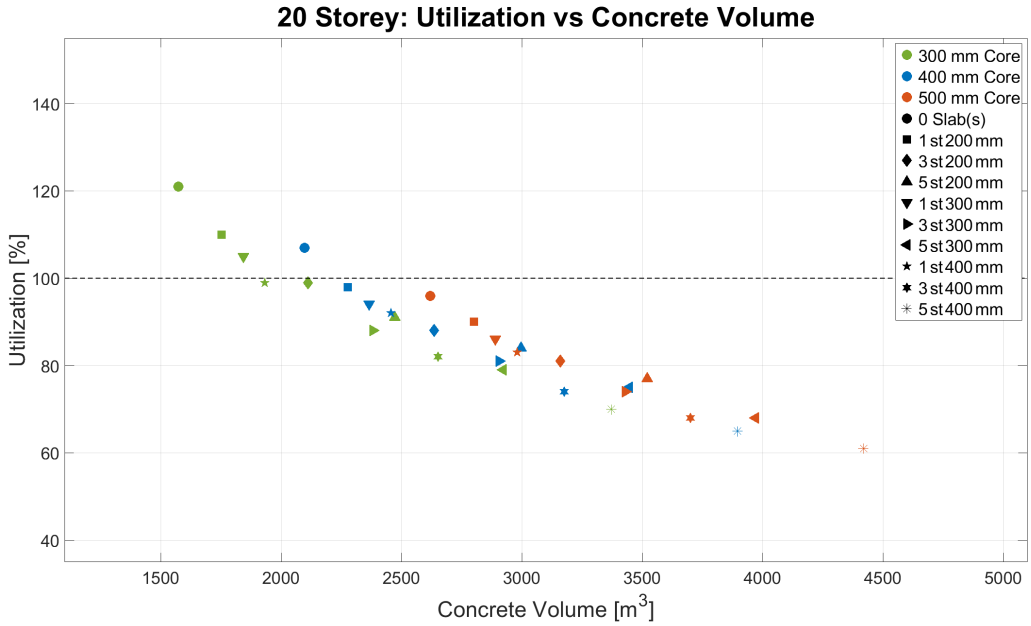

Figure 5.22: Utilization versus concrete volume for 20-storey buildings with varying combinations of core thickness and number/thickness of top concrete slabs (1-Core configuration).

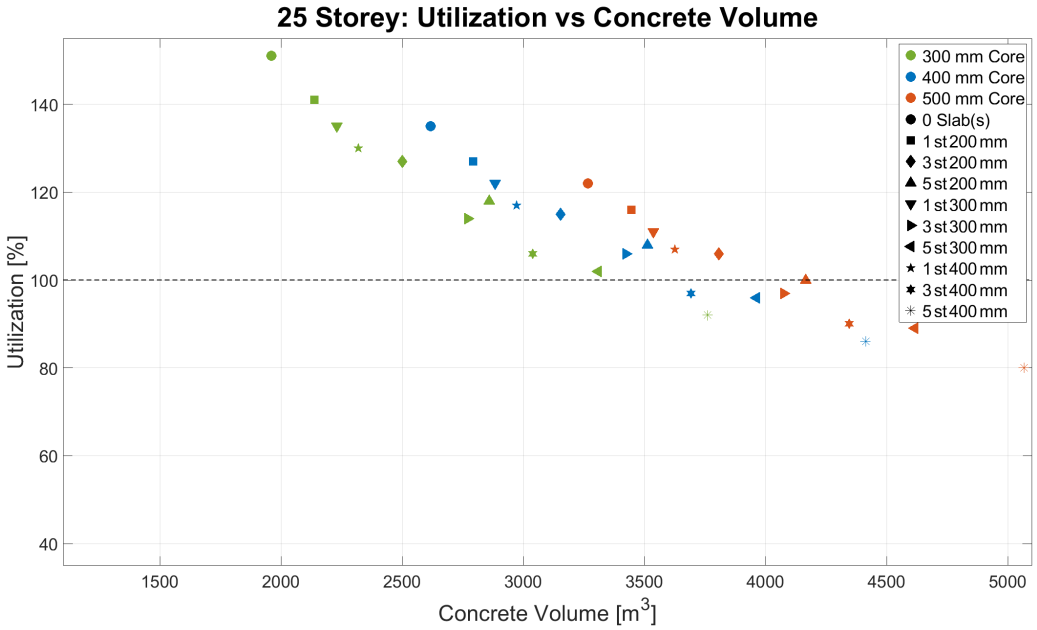

Figure 5.23: Utilization versus concrete volume for 25-storey buildings with varying combinations of core thickness and number/thickness of top concrete slabs (1-Core configuration).

5.4 Ultimate Limit State

For the ULS the most critical configurations were analysed to assess stresses within the concrete core. While ULS design checks were also performed for columns, beams and bracing elements, these components are not presented here, as they do not significantly influence the building's global dynamic behaviour. In contrast, the concrete core plays a key structural role, governing both the overall stiffness and vibrational characteristics of the building. It is therefore the primary focus of the ULS assessment, complementing the earlier SLS evaluation.

Figures 5.24– 5.27 present the maximum compressive and tensile stresses in the concrete core under ULS wind loading. The figures compare three core thicknesses (300, 400, and 500 mm) and show the influence of adding five heavy concrete slabs (400 mm) at the top, illustrating how axial and flexural stress distributions are affected by increased building height and additional mass.

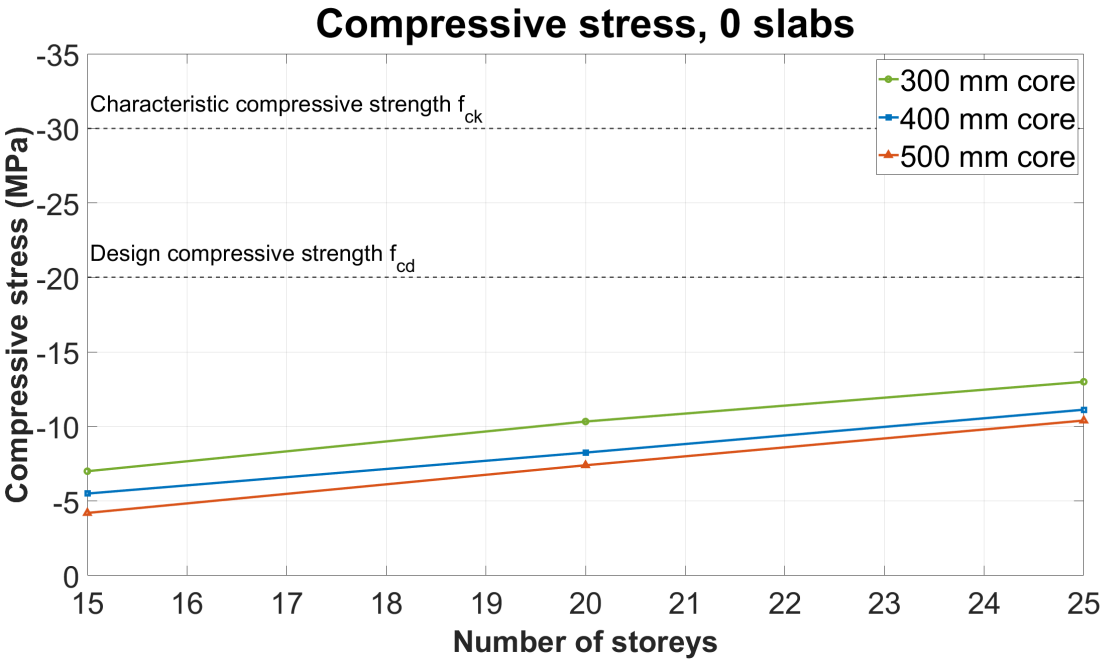

Figure 5.24: Compressive stresses in the core wall under maximum wind load for configurations with 0 slabs. Results are shown for core thicknesses of 300, 400, and 500 mm.

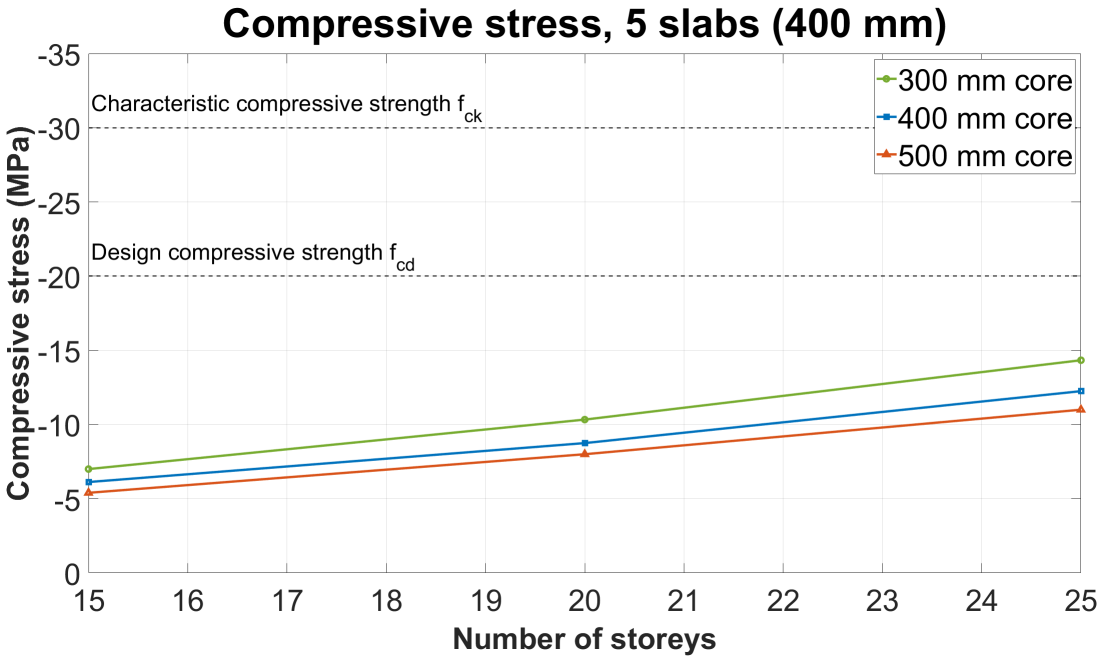

Figure 5.25: Compressive stresses in the core wall under maximum wind load for configurations with 5 concrete slabs (400 mm). Results are shown for core thicknesses of 300, 400, and 500 mm.

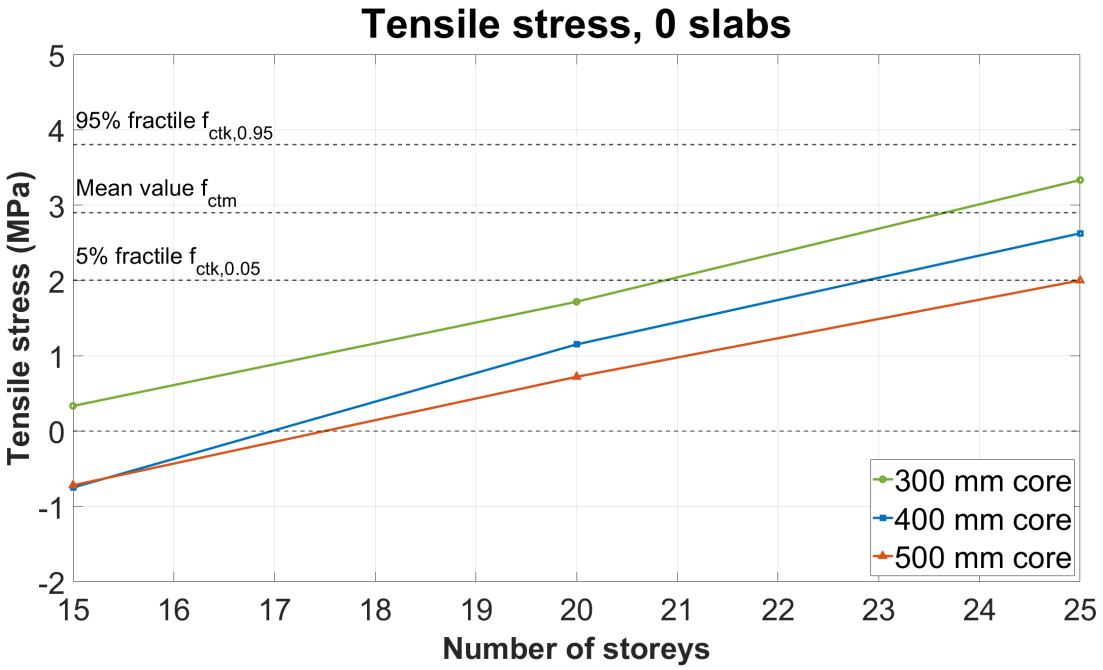

Figure 5.26: Tensile stresses in the core wall under maximum wind load for configurations with 0 concrete slabs. Results are shown for core thicknesses of 300, 400, and 500 mm.

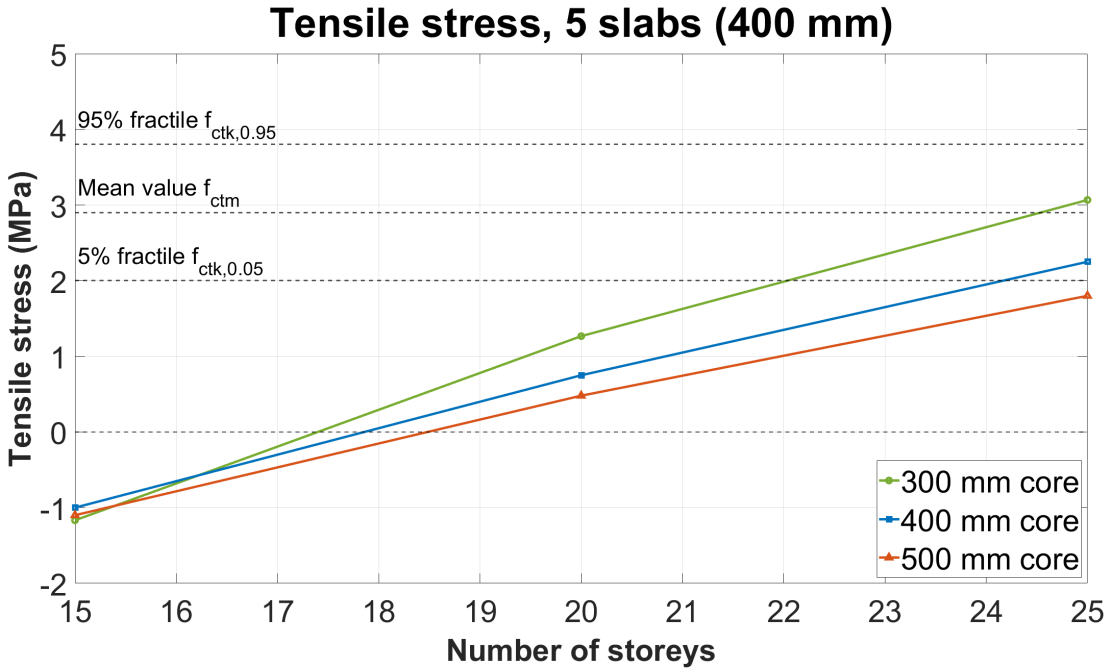

Figure 5.27: Tensile stresses in the core wall under maximum wind load for configurations with 5 concrete slabs (400 mm). Results are shown for core thicknesses of 300, 400, and 500 mm.

The results showed clear trends: increasing the core thickness led to a reduction in both compressive and tensile stresses. Conversely, as the building height increased, compressive stresses also increased, and adding concrete slabs at the top further raised these compressive forces. However, in all studied cases, the compressive stress remained well below the concrete's design strength f_{cd}, indicating no concern for crushing.

For tensile stresses, a similar pattern was observed. Thicker cores resulted in lower tensile forces, while taller buildings showed increasing tensile stress. The inclusion of concrete slabs at the top helped reduce tensile forces.

Although most configurations remained within safe limits, some approached or exceeded the 5% fractile tensile strength $f_{ctk,0.05}$. This suggests that cracking may become a concern as buildings approach 25 storeys, especially with thinner cores and minimal slab additions.

6

Discussion

This chapter discusses the results presented in the previous chapter, focusing on their relevance to the research objectives defined in section 1.4 Aim and objectives. The influence of each parameter is evaluated, emphasizing their practical relevance in the design of high-rise hybrid timber–concrete buildings. Furthermore, the ULS considerations and potential strategies for managing structural performance.

6.1 1-Core vs 2-Core layout

The 2-Core model performed slightly better than the 1-Core model in most configurations, but the differences were minor. In the weak direction (the governing case for design), both systems exhibited almost the same stiffness and thus behaved similarly. Interestingly, in the strong direction, the single-core system demonstrated higher stiffness. This is because splitting the core into two parts significantly reduces the moment of inertia, despite the total concrete volume being greater. However, this had little practical impact on the results, as accelerations in the strong direction remained well below the comfort limit and did not govern the design.

Additionally, the 2-Core model performed worse than expected in terms of torsional stiffness. This is due to the spatial separation of the cores, which resulted in an open-section behaviour with less effective resistance to torsion. In contrast, the 1-Core system, with its closed-section geometry, provided better torsional resistance and stiffness, even though it has less concrete volume.

6.2 Influence of Core Thickness

Increasing the concrete core thickness increases global stiffness, which raises the natural frequency. At the same time, the added mass from the thicker core reduces the frequency. For the building, these two effects balance each other out, resulting in a nearly unchanged natural frequency across different core thicknesses. The increased mass did have a beneficial effect on dynamic performance, as it led to a higher equivalent mass, which reduces peak accelerations. Furthermore, increasing the core thickness lowered both compressive and tensile stresses within the core due to the larger cross-sectional area, despite the increase in overall weight.

6.3 Influence of Concrete Slabs

Adding concrete slabs at the upper levels of the structure increases the equivalent mass more effectively, which in turn improves the SLS performance by reducing peak accelerations. Notably, adding mass at higher levels had the greatest impact on increasing equivalent mass. The reduction in acceleration was most noticeable when first increasing the thickness of the slabs, and then by increasing the number of slabs. As more slabs were added, the improvements became progressively smaller, showing diminishing returns.

From a ULS perspective, the increased mass from addition or thicker concrete slabs led to slightly higher compressive forces in the core due to the greater vertical load, which in turn slightly reduced tensile stresses. However, this effect was not significant enough to be considered a viable strategy to prevent cracking in the core.

6.4 Concrete Efficiency

When comparing the effect of all tested parameters, the most concrete-efficient improvement strategy for dynamic performance was to add mass at higher levels of the structure, either by increasing the slab thickness or by adding multiple slabs near the top. These measures significantly improved the equivalent mass and reduced peak accelerations more effectively. Core thickening also produced structural gains, but it was less efficient in terms of concrete use.

However, the results also indicate that adding more slabs is not universally beneficial. In some cases, configurations with five slabs resulted in higher utilization ratios than those with thicker cores, suggesting that excessive slab additions can introduce structural inefficiencies. This highlights the importance of balancing slab mass and core thickness rather than maximizing one parameter alone.

6.5 Influence of Boundary Conditions

The boundary conditions had almost no effect on the global structural response. Changing from pinned to fixed supports resulted in a marginal increase in stiffness, leading to a small increase in the building's eigenfrequency, and the changes in peak acceleration were almost non-existent.

6.6 Ultimate Limit State

The ULS analysis revealed that compressive stresses in the concrete cores remained within acceptable limits for all tested configurations. While the tensile stresses posed a more critical issue. As building height increased, tensile forces approached the tensile strength limit of concrete. In buildings exceeding 20 storeys, the tensile stresses in the core surpassed the cracking threshold, indicating that the concrete would crack under tension.

This cracking would reduce the stiffness of the core and consequently lower the building's overall frequency. A reduction in frequency would lead to higher accelerations, which may compromise comfort levels under wind loading.

To address this, an effective solution is to post-tension the concrete core. This method introduces a pre-compressive force that counteracts the tensile stresses and helps prevent cracking. With post-tensioning, even the 300 mm thick core could potentially meet the ULS criteria. However, more detailed calculations are needed, as post-tensioning increases the compressive stress in the core. This could risk exceeding the concrete's compressive strength.

6.7 Potential Sources of Error

Several assumptions in the modelling process may have influenced the accuracy of the results. While torsional modes were identified during the analysis, they were not explicitly addressed in the design process. This could underestimate wind-induced vibrations, particularly in buildings with asymmetric geometry.

Boundary conditions also present a source of uncertainty. Although variations in connection fixity were explored, the actual performance of structural connections may differ significantly in practice due to semi-rigid behaviour and deformations. Furthermore, the design and detailing of connections were not investigated in this thesis, which could impact the accuracy of the ULS assessment.

Additionally, the base of the structure was modelled as pinned, implying a rigid foundation. In reality, soil-structure interaction can introduce flexibility, potentially increasing building sway and peak accelerations.

6.8 Future Studies

This chapter outlines potential directions for future research based on the limitations observed in the current study. Addressing these aspects could improve the reliability and applicability of design strategies for hybrid high-rise structures.

Recommended areas for further study include:

- Incorporating soil-structure interaction to better represent foundation flexibility and its influence on sway and acceleration.
- Investigating the design and behaviour of structural connections and their effect on SLS/ULS performance.
- Explicitly considering torsional and higher-mode effects, particularly in asymmetrical layouts.

7

Conclusion

This thesis set out to identify the most material-efficient strategies to meet both serviceability and strength requirements in tall hybrid timber–concrete office buildings. The findings suggest that the core layout (1-Core vs. 2-Core) has minimal impact on overall structural performance, as both configurations produce similar stiffness and dynamic behaviour. Adjusting concrete slab configurations proved to be a more effective strategy. Specifically, placing fewer but thicker concrete slabs at higher levels resulted in significantly greater reductions in peak accelerations compared to distributing the same volume of concrete across multiple thinner slabs.

Increasing core thickness also improved performance, though at a greater concrete volume than adding upper-level slabs. Thicker cores showed a notably stronger influence on ULS structural capacity, becoming particularly beneficial as building height increases.

In summary, SLS conditions continue to govern the design of the analysed hybrid timber–concrete structure. For taller buildings, ULS considerations become critical and must be carefully addressed to prevent structural issues such as tensile cracking in the concrete core. Effective design strategies should thus prioritize optimal slab placement and thickness for enhanced comfort, while considering increased core thickness primarily as a complementary measure to satisfy essential ULS criteria in taller structures.

Bibliography

Al-Emrani, M., Engström, B., Johansson, M., & Johansson, P. (2013). *Bärande konstruktioner, del 1.* Institutionen för Bygg- och miljöteknik.

Alkhateb, M., & Kallmér, I. (2024). *Strength of a hybrid tower for a high-rise timber building: A study of how different parameters affect the dynamic performance of a building* [Master's thesis]. Chalmers University of Technology [Department of Architecture and Civil Engineering, Division of Structural Engineering, Lightweight Structures].

Andrew, R. M. (2019). Global co_2 emissions from cement production, 1928–2018. *Earth System Science Data*, *11*(4). https://doi.org/10.5194/essd-11-1675-2019

BIG SEE. (2022). *Hoho wien* [Accessed: 2025-04-21]. https://bigsee.eu/hoho-wien/

Blaß, H. J., & Sandhaas, C. (2017). *Timber engineering: Principles for design* [Translation by Richard Mort]. KIT Scientific Publishing. https://doi.org/10.5445/KSP/1000069616

Botis, S., & Cerbu, C. (2020). The influence of mass and stiffness distribution on torsion sensitivity of multistorey structures under dynamic loads [Accessed: 2025-07-15]. *Applied Sciences*, *10*(16), 5555. https://doi.org/10.3390/app10165555

Byggindustrin. (2021). *21 våningar av liv och kultur* [Accessed: 2025-04-21]. https://www.byggindustrin.se/alla-nyheter/arets-bygge/21-vaningar-av-liv-och-kultur/

Byggnadsarbetaren. (2021). *Se bilderna: Så tar rekordhöga plockepinnhuset form* [Accessed: 2025-04-21]. https://www.byggnadsarbetaren.se/se-bilderna-sa-tar-rekordhoga-plockepinnhuset-form/

Council on Tall Buildings and Urban Habitat. (2022). *State of tall timber: A global review of tall timber buildings* [Accessed: 2025-01-29]. https://www.ctbuh.org/resources/papers/4530-Journal2022_IssueI_StateofTallTimber+TBIN.pdf

Dahlén, J., & Niemi-Impola, J. (2023). *Dynamic optimization of high rise timber-hybrid buildings: A fem study of the effect on the dynamic response of combining timber and concrete in a high rise building* [Master's thesis]. Chalmers University of Technology [Department of Architecture and Civil Engineering, Division of Structural Engineering].

Engström, B. (1999). Distribution of horizontal load on bracing elements [Available at the Department of Structural Engineering, Chalmers University of Technology].

Foster, R. M., & Ramage, M. H. (2016). Super tall timber – oakwood tower [Accessed: 2025-04-21]. *Proceedings of the Institution of Civil Engineers - Construction Materials*, *169*(1), 1–6. https://doi.org/10.1680/jcoma.16.00034

Harada, H., Fukushima, T., Hatori, T., & Aoyagi, H. (2021). W350: The roadmap of super high-rise timber building [Council on Tall Buildings and Urban Habitat (CTBUH), Accessed: 2025-04-21].

International Timber. (2023). *How can timber be used to reduce the environmental impact of a new build?* [Accessed: 2025-01-29]. Retrieved January 29, 2025, from https://internationaltimber.com/resources/how-can-timber-be-used-to-reduce-environmental-impact-of-a-new-build/

Irwin, P., & Breukelman, B. (2001). Recent applications of damping systems for wind response [Accessed: 2025-04-21]. *CTBUH Journal*. https://global.ctbuh.org/resources/papers/download/1026-recent-applications-of-damping-systems-for-wind-response.pdf

Martinsons. (2021). *Sara kulturhus slår upp portarna* [Accessed: 2025-04-21]. https://www.martinsons.se/sv/kontakt/pressrum/nyheter/sara-kulturhus-slar-upp-portarna/

Martinsons. (2022). *Materialguide kl-trä* [Accessed: 2025-04-09]. Retrieved April 9, 2025, from https://www.martinsons.se/globalassets/travaror/martinsons/materialguide_kl-tra_05_2022.pdf

Mendis, P., Ngo, T., Haritos, N., Hira, A., Samali, B., & Cheung, J. (2007). Wind loading on tall buildings. *EJSE Special Issue: Loading on Structures*, 41–54.

Metsä Wood. (2019). *Mjøsa tower – building higher with kerto® lvl* [Accessed: 2025-04-21]. https://www.metsagroup.com/metsawood/news-and-publications/articles/mjosa-tower-building-higher-with-kerto/

Mortlock Timber Group. (2023). *Learning: Carbon footprint of timber* [Accessed: 2025-01-29]. Retrieved January 29, 2025, from https://www.mortlock.com.au/learning/learning-carbon-footprint-of-timber/

Research Institutes of Sweden (RISE). (2023). *The future of design: Reusing wooden houses in a circular economy* [Accessed: 2025-01-29]. Retrieved January 29, 2025, from https://www.ri.se/en/expertise-areas/stories/the-future-of-design-reusing-wooden-houses-in-a-circular-economy

Sæmundsson, Á. F. (2007). *Wind effects on high-rise buildings* [Master's thesis]. Lund University, Faculty of Engineering [Accessed: 2025-02-06]. https://lup.lub.lu.se/luur/download?func=downloadFile&recordOId=3172394&fileOId=4459390

Sanner, J., Snapp, T., Fernandez, A., Weihing, D., Foster, R., & Ramage, M. (2017). River beech tower: A tall timber experiment [Accessed: 2025-04-21]. *CTBUH Journal*, *2017*(Issue II). https://global.ctbuh.org/resources/papers/download/3348-river-beech-tower-a-tall-timber-experiment.pdf

Sara Kulturhus. (2025). *Sara kulturhus – ett hus fullt av liv och kultur* [Accessed: 2025-04-21]. https://www.sarakulturhus.se/sv/

Smith, B. S., & Coull, A. (1991). *Tall building structures: Analysis and design*. John Wiley & Sons, Inc.

Swedish Wood. (2016). *Limträhandbok del 2: Projektering av limträkonstruktioner* (R. Crocetti, Ed.) [Handledning för dimensionering enligt Eurokod 5]. Svenskt Trä. https://www.svenskttra.se

Swedish Wood. (2022a). Design of timber structures: Structural aspects of timber construction, volume 1.

Swedish Wood. (2022b). Tema kl-trä mälmo – johan åhlén, moelven [Accessed: 2025-04-21].

Thornton Tomasetti. (2022). *Ascent* [Accessed: 2025-04-21]. https://www.thorntontomasetti.com/project/ascent

Timber NSW. (2023). *Timber in the carbon economy* [Accessed: 2025-01-29]. Retrieved January 29, 2025, from https://timbernsw.com.au/timber-in-the-carbon-economy/

University of Melbourne. (2021). *Lightweight concrete – camph research project* [Accessed: 2025-04-21]. https://eng.unimelb.edu.au/camph/research/projects/lightweight-concrete

Woodsafe Timber Protection. (2020). *Mjøstårnet – ett projekt av woodsafe* [Accessed: 2025-04-21]. https://www.byggfaktadocu.se/woodsafe-timber-protection/foretagsprojekt-48712.html

A

FEM-Design Beam Check

This appendix contains the MathCAD PDF `Appendix_Beam_design_FEM.pdf`, showing the FEM calculations for the beam design.

B.18.1
Load combination: 'ULS_Main Load: Live Load X+'

GL 30c
(Glued laminated), Service class 1

$E_{0,05}$	=	10800	N/mm²	$f_{t,90,k}$	=	0.50	N/mm²
$G_{0,05}$	=	540	N/mm²	$f_{c,0,k}$	=	24.50	N/mm²
γ_M	=	1.25		$f_{c,90,k}$	=	2.50	N/mm²
$\gamma_{M,acc./seis.}$	=	1.00		$f_{v,k}$	=	3.50	N/mm²
k_{sys}	=	1.00					

Glulam 215x405

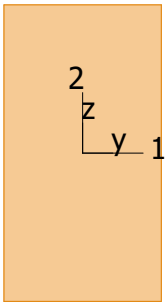

A	=	87075	mm²	$f_{t,0,k}$	=	20.28	N/mm²
W_1	=	5.878e+06	mm³	$f_{m,1,k}$	=	31.20	N/mm²
W_2	=	3.120e+06	mm³	$f_{m,2,k}$	=	33.00	N/mm²
i_1	=	117	mm				
i_2	=	62	mm				
I_2	=	3.354e+08	mm⁴				
I_t	=	8.952e+08	mm⁴				

Combined shear and torsion - 6.1.7, 6.1.8
x = 4800.00 mm

$\tau_d = 1.42\ \text{N/mm}^2 \leq f_{v,d} = 2.52\ \text{N/mm}^2$ (6.13) - OK

Lateral torsional buckling - 6.3.3
x = 2400.00 mm

$\lambda_{rel,m} = 0.461 \leq 0.75$

$$\frac{\sigma_{m,1,d}}{k_{crit} \cdot f_{m,1,d}} = \frac{8.43}{1.000 \cdot 22.47} = 0.38 \leq 1.00 \quad (6.33) - OK$$

$$\left(\frac{\sigma_{m,1,d}}{k_{crit} \cdot f_{m,1,d}}\right)^2 + \frac{\sigma_{c,0,d}}{k_{c,2} \cdot f_{c,0,d}} = \left(\frac{8.43}{1.000 \cdot 22.47}\right)^2 + \frac{0.00}{0.62 \cdot 17.64} =$$
$= 0.14 \leq 1.00$ (6.35) - OK

B.23.1
Load combination: 'ULS_Main Load: Live Load X+'

GL 30c
(Glued laminated), Service class 1

$E_{0,05}$	=	10800	N/mm^2	$f_{t,90,k}$	=	0.50	N/mm^2
$G_{0,05}$	=	540	N/mm^2	$f_{c,0,k}$	=	24.50	N/mm^2
γ_M	=	1.25		$f_{c,90,k}$	=	2.50	N/mm^2
$\gamma_{M,acc./seis.}$	=	1.00		$f_{v,k}$	=	3.50	N/mm^2
k_{sys}	=	1.00					

Glulam 215x405

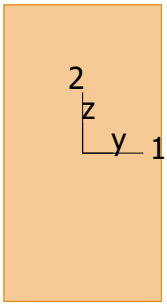

A	=	87075	mm^2	$f_{t,0,k}$	=	20.28	N/mm^2
W_1	=	5.878e+06	mm^3	$f_{m,1,k}$	=	31.20	N/mm^2
W_2	=	3.120e+06	mm^3	$f_{m,2,k}$	=	33.00	N/mm^2
i_1	=	117	mm				
i_2	=	62	mm				
I_2	=	3.354e+08	mm^4				
I_t	=	8.952e+08	mm^4				

Combined shear and torsion - 6.1.7, 6.1.8
x = 0.00 mm

$\tau_d = 1.02$ N/mm^2 $\leq f_{v,d} = 2.52$ N/mm^2 (6.13) - OK

Lateral torsional buckling - 6.3.3
x = 2400.00 mm

$\lambda_{rel,m} = 0.461 \leq 0.75$

$$\frac{\sigma_{m,1,d}}{k_{crit} \cdot f_{m,1,d}} = \frac{6.95}{1.000 \cdot 22.47} = 0.31 \leq 1.00$$ (6.33) - OK

B

FEM-Design Column Check

This appendix contains the MathCAD PDF `Appendix_Column_design_FEM.pdf`, showing the FEM calculations for the column design.

C.37.1
Load combination: 'ULS_Main Load: Live Load X+'

GL 30h
(Glued laminated), Service class 1

$E_{0,05}$	=	11300	N/mm^2	$f_{t,90,k}$	=	0.50	N/mm^2
$G_{0,05}$	=	540	N/mm^2	$f_{c,0,k}$	=	30.00	N/mm^2
γ_M	=	1.25		$f_{c,90,k}$	=	2.50	N/mm^2
$\gamma_{M,acc./seis.}$	=	1.00		$f_{v,k}$	=	3.50	N/mm^2
k_{sys}	=	1.00					

Glulam 760x765

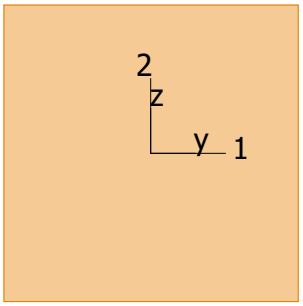

A	=	581400	mm^2	$f_{t,0,k}$	=	24.00	N/mm^2
W_1	=	7.413e+07	mm^3	$f_{m,1,k}$	=	30.00	N/mm^2
W_2	=	7.364e+07	mm^3	$f_{m,2,k}$	=	30.00	N/mm^2
i_1	=	221	mm				
i_2	=	219	mm				
I_2	=	2.798e+10	mm^4				
I_t	=	4.752e+10	mm^4				

Combined bending and axial compression - 6.1.4, 6.2.4
x = 0.00 mm

$$\frac{\sigma_{c,0,d}}{f_{c,0,d}} = \frac{6.89}{21.60} = 0.32 \leq 1.00 \quad (6.2) - OK$$

$$\left(\frac{\sigma_{c,0,d}}{f_{c,0,d}}\right)^2 + \frac{\sigma_{m,1,d}}{f_{m,1,d}} + k_m \frac{\sigma_{m,2,d}}{f_{m,2,d}} =$$
$$= \left(\frac{6.89}{21.60}\right)^2 + \frac{0.00}{21.60} + 0.70 \frac{0.00}{21.60} = 0.10 \leq 1.00 \quad (6.19) - OK$$

$$\left(\frac{\sigma_{c,0,d}}{f_{c,0,d}}\right)^2 + k_m \frac{\sigma_{m,1,d}}{f_{m,1,d}} + \frac{\sigma_{m,2,d}}{f_{m,2,d}} =$$
$$= \left(\frac{6.89}{21.60}\right)^2 + 0.70 \frac{0.00}{21.60} + \frac{0.00}{21.60} = 0.10 \leq 1.00 \quad (6.20) - OK$$

Flexural buckling around axis 1 - 6.3.2

x = 0.00 mm

$\beta_c = 0.1$ (6.29)

$$\lambda_1 = \frac{l_0}{i_1} = \frac{4500}{221} = 20.38$$

$$\lambda_{rel,1} = \frac{\lambda_1}{\pi}\sqrt{\frac{f_{c,0,k}}{E_{0,05}}} = \frac{20.38}{\pi}\sqrt{\frac{30.00}{11300}} = 0.334 \quad (6.21)$$

$$k_1 = 0.5\left(1 + \beta_c\left(\lambda_{rel,1} - 0.3\right) + \lambda_{rel,1}^{\ 2}\right) =$$

$$= 0.5\left(1 + 0.1\left(0.334 - 0.3\right) + 0.334^2\right) = 0.558 \quad (6.27)$$

$$k_{c,1} = \frac{1}{k_1 + \sqrt{k_1^{\ 2} - \lambda_{rel,1}^{\ 2}}} = \frac{1}{0.558 + \sqrt{0.558^2 - 0.334^2}} = 0.996 \quad (6.25)$$

$$\frac{\sigma_{c,0,d}}{k_{c,1} \cdot f_{c,0,d}} + \frac{\sigma_{m,1,d}}{f_{m,1,d}} + k_m \cdot \frac{\sigma_{m,2,d}}{f_{m,2,d}} =$$

$$= \frac{6.89}{0.996 \cdot 21.60} + \frac{0.00}{21.60} + 0.70 \cdot \frac{0.00}{21.60} = 0.32 \leq 1.00 \quad (6.23) \text{ - OK}$$

C

MathCAD Beam and Column Check

This appendix contains the MathCAD PDF `Appendix_Beam_and_Column_check.pdf`, showing the manual checks of beam and column designs.

Column and beam calculations

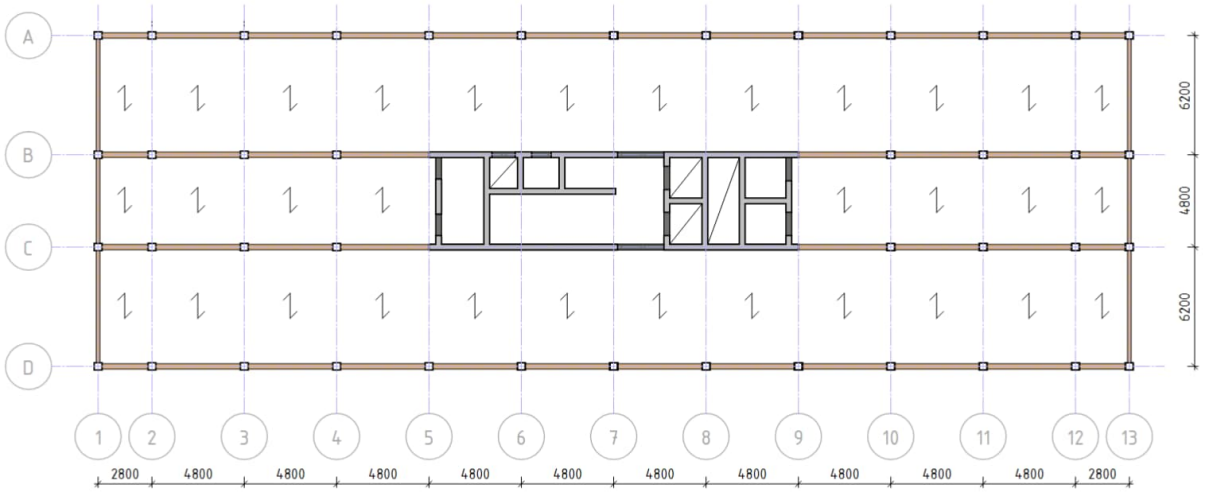

Dimensions:

·1.22AI ! () N Floor span

·1.22AW +(, N

·abcN +(, N Beam span

Beam design:

The following checks will be done:

- Bending verification
  - Laterar torsional buckling
- Shear verification
- Deformation (SLS)

Self-weight:

Self weight of facade along the beam	$d_{ef1cgckb}$ –(. $\frac{el}{N}$.
Thickness, CLT-slab	m_{122A})+1 NN
weight, CLT-slab	o_{122A} 2! (! $\frac{ed}{N^{)}}$.
Self weight, CLT-slab	d_{122A} o_{122A}4d3 1(2+5 $\frac{el}{N^{)}}$.
Self weight, of nonbearing walls and insatlations	$d_{rt\,ym}$ 1(. $\frac{el}{N^{)}}$.

Height of beam	0_{abcN} 1(+1. N
Width of beam	a_{abcN} 1()–. N
Density, glulam	$o_{Nbct\,fabcN}$ +61 $\frac{ed}{N^{6}}$.
Self weight, beam	d_{efabcN} $o_{Nbct\,fabcN}$ 4a_{abcN} 4$0_{abcN}$ 4d3 1(6! 5 $\frac{el}{N}$.

Imposed load:

Category B, office areas	5_{e})(. $\frac{el}{N^{)}}$.	C_{EnNG}	1(5
		C_{WNG}	1(6

Load combination:

Two beams need to be checked:

- Beam 1, a facade beams supports one slab and the facade.

- Beam 2, a inner beam which have two slabs at each side

Beam 1

Imposed load as main imposed load in ULS:

$$5_{kI} \quad -(6.\ 49d_{efabcN}\ 7\ 8d_{122A}7\ d_{rt\ ynE}4\cdot\cdot^{\cdot 1.22AI}\ 7\ d_{ef1cgckbN}7\ -(.\ 45_e 4\cdot\cdot^{\cdot 1.22AI}\ 3\ )\ 1()\ 16\ \cdot\cdot^{\boldsymbol{el}}_{\boldsymbol{N}}.$$

$$L_{MkI} \quad \cdot\cdot^{5_{kI}4\cdot_{abcN}}_{,}\ \cdot\ 3\ .\ ,(-,+\boldsymbol{el}\ \ 4\boldsymbol{N} \qquad\qquad P_{MkI} \quad \cdot\cdot^{5_{kI}4.abcN}_{)}\ 3\ +,(+,5\ \boldsymbol{el}$$

Beam 2

Imposed load as main imposed load in ULS:

$$5_{kW} \quad -(6.\ 49d_{efabcN}\ 7\ 8d_{122A}7\ d_{rt\ ynE}4\cdot\cdot^{\cdot 1.22AI}\ 7\ \cdot\cdot^{\cdot 1.22AW}\ 7\ -(.\ 45_e 4\cdot\cdot^{\cdot 1.22AI}\ 7\ \cdot\cdot^{\cdot 1.22AW}\ 3\ 6-(,!\ 5\ \cdot\cdot^{\boldsymbol{el}}_{\boldsymbol{N}}.$$

$$L_{MkW} \quad \cdot\cdot^{5_{kW}4\cdot_{abcN}}_{,}\ \cdot\ 3\ 2-(555\ \boldsymbol{el}\ \ 4\boldsymbol{N} \qquad\qquad P_{MkW} \quad \cdot\cdot^{5_{kW}4\cdot_{abcN}}_{)}\ 3\ 5!\ (+,-\boldsymbol{el}$$

Material parameters:

Material: Glulam		e_{N2k} 1(,	EC5: T3.1
Service class: 1	-->		
Load duration: Medium		Q_L –().	EC5: T2.3

GL30c -->

1_{Ne}	61 ***L Sc***	1_{Ve}	6(. ***L Sc***
$M_{Eff E\_}$	–1, 11 ***L Sc***	$M_{Eff Nbct}$	–6111 ***L Sc***
$h_{Eff E\_}$	. +1 ***L Sc***	h_{Nbct}	!. 1 ***L Sc***

Bending capacity 1_{Nk} e_{N2k} $\frac{1_{Ne}}{Q_L}$ 3 –2() ***L Sc***

Shear capacity 1_{Vk} e_{N2k} $\frac{1_{Ve}}{Q_L}$ 3)() + ***L Sc***

Sectional constants:

$\cdot_{.12A}$! ()+, A
$I_{.12A}$! (-! , A

$N. \; \cdot_{.12A} \, (I_{.12A}$! (! 12 $A^{)}$

$W_a. \; \frac{\cdot_{.12A} \, (I_{.12A}^{\;)}}{4}$ 5̈, (121 (+! ^{4} 7̈ $A\,A^{9}$

$b_a. \; \frac{\cdot_{.12A} \, 0I_{.12A}^{\;9}}{+)}$ 5̈+(+<0+! $^{<}$7̈ $A\,A^{-}$

Cross-section

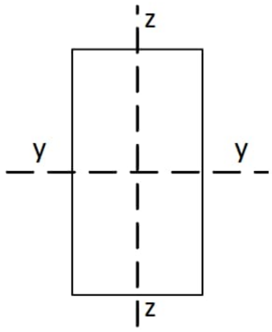

Size effect:

$c_I. \; \exists I_{.12A}$ U! (4 A +(! –

a a a A de a a NCIN a a+ 5i 5 el e el 6$I_{.12A}$ 6m 4! ! A (+! ! ! +(+ 7! (+n7 f cf 8 cf r8

[EC5: EQ 3.2]

Bending verification:

Dimensioning bending stress $f_{A\,gadk} \cdot \frac{s\ t\,x\,5l_{mko}\,zl_{mkr}\,7}{W_a}$ +, (4+, **l t 2**

$y\,I\,10c$. ∓ $f_{A\,gadk}$ “ $c_I\,(5_{A\,k}$ ”:=—•f
a ”:=—•f
NOIN
a ”| :=\ \}=—•f

Utilization ratio:

$\frac{f_{A\,gadk}}{c_I\,(5_{A\,k}}$! (21) [EC5: EQ 6.11]

Check lateral torsional buckling:

G_{15} . ! (<0C_{12A} –(9) A Simply supported, uniformly distributed load [EC5: Table 6.1]

$f_{A\,gEG}$ $\frac{!\,(21\,(.\,_{12A})}{G_{15}\,0I_{.\,12A}}$ $(m_{LgLM}$))) (, 4, **l t 2** [EC5: EQ 6.32]

$P_{ELGA} \cdot \sqrt{\frac{5_{A\,c}}{f_{A\,gEG}}}$! (942 Ratio bending slenderness [EC5: EQ 6.30]

c_{0EG} ∓ P_{ELGA} “ ! (2, +
a +
NOIN∓ ! (2, UP_{ELGA} “ +(–
a +(, 4 | ! (2, (P_{ELGA}
NOIN∓ +(–UP_{ELGA}
a +
a .
a P_{ELGA})

Critical lateral instability factor [EC5: EQ 6.34]

(no risk for buckling)

$y\,I\,10c$. ∓ $f_{A\,gadk}$ “ $c_I\,(5_{A\,k}\,(c_{0EG}$ ”:=—•f
a ”:=—•f
NOIN
a ”| :=\ \}=—•f

Utilization ratio:

$\frac{f_{A\,gadk}}{c_I\,(5_{A\,k}\,(c_{0EG}}$! (21) [EC5: EQ 6.33]

Shear verification:

c_{0E}. ! (42 for glued laminated timber

. 15 . c_{0E}C . . 12A ! (+— A effective beam width [EC5: EQ 6.13]

Q_{mko} –1(–12 cS Q_{mkr} 24(–1+ cS

V_k . +(, 0 s t x 5 Q_{mko} z Q_{mkr} 7 / I . 12A 0. 15 +(<44 l t 2 Dimensioning shear stresss [EC5: EQ 6.60]

y I 10c . ⇇ V_k “ 5_k ”:=—ƒ

a ”:=—ƒ

NOTE

a ”| :=\ \:=—ƒ

Utilization ratio:

V_k / 5_k ! (121 [EC5: EQ 6.13]

Deformation(SLS):

Beam 1

$h_{i\ o} \cdot \ n_{cg\ 12A} \parallel 5n_{5ppE} \parallel n_{de\ qCe} 7(\frac{C_{5GppEo}}{)} \parallel n_{cg5202k1} \quad 4(9, - \frac{cS}{A}$

$h_{s\ o} \cdot \ h_c 0 \frac{C_{5GppEo}}{)} \quad 2(2, \ \frac{cS}{A}$

Instantaneous deformation

Due to self weight

$u_{de\ qGj\ og\ 1ek} \cdot \ \frac{,\ (h_{i\ o} (C_{12A}^{-}}{91-(m_{LgA\ 12e} (b_a} \qquad u_{de\ qGj\ og\ 1ek} \quad)(191\ AA$

$u_{de\ qGj\ ogI\ 12E} \cdot \ \frac{+()\ 0h_{i\ o} 0C_{12A}^{)}}{1\ 0i_{A\ 12e} 0N} \qquad u_{de\ qGj\ ogI\ 12E} \quad !\ (911\ AA$

$u_{de\ qGj\ o} \cdot \ u_{de\ qGj\ og\ 1ek} \parallel u_{de\ qGj\ ogI\ 12E} \quad 9()\ )4\ AA$

Due to imposed load

$u_{de\ qGs\ og\ 1ek} \cdot \ \frac{,\ 0h_{s\ o} (C_{12A}^{-}}{91-(m_{LgA\ 12e} (b_a} \qquad u_{de\ qGs\ og\ 1ek} \quad 9(-4)\ AA$

$u_{de\ qGs\ ogI\ 12E} \cdot \ \frac{+()\ (h_{s\ o} (C_{12A}^{)}}{1\ 0i_{A\ 12e} 0N} \qquad u_{de\ qGs\ ogI\ 12E} \quad !\ (-29\ AA$

$u_{de\ qGs\ o} \cdot \ u_{de\ qGs\ og\ 1ek} \parallel u_{de\ qGs\ ogI\ 12E} \quad 9(<9, \ AA$

Total instantaneous deformation

$u_{de\ qGo} \cdot \ u_{de\ qGj\ o} \parallel u_{de\ qGs\ o} \quad 2(+4)\ AA \qquad \frac{C_{12A}}{9!\ !} \quad +4\ AA$

Final deformation

$\cdot\ _{12A} \quad !\,()$

$I_{AWb\,c} \quad I_{Wdeb\,c} - 0. \cdot _{12A} 1\ 2 \qquad I_{AWb\,c}\ 3\ 4(0)5\ f\ f$

$I_{AWg\,c} \quad I_{Wdeg\,c} + 0. \ k_{l\,N\,f\,m} \cdot _{12A} 1\ 2 \qquad I_{AWg\,c}\ 3\ 6()66\ f\ f$

Total final deformation

$I_{AWc} \quad I_{AWb\,c} \cdot I_{AWg\,c}\ 3\ 7(8!)\ f\ f \qquad \frac{q_{r2tf}}{<!}\ 3\ 0)\ f\ f$

$\frac{q_{r2tf}}{54!}\ 3\ 07(5\ f\ f$

$\frac{q_{r2tf}}{5!!}\ 3\ 56\ f\ f$

<u>Beam 2</u>

Imposed load as main imposed load in ULS:

$y_{b\,l} \quad 0_{.\,ar2tf} \cdot 0_{A55C} \cdot 0_{Wde} 1\ 2 \cdot \frac{,\ O_{A55C}}{5} \cdot \frac{O_{A55C}}{5}\ \frac{1}{2}\ 3\ 8(<5N \cdot \frac{E}{f}$

$y_{g\,l} \quad y_{.} \cdot \frac{,\ O_{A55C}}{5} \cdot \frac{O_{A55C}}{5}\ \frac{1}{2}\ 3\ 0<(N4 \cdot \frac{E}{f}$

Instantaneous deformation

Due to self weight

$I_{Wdeb\,l\,ar2W1} \quad \frac{4\ y_{b\,l}\ q_{r2tf}^{\ 6}}{<86\ G_{Laf\ 2tW}\ M} \qquad I_{Wdeb\,l\,ar2W1}\ 3\ <(N5\ f\ f$

$I_{Wdeb\,l\,adQ2tC} \quad \frac{0(5\ y_{b\,l}\ q_{r2tf}^{\ 5}}{8\ b_{f\ 2tW}\ S} \qquad I_{Wdeb\,l\,adQ2tC}\ 3\ !(4!8\ f\ f$

$I_{Wdeb\,l} \quad I_{Wdeb\,l\,ar2W1} \cdot I_{Wdeb\,l\,adQ2tC}\ 3\ 6(557\ f\ f$

Due to imposed load

$$I_{NWdeag\ l\ ar2WI} \quad \frac{4 \cdot y_{g\ l} \cdot q_{r2t\ f}^{\ 6}}{<86 \cdot G_{Laf\ 2t\ W} \cdot M_{p}} \qquad I_{NWdeag\ l\ ar2WI}\ 3\ )(065\ f\ f$$

$$I_{NWdeag\ l\ adQ2t\ C} \quad \frac{0(5 \cdot y_{g\ l} \cdot q_{r2t\ f}^{\ 5}}{8 \cdot b_{f\ 2t\ W} \cdot S} \qquad I_{NWdeag\ l\ adQ2t\ C}\ 3\ !\ (86\ f\ f$$

$$I_{NWdeag\ l} \quad I_{NWdeag\ l\ ar2WI} \cdot I_{NWdeag\ l\ adQ2t\ C}\ 3\ )(785\ f\ f$$

Total instantaneous deformation

$$I_{NWdel} \quad I_{NWdeb\ l} \cdot I_{NWdeag\ l}\ 3\ 00(500\ f\ f \qquad \frac{q_{r2t\ f}}{<!}\ 3\ 0)\ f\ f$$

Final deformation

$$I_{AWb\ l} \quad I_{NWdeb\ l} \cdot 0 \cdot \cdot_{12A} 1 \qquad I_{AWb\ l}\ 3\ )(N)\ )\ f\ f$$

$$I_{AWg\ l} \quad I_{NWdeag\ l} \cdot 0 \cdot k_{l\ N\ f\ m} \cdot_{12A} 1 \qquad I_{AWg\ l}\ 3\ 8(5<7\ f\ f$$

Total final deformation

$$I_{AW} \quad I_{AWb\ l} \cdot I_{AWg\ l}\ 3\ 04(!\ !\ 6\ f\ f \qquad \frac{q_{r2t\ f}}{<!}\ 3\ 0)\ f\ f$$

$$\frac{q_{r2t\ f}}{54!}\ 3\ 07(5\ f\ f$$

$$\frac{q_{r2t\ f}}{5!\ !}\ 3\ 56\ f\ f$$

Column design:

Storey height $Qdl_c \quad 6(4\ f \qquad Qdl \quad \lhd(4\ f$

Storeys above column $W \quad 54$

Building height $Q \quad Qd\text{-}\{WT\,0[\,.\ Qdl_c 3\ 88(4\ f$

Floor span $o_{A55Cc} 3\ )(5\ f \qquad o_{A55Cl} 3\ 6(8\ f$

Beam span $o_{r2tf}\ 3\ 6(8\ f$

The following checks will be done:

- Compression and buckling

(The wind load acting on the facade is transfered to the beams and is then transfered to the trusses/core)

Self-weight:

Height of beam

Width of beam

Density, glulam

Self weight, beam

Self weight, column (for n storeys)

Self weight and installations, floor (for n storeys)

Self weight and installations, floor (for n storeys)

Self weight, facade (for n storeys)

Self weight, beam (for n storeys)

Total Self weight on column

Total Self weight on column

Imposed load:

Snow load:

Shape coefficient for 0 °< α< 30 °

är denna rätt?

Load combination:

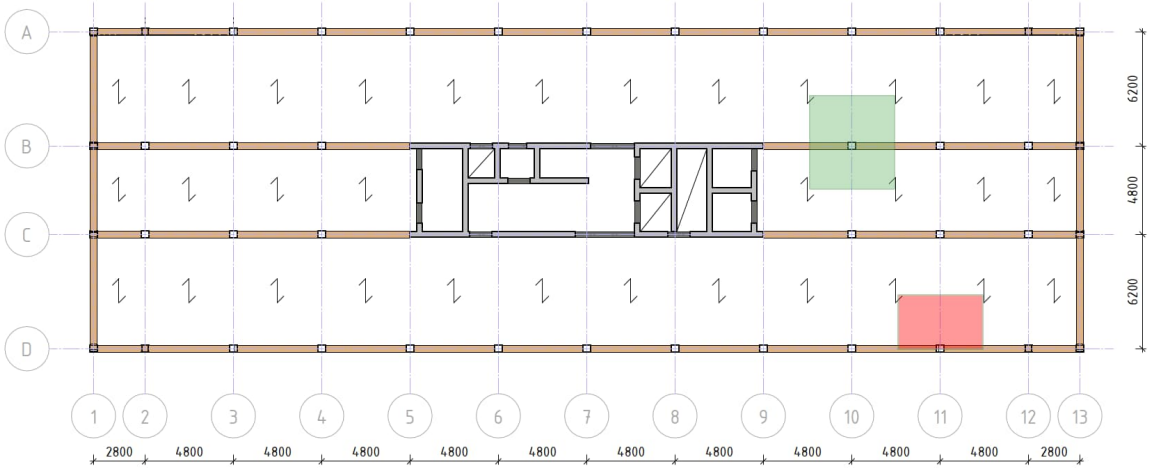

Two columns need to be checked:

- Column 1 which carries self weight, imposed loads and snow load from the area marked in green

- Column 2 which carries self weight, imposed loads, facade load and snow load from the area marked in red

Column 1

Imposed load as main imposed load in ULS:

$o_{EGWGA\,N2I\,mAb}$, 8N9 ($L_{12MdcPI\,bGW}2$, 89 (1· $_{12A\,NW}2$ · $_{12\cdot beCW}$ (0 $_{5r}$ 7! NO9K **1*o***

Snow load as main imposed load in ULS:

$o_{EGWG\cdot beC2I\,mAb}$, 8N9 ($L_{12MdcPI\,bGW}2$, 89 (1· $_{12\cdot beCW}2$ · $_{12A\,NW}$ (0 $_{5A\,N}$ 7! N49, **1*o***

Column 2

Imposed load as main imposed load in ULS:

$o_{EGjGA\,N2I\,mAb}$, 8N9 ($L_{12MdcPI\,bGj}2$, 89 (· $_{12A\,Ng}2$ · $_{12\cdot beCg}$ (0 $_{5r}$! 49TN **1*o***

Snow load as main imposed load in ULS:

$o_{EGjG\cdot beC2I\,mAb}$, 8N9 ($L_{12MdcPI\,bGj}2$, 89 (1· $_{12\cdot beCg}2$ · $_{12A\,Ng}$ (0 $_{5A\,N}$ 7! 4, <9 **1*o***

o_{E} a ef .i $o_{EGWGA\,N2I\,mAb}$ n5 0l $o_{EGWG\cdot beC2I\,mAb}$ o6! 1N8O9 (, K^{N}5 7 **1*o*** 0l $o_{EGjGA\,N2I\,mAb}$ o6 0l 1m9 $o_{EGjG\cdot beC2I\,mAb}$ o6 r7

Column Design:

$Q_{MdcPI\,b}$ Sr_{W}! =89 ***I***	Length of column
$k_{MdcPI\,b}$! K8ITU9 ***I***	Width of column
$S_{MdcPI\,b}$! K8ITU ***I***	Height of column
o_{E}! 1N8O9 (, K^{N}5 7 **1*o***	Design vertical load

Material parameters:

Material: Glulam
Service class: 1 -->
Load duration: Medium

$1_{I\,eE}$ K8O EC5: T3.1

$V_{\_}$, 849 EC5: T2.3

GL30h --> d_{M51} NK_ hm

i_{525n} , , NKK_ hm $i_{52I\,lmb}$, NUKK_ hm

p_{525n} 9=K_ hm $p_{I\,lmb}$ U9K_ hm

d_{M5E} $1_{I\,eE}\left(\frac{d_{M51}}{V_{\_}}\right)$! 4, 8U_ hm Dimensioning compression capacity

Sectional constants:

q $k_{MdcPI\,b}(S_{MdcPI\,b}$! K89<, I^{4}

s $k_{MdcPI\,b}(S_{MdcPI\,b}{}^{4}$! K8KT=I^{N}
U

u $k_{MdcPI\,b}(S_{MdcPI\,b}{}^{N}$! K8K4<$I^{=}$
, 4

v_{M5E} $\frac{o_{E}}{q}$! U8IO=_ hm Dimensioning compression stress

Check the buckling capacity:

$A \quad \sqrt{\frac{u}{q}} \; ! \; K84, O I$ Radius of gyration

$Q_{l\,dd} \quad Q_{McPI\;b} \; ! \; =89 \; I$ Effective buckling length (pinned in both ends)

$w \quad \frac{Q_{l\,dd}}{A}$ Slenderness ratio

$w_{fl\,c} \quad \frac{w}{\rho} (\sqrt{\frac{d_{M51}}{i_{525n}}} \; ! \; K8NNU$ Relative slenderness [EC5: EQ 6.21]

$\psi_M \quad K8$ for glued laminated timber and LVL [EC5: EQ 6.29]

$1 \quad K89 (_1, 2 \; \psi_M (_1 w_{fl\,c} + K8N) 2 \; w_{fl\,c}{}^4) ! \; K899<$ [EC5: EQ 6.27]

$1_M \quad \frac{?}{1 \, 2 \sqrt{1^4 + w_{fl\,c}{}^4}} \; ! \; K8OOU$ [EC5: EQ 6.25]

$\gamma\,Sl\,M$ t> $w_{fl\,c}$:=K8N ! •(| t"t\e| t\ ) ‖e| t\ |4[
ニ•(| t"t\e| t\ ) ‖e| t\ |, [
z"'z
ニ•(| t"t\e| t\ ) ‖e| t\ |4[

$\gamma\,Sl\,M$ t> $v_{M5E}{}^4 := d_{M5E}{}^4$! •| ⌊ ⫪
ニ•| ⌊ ⫪
z"'z
ニ•| | ⌋ ▌⌊ ⫪

Utilization ratio 1:

$0 \cdot \frac{v_{M5E}}{1\,d_{M5E}} \cdot 6^{54} \; ! \; K8KOO$ [EC5: EQ 6.19]

$\gamma\,Sl\,M$ t> $v_{M5E} := 1_M (d_{M5E}$! •| ⌊ ⫪
ニ•| ⌊ ⫪
z"'z
ニ•| | ⌋ ▌⌊ ⫪

Utilization ratio 2:

$\frac{v_{M5E}}{1_M (d_{M5E}} \; ! \; K8N, U$ [EC5: EQ 6.23]

Summary:

Beam:

$\cdot_{12AI}$! () ! + ***I***
1_{12AI} ! (12+ ***I***

Utilization ratio:

Bending: $\frac{N_{I\ wwW}}{c_{.}\text{-}d_{I\ b}}$! (. 01

Bending,
Lateral torsional buckling: $\frac{N_{I\ wwW}}{c_{.}\text{-}d_{I\ b}\text{-}c_{efgk}}$! (. 01

Shear: $\frac{l_{\ b}}{d_{mb}}$! (0. 0

Column:

$1_{eort\,I\ y}$! (. 3+ ***I***
$\cdot_{\ eort\,I\ y}$! (. 3 ***I***

Utilization ratio:

Compression $\frac{N_{e0b}}{d_{e0b}}$! (42+

$\frac{N_{e0b}}{c_{e}\text{–}d_{e0b}}$! (423

D

Convergence Study

This appendix summarises the results of the mesh convergence study. Columns 1–6 are numbered for compactness; their meanings are listed beneath the table.

Table D.1: Results of convergence study (see column descriptions below)

No. elems	E. Size [m]	f_1	M_{beam}	δ_{beam}	M_{CLT}	$V_{\max}$	N_{wall}
11 972.000	1.500	1.744	47.210	8.655	9.742	−5.063	−823.800
17 837.000	1.000	1.742	47.520	8.726	9.559	−5.356	−821.700
24 570.000	0.800	1.741	47.520	8.738	9.586	−5.366	−820.600
38 506.000	0.600	1.740	47.660	8.771	9.430	−5.356	−820.700
53 253.000	0.500	1.740	47.700	8.779	9.425	−5.345	−820.800
78 857.000	0.400	1.739	47.720	8.783	9.465	−5.319	−822.500
142 320.000	0.300	1.739	47.750	8.789	9.451	−5.295	−822.000

Column descriptions:

f_1 = Fundamental frequency [Hz]
M_{beam} = Maximum beam moment (self-weight) [kNm]
δ_{beam} = Maximum beam deflection (max load case) [mm]
M_{CLT} = Maximum CLT-slab moment [kNm]
$V_{\max}$ = Maximum shear force [kN]
N_{wall} = Maximum compression force in first-storey concrete wall [kN]

E

Dynamic Model Comparison

This appendix summarises the first-mode frequencies and peak accelerations for different core thicknesses and floor-slab configurations. Results are shown for both the 1-Core and 2-Core models.

Table E.1: Summary of dynamic properties (15 storeys)

Storeys	Model	Freq. 1C [Hz]	Acc. 1C [m/s²]	Freq. 2C [Hz]	Acc. 2C [m/s²]
15	300 Core, No Slab	1.036	0.052	1.028	0.051
15	300 Core, 1×200 Slab	0.972	0.047	0.967	0.047
15	300 Core, 3×200 Slab	0.882	0.043	0.884	0.043
15	300 Core, 5×200 Slab	0.835	0.041	0.841	0.041
15	300 Core, 1×300 Slab	0.932	0.045	0.932	0.044
15	300 Core, 3×300 Slab	0.810	0.040	0.821	0.039
15	300 Core, 5×300 Slab	0.753	0.037	0.772	0.036
15	300 Core, 1×400 Slab	0.897	0.043	0.903	0.042
15	300 Core, 3×400 Slab	0.755	0.037	0.775	0.035
15	300 Core, 5×400 Slab	0.693	0.034	0.722	0.032
15	400 Core, No Slab	1.046	0.044	1.034	0.044
15	400 Core, 1×200 Slab	0.988	0.041	0.980	0.041
15	400 Core, 3×200 Slab	0.905	0.038	0.903	0.038
15	400 Core, 5×200 Slab	0.861	0.037	0.863	0.036
15	400 Core, 1×300 Slab	0.952	0.040	0.948	0.039
15	400 Core, 3×300 Slab	0.837	0.036	0.845	0.035
15	400 Core, 5×300 Slab	0.781	0.035	0.797	0.032
15	400 Core, 1×400 Slab	0.919	0.038	0.921	0.040
15	400 Core, 3×400 Slab	0.783	0.033	0.800	0.032
15	400 Core, 5×400 Slab	0.722	0.031	0.749	0.029
15	500 Core, No Slab	1.052	0.040	1.036	0.040
15	500 Core, 1×200 Slab	0.999	0.038	0.987	0.039
15	500 Core, 3×200 Slab	0.922	0.035	0.917	0.034
15	500 Core, 5×200 Slab	0.880	0.033	0.879	0.033
15	500 Core, 1×300 Slab	0.965	0.036	0.958	0.035
15	500 Core, 3×300 Slab	0.857	0.032	0.862	0.031
15	500 Core, 5×300 Slab	0.803	0.031	0.816	0.030
15	500 Core, 1×400 Slab	0.935	0.035	0.934	0.034
15	500 Core, 3×400 Slab	0.805	0.030	0.819	0.029
15	500 Core, 5×400 Slab	0.746	0.028	0.769	0.027

Table E.2: Summary of dynamic properties (20 storeys)

Storeys	Model	Freq. 1C [Hz]	Acc. 1C [m/s²]	Freq. 2C [Hz]	Acc. 2C [m/s²]
20	300 Core, No Slab	0.670	0.087	0.664	0.086
20	300 Core, 1×200 Slab	0.636	0.081	0.632	0.080
20	300 Core, 3×200 Slab	0.586	0.075	0.586	0.074
20	300 Core, 5×200 Slab	0.556	0.071	0.559	0.070
20	300 Core, 1×300 Slab	0.616	0.078	0.615	0.077
20	300 Core, 3×300 Slab	0.546	0.069	0.552	0.067
20	300 Core, 5×300 Slab	0.508	0.064	0.518	0.062
20	300 Core, 1×400 Slab	0.598	0.075	0.600	0.074
20	300 Core, 3×400 Slab	0.514	0.066	0.525	0.062
20	300 Core, 5×400 Slab	0.472	0.059	0.488	0.057
20	400 Core, No Slab	0.669	0.077	0.660	0.076
20	400 Core, 1×200 Slab	0.639	0.072	0.632	0.073
20	400 Core, 3×200 Slab	0.593	0.067	0.590	0.066
20	400 Core, 5×200 Slab	0.565	0.065	0.565	0.063
20	400 Core, 1×300 Slab	0.620	0.070	0.617	0.048
20	400 Core, 3×300 Slab	0.555	0.063	0.559	0.061
20	400 Core, 5×300 Slab	0.519	0.060	0.528	0.057
20	400 Core, 1×400 Slab	0.592	0.070	0.604	0.066
20	400 Core, 3×400 Slab	0.525	0.059	0.535	0.057
20	400 Core, 5×400 Slab	0.485	0.054	0.499	0.052
20	500 Core, No Slab	0.666	0.069	0.655	0.068
20	500 Core, 1×200 Slab	0.639	0.066	0.631	0.065
20	500 Core, 3×200 Slab	0.598	0.061	0.593	0.060
20	500 Core, 5×200 Slab	0.572	0.059	0.570	0.058
20	500 Core, 1×300 Slab	0.623	0.064	0.617	0.062
20	500 Core, 3×300 Slab	0.563	0.057	0.564	0.056
20	500 Core, 5×300 Slab	0.528	0.054	0.535	0.052
20	500 Core, 1×400 Slab	0.608	0.062	0.606	0.060
20	500 Core, 3×400 Slab	0.534	0.054	0.541	0.052
20	500 Core, 5×400 Slab	0.495	0.050	0.508	0.048

Table E.3: Summary of dynamic properties (25 storeys)

Storeys	Model	Freq. 1C [Hz]	Acc. 1C [m/s²]	Freq. 2C [Hz]	Acc. 2C [m/s²]
25	300 Core, No Slab	0.477	0.126	0.472	0.125
25	300 Core, 1×200 Slab	0.457	0.120	0.454	0.118
25	300 Core, 3×200 Slab	0.426	0.111	0.425	0.110
25	300 Core, 5×200 Slab	0.405	0.106	0.407	0.104
25	300 Core, 1×300 Slab	0.445	0.116	0.444	0.114
25	300 Core, 3×300 Slab	0.400	0.103	0.404	0.101
25	300 Core, 5×300 Slab	0.374	0.095	0.380	0.094
25	300 Core, 1×400 Slab	0.434	0.113	0.436	0.110
25	300 Core, 3×400 Slab	0.380	0.098	0.387	0.094
25	300 Core, 5×400 Slab	0.350	0.088	0.360	0.085
25	400 Core, No Slab	0.472	0.113	0.465	0.112
25	400 Core, 1×200 Slab	0.454	0.108	0.449	0.107
25	400 Core, 3×200 Slab	0.426	0.101	0.424	0.099
25	400 Core, 5×200 Slab	0.407	0.097	0.407	0.095
25	400 Core, 1×300 Slab	0.443	0.105	0.441	0.103
25	400 Core, 3×300 Slab	0.403	0.095	0.405	0.092
25	400 Core, 5×300 Slab	0.378	0.089	0.383	0.086
25	400 Core, 1×400 Slab	0.434	0.102	0.434	0.100
25	400 Core, 3×400 Slab	0.384	0.089	0.390	0.086
25	400 Core, 5×400 Slab	0.356	0.082	0.365	0.079
25	500 Core, No Slab	0.467	0.103	0.459	0.102
25	500 Core, 1×200 Slab	0.451	0.099	0.445	0.097
25	500 Core, 3×200 Slab	0.426	0.093	0.422	0.091
25	500 Core, 5×200 Slab	0.409	0.089	0.407	0.087
25	500 Core, 1×300 Slab	0.442	0.096	0.438	0.094
25	500 Core, 3×300 Slab	0.405	0.087	0.405	0.085
25	500 Core, 5×300 Slab	0.382	0.082	0.385	0.080
25	500 Core, 1×400 Slab	0.433	0.093	0.432	0.091
25	500 Core, 3×400 Slab	0.387	0.082	0.392	0.080
25	500 Core, 5×400 Slab	0.360	0.076	0.368	0.073

Notes:
Freq. 1C = first-mode frequency (Hz) for the 1-core model;
Acc. 1C = peak acceleration (m/s²) for the 1-core model;
Freq. 2C = first-mode frequency for the 2-core model;
Acc. 2C = peak acceleration for the 2-core model.

F

MATLAB Script for Wind Analysis

This appendix contains the MATLAB script `Appendix_Acc.m`, used to calculate dynamic wind load and peak acceleration (ULS & SLS).

```
% appendix_wind_analysis.m
% Calculates dynamic wind load and peak acceleration (ULS & SLS)

clc; clear; close all

%% Input parameters
n_1x = 0.35;        % Natural frequency [Hz]
v = 25;             % Number of floors
h = 4.5 + (v-1)*3.5; % Total building height [m]
m_e = 318943.15;    % Equivalent mass [kg]

rho = 1.25;         % Air density [kg/m^3]
v_b = 25;           % Basic wind speed for 50-year return period [m/s]
d = 18; b = 54;     % Building width and depth [m]
h_ref = 10;         % Reference height for wind calculation [m]
z_min = 5;          % Minimum height for terrain factor [m]
z_max = 200;        % Maximum height considered [m]
z_0 = 0.3;          % Roughness length for terrain type III [m]
z_0_II = 0.05;      % Reference value of terrain roughness [m]
c_0 = 1;            % Topographic factor [-]
k_I = 1;            % Constant turbulence intensity [-]

%% Height vector
z = 0:0.5:h;        % Height vector from 0 to h with 0.5 m increments

%% Basic wind pressure
q_b = 0.5 * rho * v_b^2 / 1000; % Basic wind pressure [kN/m^2]

%% Terrain and turbulence factors
k_r = 0.19 * (z_0 / z_0_II)^0.07;         % Roughness factor
```

```
    [-]
I_v = @(z) (k_I ./ (c_0 * log(z./z_0))) .* (z>=z_min & z<=
    z_max) + ... % Turbulence intensity
        (k_I ./ (c_0 * log(z_min/z_0))) .* (z<z_min);
c_r = @(z) (k_r * log(z./z_0)) .* (z>=z_min & z<=z_max) + ...
             % Roughness factor at height
        (k_r * log(z_min/z_0)) .* (z<z_min);

%% Mean wind speed
v_m = @(z) c_r(z) * c_0 * v_b;  % Mean wind speed [m/s]
v_m_h = v_m(h);                 % At top of building

%% Frequency and reduction factors
y_c = 150 * n_1x / v_m_h;
                                                % Frequency
    factor
F = (4*y_c) / ((1+70.8*y_c^2)^(5/6));
                                    % Spectral factor
Phi_b = 1 / (1 + (3.2*n_1x*b)/v_m_h);
                                    % Width reduction factor
Phi_h = 1 / (1 + (2*n_1x*h)/v_m_h);
                                     % Height reduction factor

%% Force coefficient c_f
db_ratio = d / b; % d/b ratio
if db_ratio <= 1
    c_f0 = 0.3193*log(db_ratio) + 2.5139;    % Zone A
elseif db_ratio <= 10
    c_f0 = -0.7121*log(db_ratio) + 2.1460;   % Zone B
else
    c_f0 = -0.1443*log(db_ratio) + 1.2322;   % Zone C
end
shape_vals = [1,3,10,20,40,60,70];
psi_shape = [0.6,0.65,0.7,0.775,0.85,0.9,0.925];
psi_lambda = interp1(shape_vals, psi_shape, min(max(1.4*h/b
    ,0),70), 'linear', 'extrap');
psi_r = 1.0;                                    % No
    rounded corners [-]
c_f = c_f0 * psi_r * psi_lambda;                % Adjusted
    force coefficient

%% Damping and response factors
z_s = max(0.6*h, z_min);                        % Reference
     height for damping
delta_s = 0.10;                                 %
    Structural damping [-]
delta_a = (c_f*rho*b*v_m(z_s))/(2*n_1x*m_e);    %
    Aerodynamic damping
R = sqrt(2*pi*F*Phi_b*Phi_h / (delta_s + delta_a)); %
```

```
   Resonance response factor
B = sqrt(exp(-0.05*(h/h_ref) + (1-(b/h))*(0.04+0.01*(h/h_ref)
   ))); % Background factor
nu = n_1x * R / sqrt(B^2 + R^2);                    % Crossing
   frequency
k_p = sqrt(2*log(nu*600)) + 0.6./sqrt(2*log(nu*600)); % Peak
   factor

%% Peak velocity pressure
q_p = @(z) ((1 + 2*k_p.*I_v(z)) .* ((k_r*log(z./z_0)*c_0).^2
   * q_b)) .* (z>=z_min & z<=z_max) + ...
          ((1 + 2*k_p.*I_v(z_min)) * ((k_r*log(z_min/z_0)*c_0
             )^2 * q_b)) .* (z<z_min);

%% Structural factor and dynamic wind load
c_s_c_d = (1 + 2*k_p.*I_v(z_s).*sqrt(B^2+R^2)) / (1 + 6*I_v(
   z_s)); % Structural factor
F_w = c_s_c_d * c_f * q_p(z);       % Dynamic wind load [kN/m
   ^2]

%% Serviceability Limit State - acceleration
v_s = @(Ta) 0.75*v_b * sqrt(1 - 0.2*log(-log(1 - 1./Ta))); %
   Wind speed for Ta-year return
v_ms = @(z) c_r(z)*c_0*v_s(2);       % Mean wind speed for
   SLS [m/s]

% Mean reference pressure for SLS
q_m = @(z) 0.5 * rho * v_ms(z).^2;   % Mean wind pressure [kN
   /m^2]

y_cs = 150 * n_1x / (v_ms(h));        % Frequency factor SLS
F_s = (4*y_cs) / ((1+70.8*y_cs^2)^(5/6)); % Spectral factor
   SLS
Phi_bs = 1 / (1 + (3.2*n_1x*b)/(v_ms(h))); % Width reduction
   SLS
Phi_hs = 1 / (1 + (2*n_1x*h)/(v_ms(h)));   % Height reduction
    SLS
delta_as = (c_f*rho*b*v_ms(z_s)) / (2*n_1x*m_e); %
   Aerodynamic damping SLS
R_s = sqrt(2*pi*F_s*Phi_bs*Phi_hs / (delta_s + delta_as)); %
   Resonance SLS
nu_s = n_1x * R_s / sqrt(B^2 + R_s.^2); % Crossing frequency
   SLS
k_ps = sqrt(2*log(nu_s*600)) + 0.6./sqrt(2*log(nu_s*600)); %
   Peak factor SLS
phi_1x = @(z) (z/h).^1.5;             % Mode shape
   distribution

% Standard deviation of acceleration
```

```
96 sigma_x = @(z) (3 * I_v(h) * R_s * q_m(h) * b * c_f .* phi_1x
       (z)) ./ m_e;
97
98 % Peak acceleration
99 X_max = @(z) k_ps .* sigma_x(z);
100
101 % Calculate and display peak acceleration at top of building
102 X_max_top = X_max(h);
103 fprintf('Peak␣acceleration␣at␣h␣=␣%.1f␣m:␣%.3f␣m/s^2\n', h,
       X_max_top);
104
105 %% Export dynamic wind load table
106 F_w_table = table(z',␣F_w', 'VariableNames', {'Height_m', '
       WindLoad_kN_m2'});
107 disp(F_w_table);
108 writetable(F_w_table, 'F_w_wind_load.xlsx', 'Sheet', 'Wind␣
       Load');
109
110 %% Export selected heights results
111 z_select = [0, 4.5 + (0:ceil((h-4.5)/3.5))*3.5];
112 z_select = z_select(z_select <= h);
113 F_w_sel = c_s_c_d * c_f .* q_p(z_select);
114 X_max_sel = X_max(z_select);
115 result_table = table(z_select',␣F_w_sel', X_max_sel',␣...
116 ␣␣␣␣'VariableNames',␣{'Height_m',␣'WindLoad_kN_m2',␣'
       PeakAccel_mps2'});
117 disp(result_table);
118 writetable(result_table,␣'Selected_WindResults.xlsx',␣'Sheet'
       ,␣'Selected Heights');
```

Listing F.1: `Appendix_Acc.m` – Dynamic wind load & acceleration analysis

G

MATLAB Script for Mass and Equivalent Mass Calculation

This appendix contains the MATLAB script `Appendix_Mass.m`, used to compute floor, wall and column masses and the equivalent mass m_{eq}.

```
format long g
clc

% --------- Core model selection ('1-Core' or '2-Core') ---------
core_model = '1-Core';  % <-- Change to '2-Core' if needed

% --------- Parameters ---------
n_floors_total = 20;       % Total number of floors
n_conc_floors = 3;         % Number of top floors made of concrete instead of CLT

% Total height of the building (m)
h = 4.5 + (n_floors_total - 1) * 3.5;

% Modal shape exponent
zeta = 1.5;

% Vertical discretization for integration
n_z = 1000;
z = linspace(0, h, n_z);
dz = z(2) - z(1);
phi = (z / h).^zeta;

% --------- Floor properties ---------
switch core_model
    case '1-Core'
        area_office = 834.56;      % m2
        area_core   = 65.209;      % m2
        n_columns   = 42;
    case '2-Core'
        area_office = 829.76;      % m2
        area_core   = 60.96;       % m2
        n_columns   = 40;
    otherwise
        error('Invalid core_model. Choose ''1-Core'' or ''2-
```

```
            Core''.');
end

% Material densities (kg/m3)
rho_CLT   = 402.5;
rho_conc  = 2550;

% Floor thicknesses (m)
thick_CLT   = 0.24;
thick_conc  = 0.4;

z_floors = 4.5 : 3.5 : h;
phi_floors = (z_floors / h).^zeta;

idx_CLT  = 1:(n_floors_total - n_conc_floors);
idx_BTGO = (n_floors_total - n_conc_floors + 1) :
   n_floors_total;

% --------- Columns, walls, bracing ---------
rho_column = 480;

% Column cross-sectional areas per block (m2), from top to
   bottom
A_vec = [0.1368 0.17415 0.33345 0.4644 0.5814 0.6966 0.7353];
% Column dimensions [mm]: 380x360, 430x405, 570x585, 645x720,
    760x765
block_size = 5;
n_blocks = ceil(n_floors_total / block_size);
A_columns = zeros(1, n_blocks);

for i = 1:n_blocks
    A_columns(i) = A_vec(n_blocks - i + 1); % Decreasing area
        upward
end

% Heights and z-positions of each floor's bottom
floor_heights = [4.5, 3.5 * ones(1, n_floors_total-1)];
z_floor_bottoms = [0, cumsum(floor_heights(1:end-1))];

% Initialize mass distribution of columns along z
m_columns = zeros(size(z));

% Distribute column mass per floor segment
for i = 1:n_floors_total
    z_start = z_floor_bottoms(i);
    z_end = z_start + floor_heights(i);
    block_idx = ceil(i / block_size);
    A = A_columns(block_idx);
    M = rho_column * n_columns * A;
```

```
    m_columns(z >= z_start & z < z_end) = M;
end

% Integrate to get total column mass (kg)
mass_columns = sum(m_columns) * dz;


% --------- Wall and Bracing Mass ---------
scale_wall = 4 / 3;  % Wall thickness scaling (e.g. 400/300 or 500/300); default = 300 mm --> 1.0

m_wall = zeros(size(z));
m_wall(z < 4.5)    = 5.757e4 * scale_wall;   % Bottom wall segment
m_wall(z >= 4.5)   = 5.635e4 * scale_wall;   % Upper wall segment
mass_wall = sum(m_wall) * dz;

% Bracing is assumed constant over height
m_bracing = 1.803e3;
mass_bracing = m_bracing * h;

% Total continuous mass distribution (columns + walls + bracing)
m_continuous = m_columns + m_wall + m_bracing;

% --------- Point Masses per Floor ---------
M_CLT_office  = rho_CLT  * thick_CLT  * area_office;
M_conc_office = rho_conc * thick_conc * area_office;
M_conc_core   = rho_conc * thick_conc * area_core;

% Facade mass
q_facade = 1500 / 9.81;                    % Line load in kg/m
perimeter = 2 * (17.2 + 53.6);             % Approximate building perimeter
M_facade = q_facade * perimeter;

% Surface load mass (non-structural weight on floor)
q_surface = 500 / 9.81;
total_area = area_office + area_core;
M_surface = q_surface * total_area;

% Live load (nyttig last)
load_CLT  = 2.5e3 * area_office / 9.81;
load_conc = 3.0e3 * area_core   / 9.81;
M_live = 0.3 * (load_CLT + load_conc);    % 30% of live load is considered

% Remove top floor from live load
```

```
122 phi_live = phi_floors(1:end-1);
123 n_floors_live = numel(phi_live);
124
125 % Beam mass per floor
126 rho_beam = 430;
127 A_b1 = 0.087; len_b1 = 176;
128 A_b2 = 0.048; len_b2 = 34.4;
129 M_beams = rho_beam * (A_b1 * len_b1 + A_b2 * len_b2);
130
131 % Mass per floor (point masses)
132 M_floors = zeros(1, n_floors_total);
133 for i = 1:n_floors_total
134     % Determine office slab material (CLT or concrete)
135     if ismember(i, idx_CLT)
136         M_office = M_CLT_office;
137         core_thick = 0.20; % Standard core thickness for CLT
              floors
138     else
139         M_office = M_conc_office;
140
141         % Assume concrete core matches concrete slab
              thickness
142         core_thick = thick_conc;
143         if exist('thick_conc_variable', 'var')
144             core_thick = thick_conc_variable; % Optional
                  override
145         end
146     end
147
148     % Core mass for this floor
149     M_core = rho_conc * core_thick * area_core;
150
151     % Sum all point mass components
152     M_floors(i) = M_office + M_core + M_facade + M_surface +
          M_beams;
153
154     % Add live load (except top floor)
155     if i < n_floors_total
156         M_floors(i) = M_floors(i) + M_live;
157     end
158 end
159
160 % --------- Equivalent Mass Calculation ---------
161 numerator_cont  = sum(m_continuous .* phi.^2) * dz;
162 numerator_point = sum(M_floors .* phi_floors.^2);
163 denominator     = sum(phi.^2) * dz;
164 m_eq = (numerator_cont + numerator_point) / denominator;
165
166 % --------- Mass Summary ---------
```

```
167 mass_CLT_office     = M_CLT_office * numel(idx_CLT);
168 mass_conc_office    = M_conc_office * numel(idx_BTGO);
169 mass_conc_core      = M_conc_core   * n_floors_total;
170 mass_facade         = M_facade      * n_floors_total;
171 mass_surface        = M_surface     * n_floors_total;
172 mass_beams          = M_beams       * n_floors_total;
173 mass_live           = M_live        * (n_floors_total - 1);
174 mass_slab_total     = sum(M_floors);
175
176 mass_total = mass_columns + mass_wall + mass_bracing +
       mass_slab_total;
177
178
179 fprintf('\n----------␣Mass␣Breakdown␣----------\n');
180 fprintf('Columns:␣␣␣␣␣␣␣␣␣␣␣␣␣␣␣␣%.1f␣kg\n', mass_columns);
181 fprintf('Concrete␣walls:␣␣␣␣␣␣␣␣␣%.1f␣kg\n', mass_wall);
182 fprintf('Bracing␣(diagonals):␣␣␣␣%.1f␣kg\n', mass_bracing);
183 fprintf('Floor␣slabs␣(office␣+␣core):␣%.1f␣kg\n',
       mass_slab_total);
184 fprintf('␣-␣CLT␣(office):␣␣␣␣␣␣␣␣%.1f␣kg\n', mass_CLT_office)
       ;
185 fprintf('␣-␣Concrete␣(office):␣␣␣%.1f␣kg\n', mass_conc_office
       );
186 fprintf('␣-␣Concrete␣(core):␣␣␣␣␣%.1f␣kg\n', mass_conc_core);
187 fprintf('Facade:␣␣␣␣␣␣␣␣␣␣␣␣␣␣␣␣%.1f␣kg\n', mass_facade);
188 fprintf('Surface␣load:␣␣␣␣␣␣␣␣␣␣%.1f␣kg\n', mass_surface);
189 fprintf('Beams:␣␣␣␣␣␣␣␣␣␣␣␣␣␣␣␣%.1f␣kg\n', mass_beams);
190 fprintf('Live␣load:␣␣␣␣␣␣␣␣␣␣␣␣%.1f␣kg\n', mass_live);
191 fprintf('-------------------------------------\n');
192 fprintf('TOTAL␣MASS:␣␣␣␣␣␣␣␣␣␣␣%.1f␣kg\n', mass_total);
193 fprintf('Equivalent␣mass␣(m_eq):␣%.2f␣kg/m\n', m_eq);
```

Listing G.1: `Appendix_Mass.m` – Mass & equivalent mass calculation

H

MATLAB Script for Acceleration Limit and Total Concrete Volume

This appendix contains the MATLAB script `Appendix_Conc.m`, used to compute the acceleration limit dependent on the frequency and the total concrete volume for each model.

```
%% Find acceleration limit
officeLimit(0.368) % Limit dependent on the Frequency


%% Total Concrete Volume
% === Input Data ===
clc; clear;

numStoreys      = 25;       % Number of storeys (20, 25, 30)
coreThickness   = 500;      % Core thickness in mm (300, 400, or 500)
numSlabs        = 5;        % Number of concrete slabs
slabThickness   = 400;      % Slab thickness in mm (default is 200 mm for base volumes)

% Base slab volumes per unit at reference thickness 200 mm
baseSlabVol1    = 180;      % m3 per slab (1-Core) at 200 mm thick
baseSlabVol2    = 178;      % m3 per slab (2-Core) at 200 mm thick

% Scale base volumes by actual slabThickness:
slabVolumePerUnit  = baseSlabVol1 * (slabThickness / 200);
slabVolumePerUnit2 = baseSlabVol2 * (slabThickness / 200);


% === Heights ===
firstStoreyHeight = 4.5;    % m (height of first storey)
otherStoreyHeight = 3.5;    % m (height of each subsequent storey)
totalHeight       = firstStoreyHeight + (numStoreys - 1) * otherStoreyHeight;


% === Core volume per metre (m3/m of height) maps ===
coreVolumePerMeter = containers.Map( ...
```

```
    {300, 400, 500}, ...
    [22.14084507, 29.52112676, 36.90140845] ...
);

coreVolumePerMeter2 = containers.Map( ...
    {300, 400, 500}, ...
    [23.94366197, 31.92488263, 39.90610329] ...  % (2-Core) m3/m
);


% === Volume calculations ===
coreVolume  = totalHeight * coreVolumePerMeter(coreThickness);     % m3 for 1-Core
slabVolume  = numSlabs    * slabVolumePerUnit;                     % m3 for 1-Core
totalVolume = coreVolume + slabVolume;                             % m3 for 1-Core

coreVolume2  = totalHeight * coreVolumePerMeter2(coreThickness);   % m3 for 2-Core
slabVolume2  = numSlabs    * slabVolumePerUnit2;                   % m3 for 2-Core
totalVolume2 = coreVolume2 + slabVolume2;                          % m3 for 2-Core



% === Print Results ===
fprintf('==========================\n');
fprintf('1-Core Configuration\n');
fprintf('==========================\n');
fprintf('Total concrete volume:    %.1f m3\n', totalVolume);
fprintf('  Core volume:            %.1f m3    (%.2f m height x %.3f m3/m)\n', ...
        coreVolume, totalHeight, coreVolumePerMeter(coreThickness));
fprintf('  Slab volume:            %.1f m3    (%d slabs x %.1f m3 each)\n\n', ...
        slabVolume, numSlabs, slabVolumePerUnit);

fprintf('==========================\n');
fprintf('2-Core Configuration\n');
fprintf('==========================\n');
fprintf('Total concrete volume:    %.1f m3\n', totalVolume2);
fprintf('  Core volume:            %.1f m3    (%.2f m height x %.3f m3/m)\n', ...
        coreVolume2, totalHeight, coreVolumePerMeter2(coreThickness));
```

```
fprintf('  Slab volume:           %.1f m3   (%d slabs x %.1f m3 each)\n\n', ...
        slabVolume2, numSlabs, slabVolumePerUnit2);


%% --- Local function: SS-ISO 10137 office acceleration limit ---
function A = officeLimit(f)
    % OFFICELIMIT Returns the SS-ISO 10137 office acceleration limit [m/s^2].
    %
    %   A = officeLimit(f) interpolates on a log-log scale between:
    %     f_iso = [0.06, 1,   2,   5] Hz
    %     A_pts = [0.21, 0.06,0.06,0.15] m/s^2
    %
    %   Example: officeLimit(1) --> 0.06

    f_iso = [0.06, 1,   2,   5];
    A_pts = [0.21, 0.06,0.06,0.15];
    A = 10.^interp1(log10(f_iso), log10(A_pts), log10(f), 'linear', 'extrap');
end
```

Listing H.1: `Appendix_Conc.m` – Mass & equivalent mass calculation

I

MATLAB Script for Eigenfrequency Calculations

This appendix contains the MATLAB script `Appendix_Freq.m`, which is used for:

- Analytical calculation of bending and torsion frequencies.
- Numerical FEM calculation of bending frequencies.
- Numerical FEM calculation of torsional frequencies.

```
% Appendix: Analytical eigenfrequencies for cantilevers
% Bending (Euler-Bernoulli, Fixed-Free)
% Torsion (Saint-Venant, Fixed-Free)
clear; clc;

%% Section definitions:
% name         L [m]    b [m]   h [m]    E [Pa]    rho  [kg/m^3]    nu     isHollow   t_wall [m]
elements = { ...
  'GlulamBeam',    10.0, 0.14, 0.14, 13e9,    430,     0.2,     false,    0.0; ...
  'SteelTube',     10.0, 0.45, 0.25, 210e9,  7850,     0.3,     true,    0.016; ...
  'ConcreteCore', 88.5, 19.2,  4.8,  33e9,   2550,     0.2,       true,    0.50; ...
};

% Eigenvalue constants
beta_EB  = [1.875104, 4.694091, 7.854757];      % fixed-free bending
alpha_SV = (2*(1:3)-1)*pi/2;                    % fixed-free torsion

% Table header
fprintf('\n%-20s %-8s %-12s %-12s\n','Type','Mode','Bending [Hz]','Torsion [Hz]');
fprintf('%s\n', repmat('-',1,56));

for i = 1:size(elements,1)
  name     = elements{i,1};
  L        = elements{i,2};
  b        = elements{i,3};
```

```
26  h         = elements{i,4};
27  E         = elements{i,5};
28  rho       = elements{i,6};
29  nu        = elements{i,7};
30  isHollow  = elements{i,8};
31  t_wall    = elements{i,9};
32
33  %% 1) Cross-sectional properties
34  if isHollow
35    b_o = b + t_wall;  b_i = b - t_wall;
36    h_o = h + t_wall;  h_i = h - t_wall;
37    A  = b_o*h_o - b_i*h_i;
38    Iz = (b_o*h_o^3 - b_i*h_i^3)/12;
39    Iy = (h_o*b_o^3 - h_i*b_i^3)/12;
40    Jp = Iz + Iy;
41    % Saint-Venant torsion constant (thin-wall)
42    Bm = b_o; Dm = h_o; t = t_wall;
43    pm = 2*((Bm-t)+(Dm-t));
44    Am = (Bm-t)*(Dm-t);
45    Jt = (1/3)*t^3*pm + 2*(2*Am*t/pm)*Am;
46  else
47    A  = b*h;
48    Iz = b*h^3/12;
49    Iy = h*b^3/12;
50    Jp = Iz + Iy;
51    % Approximate solid torsion constant
52    b1 = max(b,h); h1 = min(b,h);
53    Jt = b1*h1^3*(1/3 - 0.21*(h1/b1)*(1 - h1^4/(12*b1^4)));
54  end
55
56  G = E/(2*(1+nu));  % shear modulus
57
58  %% 2) Analytical bending frequencies (Euler-Bernoulli)
59  for n = 1:3
60    f_b(n) = (beta_EB(n)^2)/(2*pi*L^2) * sqrt(E*Iz/(rho*A));
61  end
62
63  %% 3) Analytical torsion frequencies (Saint-Venant)
64  if isHollow
65    for n = 1:3
66      f_t(n) = (alpha_SV(n)/(2*pi*L))*sqrt(G*Jt/(rho*Jp));
67    end
68  else
69    f_t = NaN(1,3);  % no hollow torsion for solid beam
70  end
71
72  %% 4) Print results
73  for n = 1:3
74    fprintf('%-20s␣Mode%-1d␣␣␣%8.4f␣␣␣␣␣␣␣%8.4f\n', ...
```

```
            name, n, f_b(n), f_t(n));
  end
  fprintf('\n');
end



% Appendix: Numerical bending eigenfrequencies (Timoshenko)
clear; clc;

%% 1. Section definitions:
% name, span L [m], H_sec [m], B_sec [m], E [Pa], rho [kg/m^3], nu [-],
% isHollow, wall thickness t [m]
sections = { ...
  'GlulamBeam',   10.0, 0.14,   0.14, 13e9,  430,   0.2,  false, 0.00; ...
  'SteelTube',    10.0, 0.45,   0.25, 210e9, 7850,  0.3,  true,  0.016; ...
  'ConcreteCore', 88.5, 19.20,  4.80, 33e9,  2550,  0.2,  true,  0.50; ...
};

%% 2. FEM settings
Nelem       = 30;       % number of beam elements
ndof_per_nd = 2;        % DOFs per node: [w; phi]
kappa       = 5/6;      % shear correction factor

fprintf('\n%-16s %-6s %-12s\n','Element','Mode','Bending [Hz]');
fprintf('%s\n',repmat('-',1,38));

for s = 1:size(sections,1)
    %% 3. Unpack parameters
    [name, L_span, H_sec, B_sec, E, rho, nu, isHollow, t_wall] = deal(sections{s,:});

    %% 4. Cross-section geometry
    if isHollow
        h_in = H_sec - 2*t_wall;
        b_in = B_sec - 2*t_wall;
    else
        h_in = 0;
        b_in = 0;
    end
    A_sec  = H_sec*B_sec - h_in*b_in;
    Iz_sec = (B_sec^3*H_sec - b_in^3*h_in)/12;

    %% 5. Select shear modulus & mass matrix type
```

```
    if strcmp(name,'GlulamBeam')
        G       = 650e6;          % measured for glulam
        massMat = 'lumped';       % lumped mass
    else
        G       = E/(2*(1+nu));   % isotropic
        massMat = 'consistent';   % consistent mass
    end

    %% 6. FEM mesh & globals
    Ne   = Nelem;
    Nn   = Ne + 1;
    totD = Nn * ndof_per_nd;
    Le   = L_span / Ne;
    K    = zeros(totD);
    M    = zeros(totD);

    EI  = E * Iz_sec;
    kGA = kappa * G * A_sec;
    phi = 12*EI / (kGA*Le^2);

    % element stiffness (Timoshenko 2DOF)
    Ke = EI/(Le^3*(1+phi)) * [ ...
         12,    6*Le,   -12,    6*Le;
         6*Le, (4+phi)*Le^2, -6*Le, (2-phi)*Le^2;
        -12,   -6*Le,    12,   -6*Le;
         6*Le, (2-phi)*Le^2, -6*Le, (4+phi)*Le^2 ];

    % assemble elements
    for e = 1:Ne
        % choose mass matrix
        me  = rho * A_sec * Le;
        Irt = rho * Iz_sec * Le;
        switch massMat
            case 'lumped'
                Me = diag([me/2, Irt/2, me/2, Irt/2]);
            case 'consistent'
                % Consistent mass matrix (beam theory)
                Me = me/420 * [ ...
                  156,   22*Le,  54,   -13*Le;
                  22*Le, 4*Le^2, 13*Le, -3*Le^2;
                   54,    13*Le, 156,   -22*Le;
                 -13*Le,-3*Le^2,-22*Le, 4*Le^2 ];
        end

        idx = (e-1)*ndof_per_nd + (1:4);
        K(idx,idx) = K(idx,idx) + Ke;
        M(idx,idx) = M(idx,idx) + Me;
    end

```

```
    %% 7. Apply fixed-base BC: remove DOFs 1 & 2
    free = 3:totD;
    Kf   = K(free,free);
    Mf   = M(free,free);

    %% 8. Solve eigenvalue problem
    [Vb,Db] = eig(Kf,Mf);
    lamb    = sort(diag(Db));
    freq_b  = sqrt(lamb(lamb>0))/(2*pi);

    %% 9. Print first five bending modes
    for m = 1:5
        if m <= numel(freq_b)
            fprintf('%-16s Mode%-1d    %8.4f\n', name, m,
                freq_b(m));
        else
            fprintf('%-16s Mode%-1d    %8s\n', name, m, '-');
        end
    end
    fprintf('\n');
end




% Appendix: Numerical torsional eigenfrequencies (1-DOF bar
    elements)
clear; clc

%% 1. Define the torsion members
%   name            L [m]   B_out [m]  H_out [m]  t_wall [m]
      E [Pa]      rho [kg/m^3]  nu
secs = { ...
 'SteelTube'    , 10.0 ,   0.25 ,    0.45 ,   0.016 ,  210e9 ,
       7850 ,   0.30 ; ...
 'ConcreteCore', 88.5 ,   19.2 ,     4.8 ,   0.50  ,   33e9 ,
       2550 ,   0.20 ;
};

Ne       = 100;      % number of elements
numModes = 3;        % number of torsional modes to compute

fprintf('%-14s  %-10s  %-10s  %-10s\n', 'Section', 'f1 [Hz]',
    'f2 [Hz]', 'f3 [Hz]');
fprintf('%s\n', repmat('-',1,46));

for k = 1:size(secs,1)

```

```
210     %% 2. Geometry & material
211     [name, L, B, H, t, E, rho, nu] = deal(secs{k,:});
212     G = E/(2*(1+nu));  % shear modulus
213
214     %% 3. Compute cross-section torsion and mass properties
215     Bi = B - 2*t;  Hi = H - 2*t;
216     if Bi<=0 || Hi<=0
217       error('%s: wall thickness %.3f m too large for %.2fx%.2
            f m section.', name, t, B, H);
218     end
219
220     % Thin-wall Saint-Venant torsion constant
221     b_mid = B - t;  h_mid = H - t;
222     A_enc = b_mid * h_mid;            % mid-surface enclosed
          area
223     p_mid = 2*(b_mid + h_mid);        % mid-surface perimeter
224     Jt = 4 * A_enc^2 * t / p_mid;
225
226     % Polar mass moment per unit length
227     Ix = (B*H^3 - Bi*Hi^3)/12;
228     Iy = (H*B^3 - Hi*Bi^3)/12;
229     Jp = Ix + Iy;                     % polar area moment
230     Ip = rho * Jp;                    % polar mass moment per
          length
231
232     %% 4. Build global K & M for torsion bar model (1 DOF per
           node)
233     Le   = L / Ne;
234     Nn   = Ne + 1;
235     Kb   = sparse(Nn, Nn);
236     Mb   = sparse(Nn, Nn);
237
238     % Element stiffness & mass
239     Ke = (G*Jt/Le) * [1 -1; -1 1];
240     Me = (rho*Jp*Le/6) * [2 1; 1 2];
241
242     % Assemble
243     for e = 1:Ne
244       idx = e:e+1;
245       Kb(idx,idx) = Kb(idx,idx) + Ke;
246       Mb(idx,idx) = Mb(idx,idx) + Me;
247     end
248
249     %% 5. Apply fixed-base BC
250     free = 2:Nn;
251     Kf   = Kb(free,free);
252     Mf   = Mb(free,free);
253
254     %% 6. Solve eigenproblem
```

```
255     opts.issym = true;
256     opts.isreal = true;
257     [~, D] = eigs(Kf, Mf, numModes, 'SM', opts);
258     omega = sqrt(diag(D));          % rad/s
259     f     = sort(omega)/(2*pi);     % convert to Hz
260
261     %% 7. Print first three torsional frequencies
262     f_out = nan(1,3);
263     f_out(1:length(f)) = f;
264     fprintf('%-14s␣␣%10.3f␣␣%10.3f␣␣%10.3f\n', name, f_out);
265 end
```

Listing I.1: `Appendix_Freq.m` – Analytical and numerical eigenfrequency calculations

DEPARTMENT OF SOME SUBJECT OR TECHNOLOGY
CHALMERS UNIVERSITY OF TECHNOLOGY
Gothenburg, Sweden
www.chalmers.se

CHALMERS
UNIVERSITY OF TECHNOLOGY